Quays Rather Than Boilers

Extracting Heat From Water and Soil Through Energy Sheet Piles

J. P. de Vries

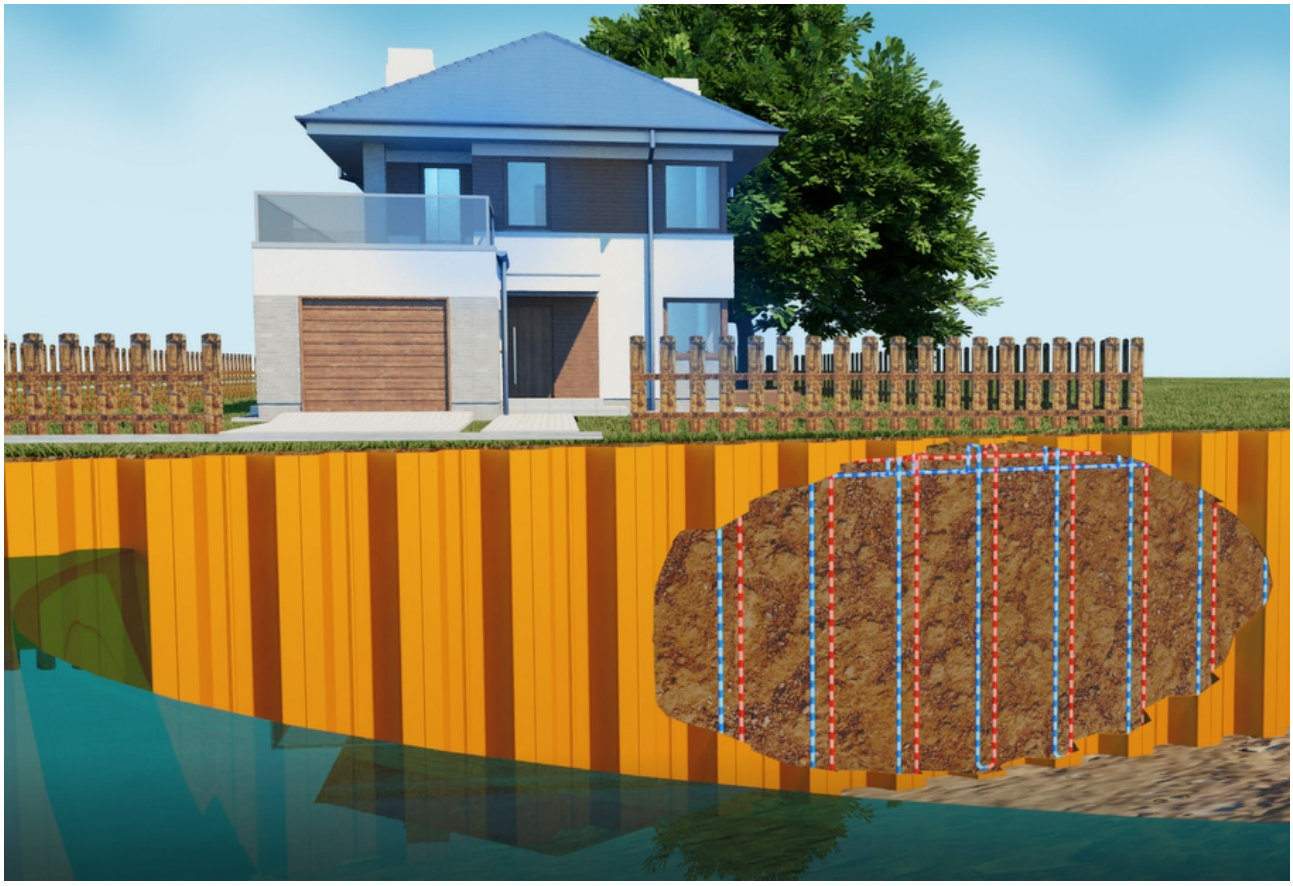

Source: *Inzending Handelmaatschappij Gooimeer BV - Categorie: Product Innovatie.* (2020, 27 oktober). [Video]. YouTube. https://www.youtube.com/watch?v=-zdeHxZ9ock&ab_channel=InfraTechNL

Quays Rather Than Boilers

Extracting Heat From Water and Soil Through Energy Sheet Piles

by

J. P. de Vries

to obtain the degree of Master of Science
at the Delft University of Technology,
to be defended publicly on Friday May 14, 2021 at 15:00.

Student number:	4615514	
Project duration:	April 20, 2020 – March 17, 2021	
Thesis committee:	Assoc. Prof. ir. P. J. Vardon,	TU Delft, Geoscience and Engineering, (Chair)
	Dr. Ing. M. Z. Voorendt,	TU Delft, Hydraulic Engineering
	Ir. I. A. Pantev,	TU Delft, Geoscience and Engineering
	Ing. K. de Jong	CRUX Engineering B.V.

This thesis is confidential and cannot be made public until May 14, 2022.

An electronic version of this thesis is available at `http://repository.tudelft.nl/`.

TU Delft

Preface

I hereby proudly present my thesis 'Energy sheet pile wall'. This report contains the conducted literature study, research and conclusions of my master degree thesis at the faculty of Civil Engineering and Geosciences of Delft University of Technology. As part of the Civil Engineering track, this report marks the end of my time as Msc student Geo-Engineering and start as Engineer.

As a student-assistent Soil Mechanics, I encountered one of Phil Vardon's fields of expertise, coupled numerical modelling in geomaterials, a number of times and it caught my attention immediately. Therefore, it didn't take long to make up my mind when presented this topic. The incredibly interesting idea of utilizing the earth's temperature in combination with the isolating effect of soil and the energy in flowing water resulting in a almost infinite source of renewable energy speaks to my, and probably everyone's, imagination.

This thesis subject brings together two of my interests: renewable energy and soil mechanics, the latter of which became clear during my BSc internship at Royal HaskoningDHV. Not being able to work on the project I was originally hired for, I had to fend for myself within the company, in the end managing to work in every field civil engineering spans. Out of all assignment I did for my colleagues, the ones for geo-engineering where the ones which I enjoyed the most. Starting with my dad's advice to study civil engineering, you could say that me ending up here is a series of fortunate events. As I yet had to find out back then, the applications and characteristics of soil go way beyond agriculture and building material, as is perfectly shown by this topic. This insight, among others, make me realize the time at the university is well spend. Moreover, combining the two subjects in this thesis fulfil a desire to actively contribute to changing society for the better and if possible, even make a career out of it.

Jorrit de Vries
May 9, 2021
Delft

Abstract

As part of the effort to make the Dutch waterways CO_2-neutral, a consortium consisting of, among others, CRUX Engineering BV and Delft University of Technology, initiated a case study in which the thermal and mechanical performance of an energy sheet pile wall is studied. This technology allows for the extraction of energy from the water and soil by means of collectors, i.e. a system of pipes welded to the sheet piles. The fluid flowing through these pipes is directed to a heat pump after which the extracted energy can be used to heat buildings. Moreover, during summer, the system provides the opportunity to be used to cool homes by storing heat in the subsurface. The primary objective of a sheet pile wall is to assure stability of the quay and by giving the sheet pile wall an additional purpose, that of heat sink or source, previously not present thermal loads are applied to the wall. In this thesis the temperature change of the sheet pile wall and soil is investigated after which the deformation of the sheet pile wall is analysed in order to answer the main research question: 'Can the structural safety of a sheet pile quay be guaranteed when the sheet pile is thermally activated?'.

In the town of Zweth, part of the municipality of Rotterdam, an investigation into the performance and consequences of thermally activating a sheet pile wall was conducted in the form of a case study. A sheet pile wall with a width of approximately 7.5 meters and a depth of 15 meters was placed. Two sets of loops were welded on the sheet pile: loops running to the bottom of the wall and loops running to a depth of 3 meters. The influence on the surroundings of these separately investigated loops was monitored by means of thermistor strings. The deformation of the sheet pile was measured with inclinometers. This thesis starts with the analysis of the collected data from the field test. To investigate the long-term behaviour of the sheet pile wall two models are developed in this thesis: a heat conduction model and a geotechnical stability model. The former is a thermal calculation only and aims to model the temperature changes in the subsurface as well as the heat extraction. The latter consists of a time dependent Thermo-Hydro-Mechanical (THM) analysis in PLAXIS and used the sheet pile temperature determined in the heat conduction model as thermal boundary condition on the sheet pile. The resulting temperature change of the sheet pile and subsurface in combination with mechanical loads results in a deformation of the sheet pile. Using the data acquired in the field test, these two models are validated. With the help of the validated geotechnical stability model, the thermal component in the total distortion of the sheet pile is investigated. Finally, a calculation with with a time span of 4 years is performed to see the long-term reaction of the sheet pile wall. Based on this research the main question is answered.

In the Netherlands, soil temperatures below 6 meters of depth stays approximately 12 °C all year. Above that, the soil temperature changes with the seasons, yet with a delay. The test ran in the autumn and winter and due to the time of the year, the soil at a few meters depth still had the summer heat stored while the soil close to the surface already started to cool down. The interpretation of the collected data started with recognizing from the thermistor string data that the soil in the quay adjacent to the canal is heavily influenced by the water temperature. Deeper down, the heat extraction is the only external influence. Investigations into heat extraction based on the numbers of loops activated showed that there was no linear relation between the concentration of activated loops and the soil temperature decrease. When twice as many loops were activated on the same sheet pile wall area, the soil temperature decrease was only slightly higher. The maximum deformation of the sheet pile wall oscillated throughout the testing period. No direct correlation between thermal activation and deformation was identified.

The validation of the heat conduction model showed that the the soil temperatures in the model were generally too low in the subsurface below 6 meters in the comparison between the in-situ measured temperatures and the numerically determined soil temperatures. The numerically approached temperatures in the quay adjacent to the canal were strongly influenced by the canal water temperature. So much that the heat extraction was barely visible in the data. This emphasizes the importance of good water temperature data. Moreover, part of the energy extracted is a result of the turbulent flow of the canal water parallel to the sheet pile wall. This is not simulated in the model yet important to add. Despite this, the numerically determined extracted heat and the measured heat showed a reasonably good fit.

The comparison of in-situ measured deformation of the sheet pile wall and the numerically approached deformation was in the same order of magnitude as the measured data. The influence of the thermal component on the distortion of the sheet pile was found to be small. During the calculation, the distortion slightly oscillated in the range of tens of millimetres which falls within the numerical accuracy of the model. The measured oscillation was assumed to be caused by changing water levels and soil saturation as well as measurement errors. To investigate the long-term reaction of a thermally activated sheet pile wall, three THM computations with a time span of 4 years were conducted: one without thermal activation, one with natural soil temperature regeneration during summer and one with forced regeneration by the energy sheet pile wall. All had a sinus-like course with an accumulating deformation over time which was intensified by the amount of influence of the energy sheet pile. The computation with the forced regeneration – i.e. the most influence – by the energy sheet pile wall ended with the largest amount of deformation which was 5 millimetres larger than the computation without thermal activation. Extrapolating the results, the maximum deformation was determined to be approximately 6 millimetres after 6 years.

The thermal load on the sheet pile wall is not a design parameter and is generally not investigated in detail. Therefore, it is strongly advised to conduct additional research. However, based on these findings, it is concluded that the deformation resulting from the thermal activation of a sheet pile wall is not excessively large. This means the primary objective of keeping the quay stable won't be compromised. This leads to the conclusion that the technology is safe to be applied on a large scale to decrease the carbon footprint and contribute to a more sustainable society without interfering with the quay's primary function.

Contents

Chapter 1

Relevancy of this Thesis

In recent years, the negative human impact on the environment has become increasingly clear. The ever increasing thirst for energy has lead us to use more fossil fuels and other polluting energy sources than ever. As more and more people realize this, the demand for change is growing. With this increasing awareness, people search for ways to contribute to a more CO_2 neutral society.

One of the possible ways to realize this, is to use the freely available energy from aquathermy with the help of an energy sheet pile wall. Since most of the domestic used energy is for heating, it makes sense to focus on using this energy more efficiently. An energy sheet pile wall gives the possibility to extract, and generate, heat stored in the ground and use it to heat homes when necessary. At the same time, the subsurface is cooled down giving the possibility to cool houses in the summer by extracting the coolness. Considering the Dutch climate, the relatively large summer/winter temperature difference and the widespread use of sheet piles gives this technology a lot of potential to drastically decrease the household carbon footprint. Besides that, innovation is the engine of a knowledge economy. Where Dutch hydraulic engineers are already considered the best of the world – exporting their knowledge and expertise far and wide – innovative technologies such as these can broaden this reputation to include small scale energy effective solutions making a large impact.

Partly due to the promising results from recent experiments with innovative technologies, the Dutch province of Zuid-Holland decided to fund several pilots, one of which was awarded to a consortium consisting of Delft University of Technology, Eindhoven University of Technology, CRUX Engineering B.V., Gooimeer B.V. and Groep Duurzame Energie. One of the pilots is carried out near the village of Zweth along the canal Delftsche Schie in the Netherlands. The energy sheet pile wall has been installed on June 16, 2020. The patented design has so-called activation loops on the soil-side of the sheet pile through which a fluid is pumped to harvest heat from the soil and slow streaming water in the Delftsche Schie. The configuration and means of measurement is set out in Chapter 4. The objective of the pilot is to collect in-situ data to validate numerical models needed for future design processes and determine the feasibility of using energy sheet pile wall to store and generate energy in the quay which can be used to heat adjacent households.

Chapter 2

Problem Analysis

This chapter contains an analysis of the so far available information and aims to define pitfalls and unknowns of the research process. The current state of knowledge is analysed and this chapter ends with a problem statement.

2.1 Analysis of the Current State of Knowledge

The use of the subsurface as heat source has been growing for several decades and is receiving increasing attention. Since the 1970's, the global use of Ground Source Heat Pump (GSHP) and Underground Termal Energy Storage (UTES) systems have soared drastically. It is estimated that the worldwide capacity has increased almost twenty-fold between 1995 and 2010 from approximately 1854 MW_{th} to 35.236 MW_{th}. In Europe, the installed capacity up to 2012 is estimated to be 16.500 MW_{th} (Bourne-Webb et al., 2016).

One of these UTES systems is the energy sheet pile wall. For it is a relatively new technology, there is little experience among geo-engineers. To get a better grip on the subtleties of this new technology, several large-scale tests were carried out recently. Another reason for the rise of researching this topic, is the ability to numerically model the energy transfer through the soil which became possible relatively recent due to the increase in computing power. Hence, several papers have been written in which a large scale laboratory test are compared with numerical analyses. This study considers three papers: Kürten et al. (2014), Kürten et al. (2015) and Ziegler et al. (2019).

In 2014, Kürten et al. (2014) published a paper in which their conclusions of the coupling of a semi-analytical model with a numerical code was validated with a large-scale test is explained. Starting with the experiment, a 3 m x 3 m x 2 m testing station was constructed in which a thermo-active seal panel – consisting of activation loops integrated in a concrete protection slab – was placed to simulate a thermally active basement wall, shown in Figure 2.1. Water runs from the left hand side to the right hand side in a flow perpendicular to the seal panel. Meanwhile, a conduction fluid was circulated through the activation loops to extract heat from the soil. The experiment was started with a thermal response test. The inlet temperature and flow rate of the conduction fluid was kept constant and the energy output was determined by measuring the outlet temperature and outlet flow rate over a period of 7 hours. The soil and outside of the seal panel where also monitored for temperature change. To assess the influence of different system conditions, pipe arrangement, pipe diameter, pipe materials and flow rates as well as different groundwater velocities where varied to find the optimal system set-up. This concluded in the recommendation to use a large pipe diameter and the mounting of activation loops in series to get an area as large as possible. Promising results where acquired; energy output was found to be between 30 and 300 $W m^{-2}$ depending on conditions.This is considerably higher than energy diaphragm walls (up to 100 $W m^{-2}$), ground slabs (up to 30 $W m^{-2}$) and energy tunnels (up to 70 $W m^{-2}$).

The numerical part of the experiment has been based on the general code SHEMAT, which is for modelling heat and mass transport in porous media. Coupling a thermal resistance equivalent star network model with SHEMAT-suite, an extension of SHEMAT, resulted in a tool capable of analysing the element and surrounding soil in terms of thermic behaviour. Recognising the fact that the geometry of the construction element changes very little in radial direction, the horizontal heat transfer was calculated using thermal resistance while vertical change was calculated by finite difference methods. Hence, the used model is a 2D finite difference code reducing computing times drastically by avoiding a full discretization.

Validation was done by using a fully discretized COMSOL model. The first run gave a good agreement: a fixed inlet temperature of 1°C gave an output of 1.59°C (COMSOL) and 1.57°C (SHEMAT-Suite). The large-scale testing set-

up was rerun with boundary conditions which made comparing the analytical and semi-analytical model possible. The results show good agreement. Nevertheless, two possible improvements where identified. Firstly, perpendicular groundwater flow causes spacious flow around the wall, resulting in a so called 'dead zone' due to the decreasing velocity near the seal panel as water flow is directed to the bottom of the wall (Figure 2.1). This prevents the full utilization of the heat conduction capacity of the groundwater, soil and thermo-active seal panel as the groundwater stays relatively long near the wall. It's concluded that future experiments will have parallel groundwater flow to the thermal structures. Secondly, seasonal temperature fluctuations will affect the shallow subsurface in real life thus this influence should be simulated in both the laboratory set-up as well as the (semi-)analytical model.

The second paper sets off where the previous paper stopped. The same authors, S. Kürten, D. Mottaghy and M. Ziegler, build another laboratory set-up in which the 'lessons learned' where applied and described their results in Kürten et al. (2015). Moreover, two different pipe systems where incorporated in the seal panel: U-shaped and W-shaped pipes. Experiments pointed out return temperatures increased with longer exposure to the soil. Therefore, longer loops are preferred thus it can be concluded the W-shape is more efficient. Furthermore, in line with expectations, the specific power, dependent on the flow rate and in- and outlet temperature difference, increased with increasing flow rate. However, with increasing flow rate, the exposure of the fluid in the pipe system to the soil warmth decreased hence the in- and outlet temperature difference decreased as well. Further investigations showed the flow rate has the most influence of the pair meaning a high flow velocity is the most efficient way to maximize the specific energy output. A side note has to be added to this conclusion because only the output energy was assessed in this study, not the input. When the flow rate is high at the exit of the system, the velocity has to be high at the entrance as well. It would be more appropriate to look at the specific power after the power needed to pump the liquid through the system has been subtracted.

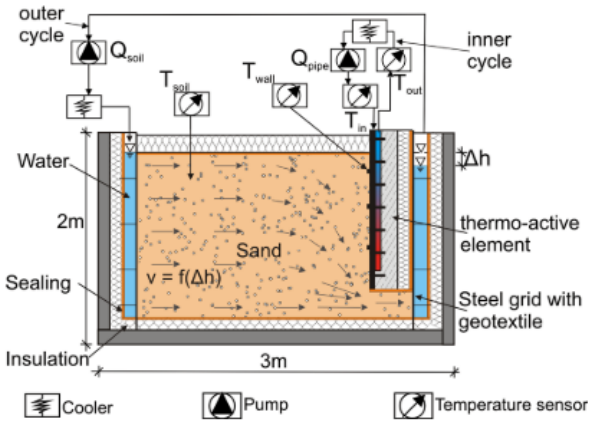

Figure 2.1: Schematic overview of the large-scale testing station used by Kürten et al. (2014)

Key to designing the most efficient energy geostructure as possible is to know which parameters yield the most influence. Kürten et al. (2015) conducted a parametric study to assess the controlling factors. Roughly two types of parameters can be identified: technical and soil parameters, of which the latter is site specific and thus cannot be tweaked. The technical parameters, which can be adjusted, are subdivided in two classes applying to the constructive elements and operating the energy structure.

Table 2.1: Investigated parameters in Kürten et al. (2015)

Constructive parameters	**Operational parameters**	**Soil parameters**
Thermal properties	Type of heat carrier fluid	Thermal ground properties
Pipe diameter	Volumetric flow rate	Ground water flow velocity
Spacing of the pipes	Inlet temperature of fluid	Ground temperature incl. seasonal variations
Location of pipes within the wall		Properties of the far side of the ground (inner part)
Arrangement of pipes (number of loops, serial/parallel)		

Table 2.1 shows the parameters looked at. Figure 2.2 show the normalized results. The operational and constructive parameters where determined in accordance with the (site specific) boundary conditions. It's key to get the constructive parameters right in the designing stage as they cannot be changed afterwards, in contrast to the operational parameters which can be altered during the complete lifespan. The most important factors are identified as: flow rate, thickness pipe cover, thickness pipe layer (insulated), shank space (the spacing between pipes) and the groundwater.

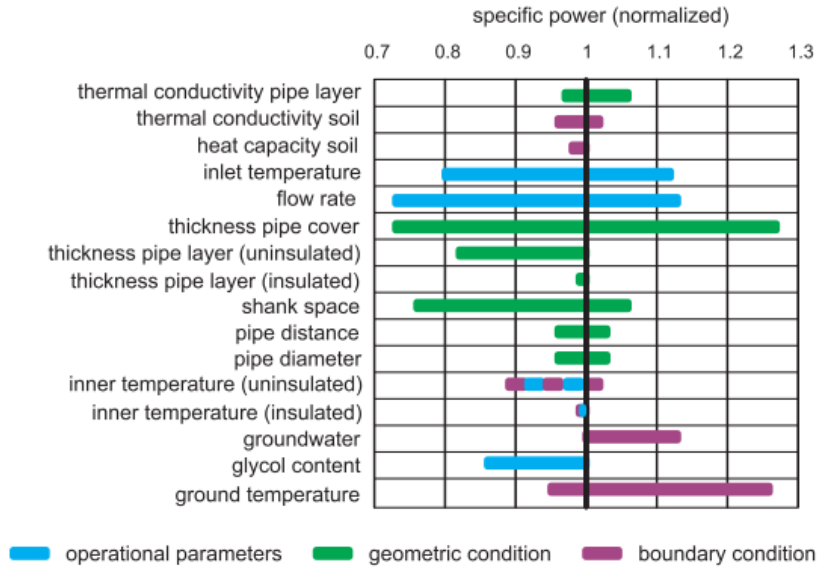

Figure 2.2: Normalized results of the parameter study by Kürten et al. (2015)

Several general recommendations are made:

- Increasing flow rate leads to the decreasing of return temperature. In addition, pressure loss due to friction decreases the specific energy so a very high velocity is not convenient. Therefore, the flow through the pipes should be in the transition zone between laminar and turbulent flow.
- Inlet temperature should be chosen with site specifications in mind. If the fluid temperature is a bit colder than the soil, the fluid can be heated to soil temperature in the limited amount of time it's exposed.
- Heat output is higher with the presence of groundwater flow. Also, the geostructure should be placed in such a way it's parallel to the flow direction.
- The arrangement of the pipes is of importance (series or parallel). A large pipe length leads to a longer exposure to the soil's heat resulting in the biggest in- and outlet temperature difference. Parallel loops yield a higher redundancy and low pressure loss. However, the fluid volume is split while flow through different sections decreasing the flow rate thus decreasing the specific energy. Therefore, loops in series are recommended.

The final paper considered is the most applicable to this thesis. Titled 'Energy sheet pile walls - Experimental and Numerical Investigation of Innovative Energy Geostructures' by Ziegler et al. (2019), a large-scale test set-up is build in which an energy sheet pile is placed with sand on one side and water on the other, as shown in Figure 2.3. Water flows on both sides parallel to the sheet pile. Each test lasted for 8 hours. The initial temperature of the water and sand surrounding the sheet pile was 12 - 13°C and the heat carrier fluid was 3°C.

In the test, the influence of the flow velocity of the open water, flow rate of the heat carrier fluid through the activation loops and the groundwater flow velocity was investigated. Moreover, the optimal configuration of the activation loops was assessed, testing pipes mounted in both series and parallel. A limited influence of the groundwater flow was established thus the velocity was set at 2.0 m/d. The flow rate of the heat carrier fluid proved to achieve ideal convective heat transport with turbulent flow conditions. Return rates of 430 W/m with and 285 W/m without open water flow where measured. These differences prove the large influence of the water flow along the sheet piles on the return energy. With velocities up to 0.3 m/s, turbulent flow was achieved near the sheet piles immediately regenerating the temperature of the water. The results are displayed in Figure 2.4a.

Similar to the previously discussed papers, the efficiency of the activation loops in series was deemed to be much higher than when attached parallel. The series connection almost doubled the in- and outlet temperature difference, resulting in the heat pump at the end of the system working much more efficient. The authors recommend to connect individual U-loops in series.

Figure 2.4b show the results of the same experiment but with activation panels. These add-ons are attached to the water side of the sheet piles thus are in direct contact with the water. Considerably high extraction rates have been achieved even without open water flow. This can be explained by the fact that the panel is surrounded by water creating a large area to extract heat from and the constant supply of 'fresh' water unaffected by the heat extraction.

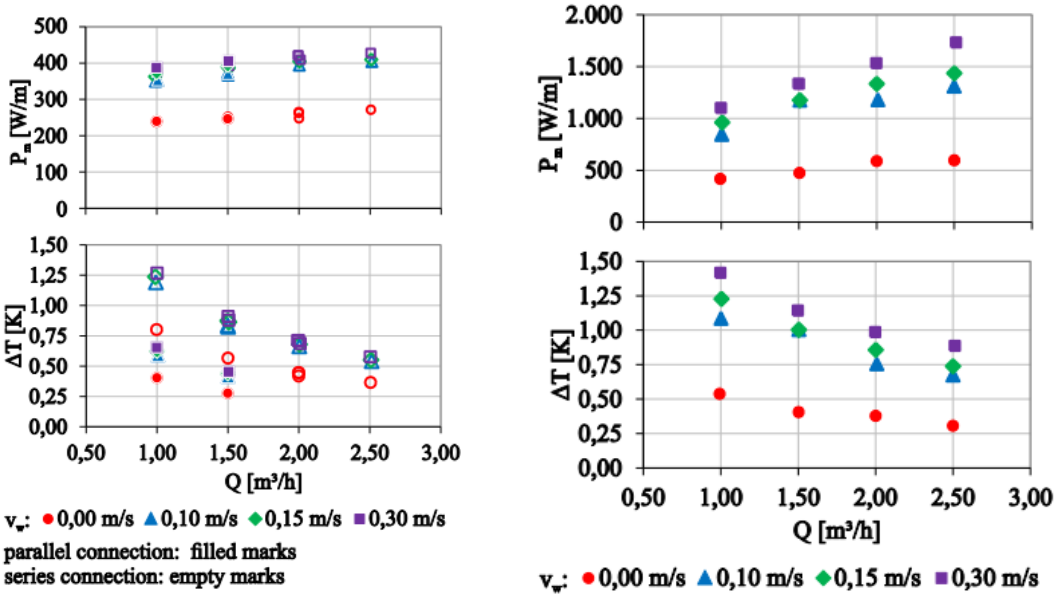

(a) Results for the activation loops

(b) Results for the activation panel

Figure 2.4: The heat extraction rate P_m and temperature difference ΔT connection in parallel and series for different flow velocities of the water v_w related to various to volumetric flows Q through the loops by Ziegler et al. (2019)

The test set-up validation is very comparable to Kürten et al. (2014) and Kürten et al. (2015). Using semi-analytical models based on SHEMAT, the heat transport processes in the loops is coupled with the finite element model. Furthermore, a fully discretized model was defined in COMSOL which was used to validate the SHEMAT-suite semi-analytical approach. The numerically calculated outcomes showed a good agreement with the large scale test results.

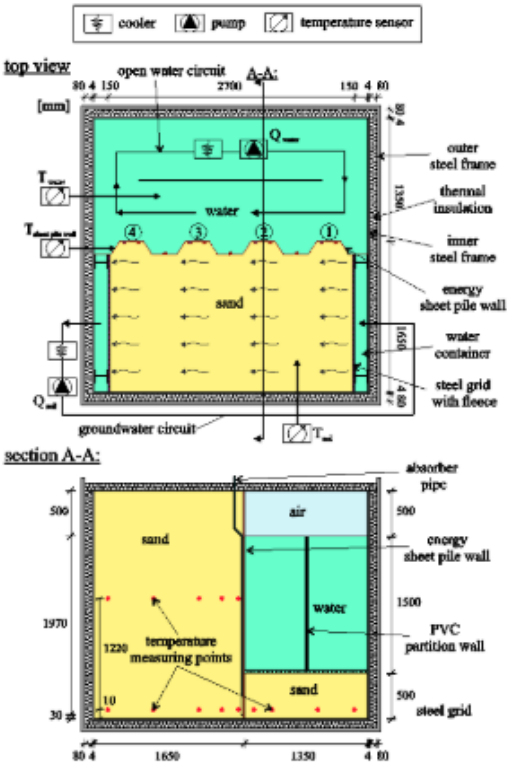

Figure 2.3: Test set-up by Ziegler et al. (2019)

2.2 Problem Statement

The knowledge gaps identified in the problem analysis are as follows:

1. there is a lack of knowledge about the long-term response of the subsurface on temperature change.
2. there is a lack of knowledge of the response of the sheet pile wall to the temperature change.
3. there is a lack of knowledge about the necessity to do a full thermal calculation to determine the structural safety of the sheet pile wall.
4. there is a lack of knowledge about how to implement the changes in temperature of the subsurface in a technical sheet pile wall design.
5. there is a lack of knowledge about the way the energy sheet piles have to be operated to achieve the best energy yield;

Chapter 3

Objective and Methodology

This chapter contains the description of the objective of this thesis and the methodology to reach this goal. The first section holds the objective, scope, main question and research questions. The second section holds the methodology and report outline in which the steps that are taken to answer the research questions and in which chapter this is done are described.

3.1 Objective and Research Questions

As a result of the previously conducted research and the defined knowledge gaps, the objective and scope of this thesis are specified in this section. Based on these, the main question and research questions are determined. The research questions serve as guideline to solving the main question.

Objective

As already mentioned in Chapter 1, the energy sheet pile technology has much potential to reduce the carbon footprint of households. However, as concluded in Chapter 2, long-term and large-scale test have not been performed yet, making it difficult to predict the behaviour of the subsurface and sheet pile. The thermal activation of the sheet pile wall cannot compromise the primary function of the wall, which is ensuring the stability of the quay. Therefore, based on the monitored data from the field test and two finite element models, the objective for this thesis is to investigate the behaviour of the sheet pile wall under thermal loading and assess if it is safe to thermally activate the sheet pile wall.

Scope

This thesis focusses solely on the technical aspects of an energy sheet pile wall. The financial feasibility is not investigated. Moreover, the energy yield is left out of consideration. With the focus on structural safety, a constant load in the form of a low and fixed temperature is imposed on the sheet pile wall to investigate the behaviour under such conditions. A more realistic approach would be te use a heat flux changing over time.

Main question

The main question has been defined as follows:

Can the structural safety of a sheet pile quay wall be guaranteed when the sheet pile is thermally activated?

Research questions

Based on the problem analysis, objective and the identified knowledge gaps, the following research questions are drawn up:

1. What is the magnitude of temperature changes of the subsurface as a result of the thermal activation of the energy sheet pile?
2. What is the response of the sheet pile wall to the temperature change?
3. Can an industry standard finite element method program capture the long-term thermal and mechanical behaviour of an energy sheet pile quay and the subsurface?

Research questions 1 and 2 arise from need to understand the influence the thermal activation has on the sheet pile wall and the surroundings. Without this understanding, the subsurface cannot be accurately modelled and the output from the calculation not assessed. This applies to the third research question. With the two models, which are validated using the field test data, the behaviour of the sheet pile wall and subsurface can be predicted. This leads to the main question which is to determine if the sheet pile wall can be thermally activated while the stability of the quay is ensured.

3.2 Methodology and Report Outline

As is defined in the problem statement, the long-term effects of a thermally activated sheet pile on the sheet pile and adjacent subsurface are not known making it difficult to predict the aforementioned behaviour. In the effort of seeking clarification on this matter, a field test is conducted in which extensive measurements are conducted to capture both the thermal and mechanical reaction.

To be able to answer the research questions involving modelling, two different programs are needed: COMSOL Multiphysics and PLAXIS 2D. The choice for two different FEM programs is due to the characteristics of the programs. COMSOL is good in modelling heat conduction but less useful for a geotechnical assessment. PLAXIS is specialized in modelling soil behaviour but less so in heat conduction calculations. Question 3 involves the ability to correctly predict the behaviour of the soil and sheet pile using FEM software. The data acquired in the field test is used to validate the models providing an answer to this question. Based on the analysis of the field test data and the computations performed with both models, the main research questions is answered.

The following table shows which steps serve to answer which research question:

Table 3.1: Methodological process to solve the research questions.

Research question	Step	Chapter
1, 2	1	4
3	2, 3, 4	5, 6, 7

Step 1: Interpret the Field Test Measurement Data

To understand the large-scale and long-term influence of the thermal activation of the sheet pile, a full-scale field test is conducted near Zweth. In this test, inclino measurements are performed to measure the deformation of the sheet pile and thermistor string measurements to capture the temperature change of the subsurface. The inclinometers are mounted on the sheet pile wall and thermistor strings are placed in its vicinity. By interpretation these measurements, research questions 1 and 2 are answered.

Step 2: Investigate heat transfer physics packages and develop a Heat Conduction Model

COMSOL multiphysics provides several heat transfer packages which are applicable to a range of materials. To investigate the differences and determine the best applicable packages, an investigation is carried out. In this model, only the heat conduction is analysed - the mechanical component is ignored. Based on this investigation, a heat conduction model is developed which is used to model the temperature change in the subsurface resulting from external influences (e.g. water and air temperature) and heat extraction. The temperature of the energy sheet pile can be derived from this program, which is then used in the analysis in PLAXIS. This step is part of the endeavour to answer research questions 3.

Step 3: Investigate a Thermo-Hydro-Mechanical Analysis and Develop Geotechnical Stability Model

Chapter 6 contains the description of the construction of a geotechnical deformation assessment model in PLAXIS and is the third step in Figure 3.1. A Thermo-Hydro-Mechanical analysis is used to model the deformation and temperature change of the energy sheet pile. As with the heat conduction model, an investigation was first carried out into the operation of the software. A geotechnical stability model has been developed based on the findings. In step 2 is the temperature of the energy sheet pile determined. This temperature is imposed on the sheet pile in PLAXIS. This step is part of the endeavour to answer research questions 3.

Step 4: Validation of the Models

This thesis covers three measuring phases, two of which last for a month and one for 2 weeks; and all with a different activated activation loop scheme. Each phase results in two datasets, one with heat measurements and the other one with displacements of the sheet pile wall. The data acquired by the thermistor string is used to validate the heat conduction model. The displacements resulting from the geotechnical analysis in PLAXIS is validated with the measurements from the inclinometers. To be clear, two different FEM models will be validated with field test data. The aforementioned process of validating the heat conduction model and the geotechnical analysis of the quay wall is conducted for each phase. Referring back to Figure 3.1, this is done in step 1. At the end of this step are research question 3 answered with the help of the validated models.

As support in explaining the methodology, Figure 3.1 shows four steps. Each of the steps corresponds to a chapter in this report which is mentioned underneath the step number.

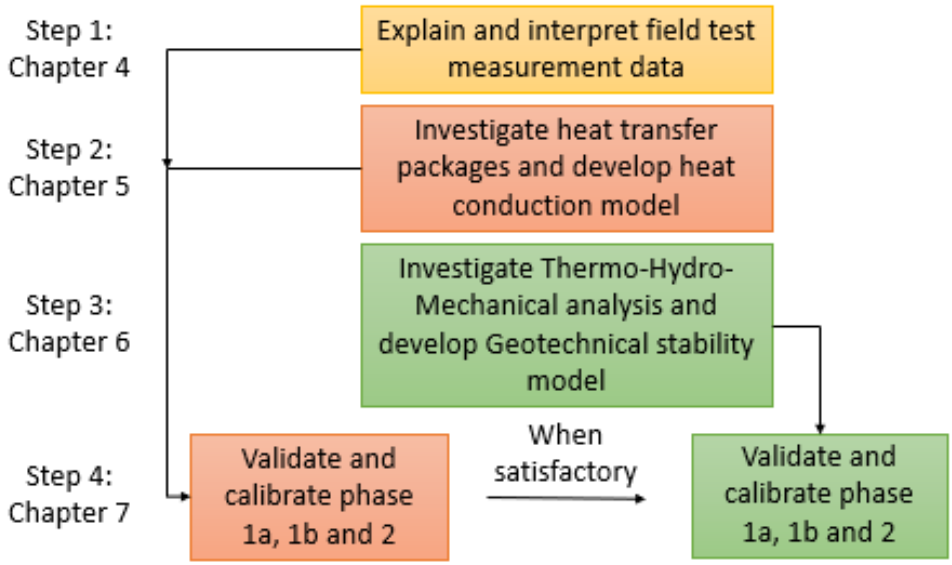

Figure 3.1: The visual representation of the methodology

Chapter 4

Explanation of the Field Test

This chapter contains the site soil specifications, the explanation of the field test and monitoring scheme; and the interpretation of the acquired monitoring data. The temperature changes of the soil are investigated as well as the deformation of the sheet pile - which is methodological step 1. Based on this analysis, the first and second research question is answered: 'What is the magnitude of temperature changes of the subsurface as a result of the thermal activation of the energy sheet pile' and 'What is the response of the sheet pile wall to the temperature change?', respectively. Understanding the effects of the thermal activation results in a better model and assessment of the computations of the model.

4.1 General Information of the Field Test

On June 16th 2020, a field installation was placed at the testing site along the Delftsche Schie near the village of Zweth in the municipality of Rotterdam in the province of Zuid-Holland in the Netherlands. This installation is part of an endeavour to make the Dutch waterways CO_2 neutral and serves two purposes: 1) to prove sheet piles can be thermally activated without compromising their water retaining function and 2) investigate the energy yield from the energy sheet piles. The sheet pile wall, with dimensions of approximately 7 metres wide and 15.7 metres deep, was designed by a consortium consisting of Delft University of Technology, Eindhoven University of Technology, CRUX Engineering B.V., Gooimeer B.V. and Groep Duurzame Energy.

4.2 Soil Profile at the Testing Site

The area in which the field test is executed is deltaic. After the formation of the Holocene sand layer, subsequent relocating river courses prior to the reclamation of the area resulted in a subsurface with clays, silts and peats alternating. As part of the human endeavour to dewater the bogs located between Delft and Rotterdam, the Delftsche Schie was (at least partly) dug to make it fit for agriculture. The dewatering resulted in a substantial subsidence of the land around the waterway raising the need for flood defences. The quay is supported by a sheet pile wall and a small dike protects the hinterland.

A soil profile of the location is composed, shown in Figure 4.1. The Holocene sand layer ends at a depth of NAP -17 m. Above that lies 7.5 metres of clay up until NAP -9.5 metre. Three relatively thin layers lie above that: clay, weakly silty; clay, strongly sandy; and clay, weakly silty again with thicknesses of 1.5 metre, 2.5 metre and 1 metre thickness. Starting at a depth of NAP -5.5 metres, the soil consists of peat up to a height of NAP -1.75 metres. The top layer, ending at NAP +0.2 metre, is a man made sand layer which is used for the construction of the dike.

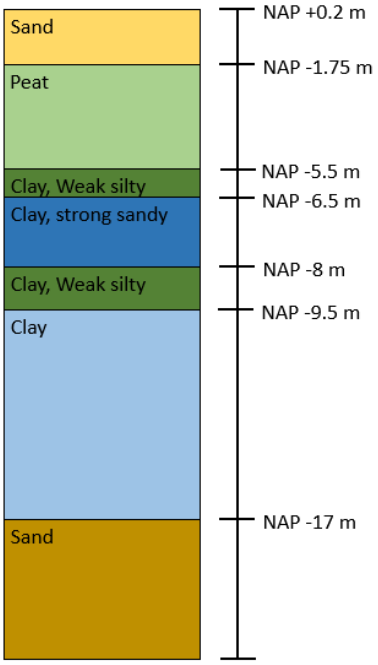

Figure 4.1: The soil profile at the testing location.

4.3 How the Energy Sheet Pile Works

By thermally activating the sheet piles, it starts to act as a heat exchanger. This is achieved by pumping a fluid through a set of pipes welded on the soil side to the sheet piles resulting in the possibility to extract warmth or coolness from the canal water and subsurface. These pipes are connected to a heat pump which then converges the temperature to make it fit for domestic use. A step-by-step explanation is shown in Figure 4.2. The numbers correspond to the following enumeration:

1. A regular Z-shaped sheet pile;
2. A U-shaped pipe is attached to the diagonal side of the sheet pile on the soil side. These pipes are welded on to the sheet pile before installation;
3. A U-shaped pipe is attached to every other sheet pile;
4. The pipes are attached to each other by means of a connection piece. The connection is made after installation of the sheet piles.
5. A U-shaped pipe (blue) is attached to unused sheet piles in between;
6. The U-shaped pipes (blue) are connected to each other. Depicted are the entrance and exit of the activation loops as well. The entrance and exit pipes are attached to a main entrance/exit pipe which are connected to the heat pump. With the help of valves can the loops be turn on or off - making it possible to operate the loops independently from each other.

Two set-ups are tested in the field test, one where the depth of the U-shaped pipes runs to the bottom of the canal and one where the pipes run to the bottom of the sheet piles. Two times two loops, so twice the loops shown in Figure 4.2.6, are placed in the quay of the Delftsche Schie. Two loops run to the bottom of the canal and two run to the bottom of the sheet pile. Figure 4.4 shows this. Figure 4.5 shows a picture of the in-situ situation.

Another scheme tested is the activation panel. Shown in Figure 4.3, this panel is attached after installation of the sheet piles whereas the pipe system is welded on the sheet piles before placing them. This has the advantage that they can be placed on existing sheet piles. The panels are mounted on the water side of the sheet piles resulting in the water flowing directly past them. The panels have approximately the same length as the depth of the canal (3 metre).

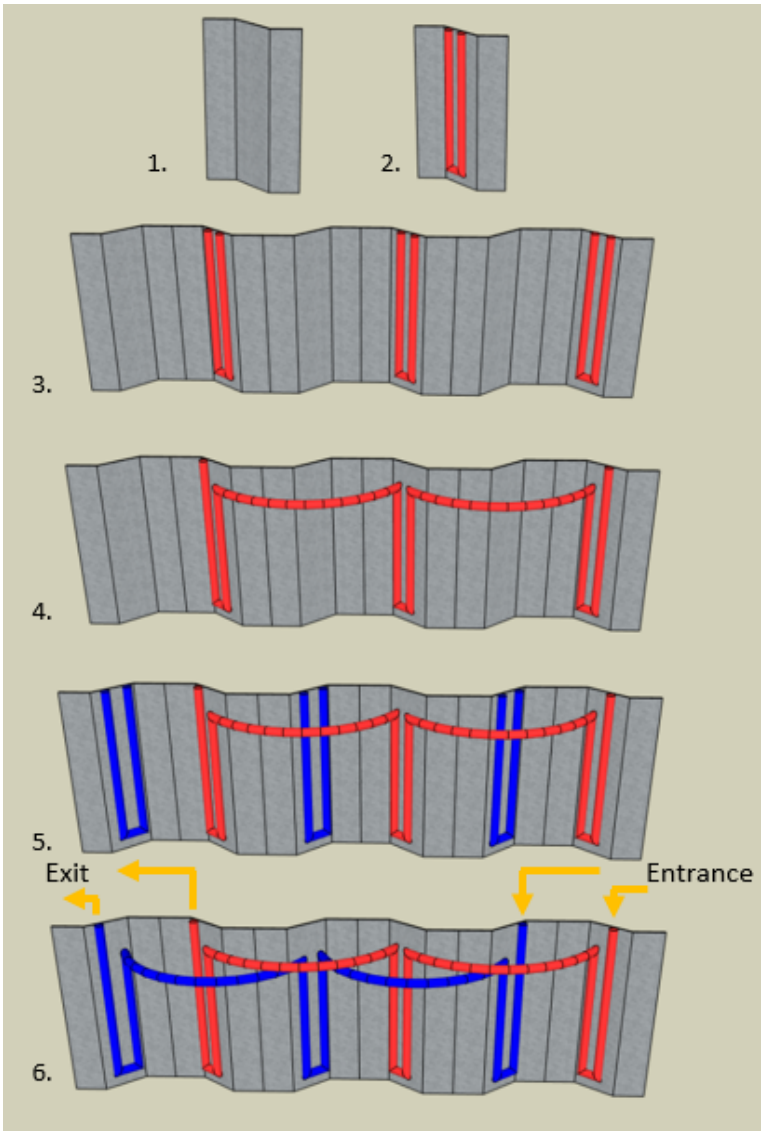

Figure 4.2: Roadmap of the activation loops attached to the sheet pile.

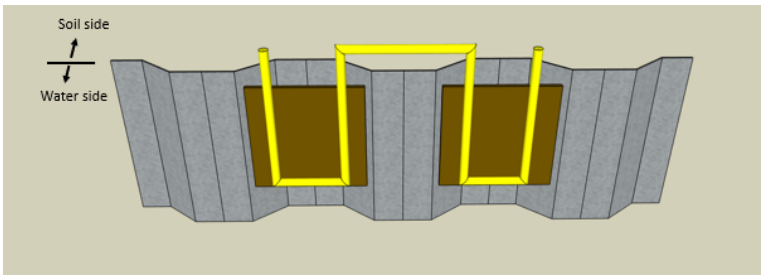

Figure 4.3: The activation panel from the canal point of view.

4.4 Phasing of the Field Test

Not all the loops are used at the same time. To test different schemes, different loops will be tested in different phases. These are as follows:

- Phase 1: Single side activation of the sheet piles for both shallow and deep systems (the loops in blue and purple in Figure 4.4);

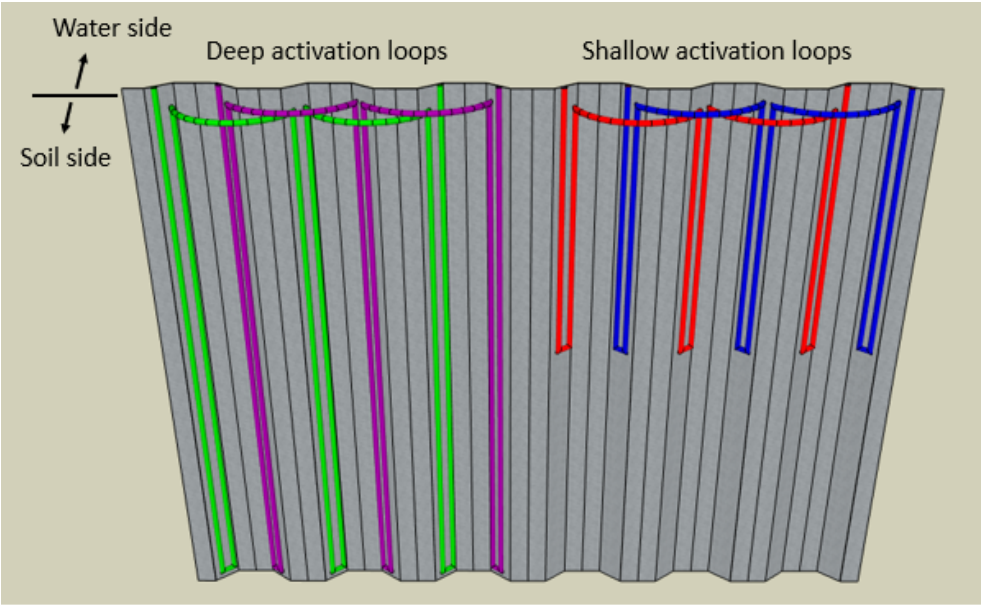

Figure 4.4: Overview of the set-up with the shallow activation on the right hand side and the deep activation on the left hand side.

- Phase 2: Double side activation of the sheet piles for both shallow and deep systems (all activation loops in figure 4.4);
- Phase 3: A choice is made between shallow or deep activation based on the previously collected data. Activation panels are placed on the deep activation side on the water side.

In total, the pilot consists of four phases. The first three last each one month and the fourth 21 months. However, this thesis only covers the analysis and assessment of the first three.

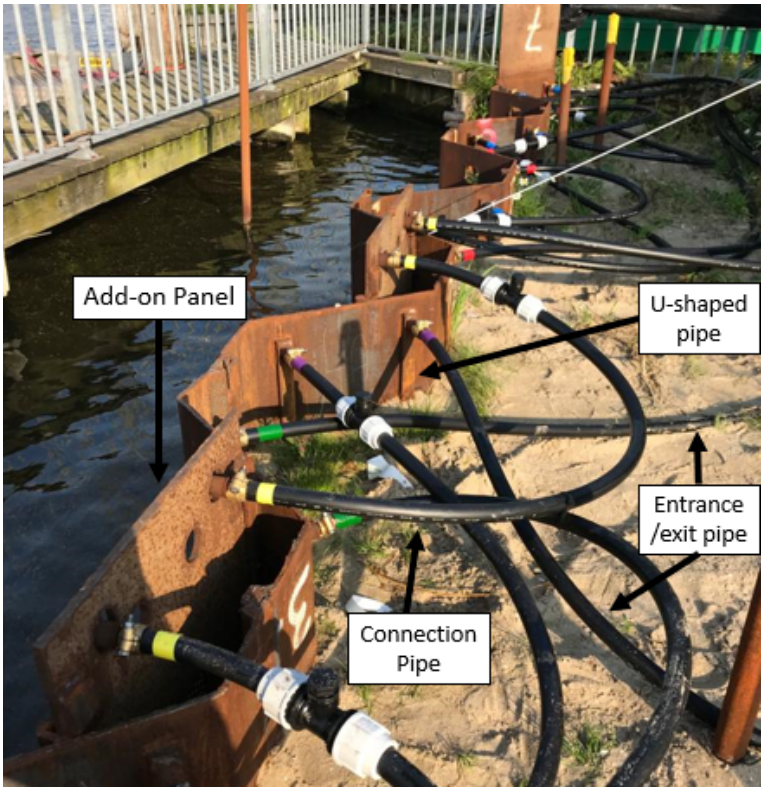

Figure 4.5: An image of the setup.

4.5 Monitoring Plan

To be able to assess the geotechnical and thermodynamic response; and the change in temperature of the soil, several tilt-meters and thermistor strings are placed. The tilt-metrers are mounted on the sheet piles to measure the response of the sheet piles. Temperature change is measured using thermistor strings placed in the direct vicinity of the sheet pile as well as further way, both on the soil and water side. Figure 4.6 shows the locations of the measurement devices on the sheet piles and in its vicinity including the abbreviations of the thermistor location names. Table 4.1 contains the explanation of the abbreviations.

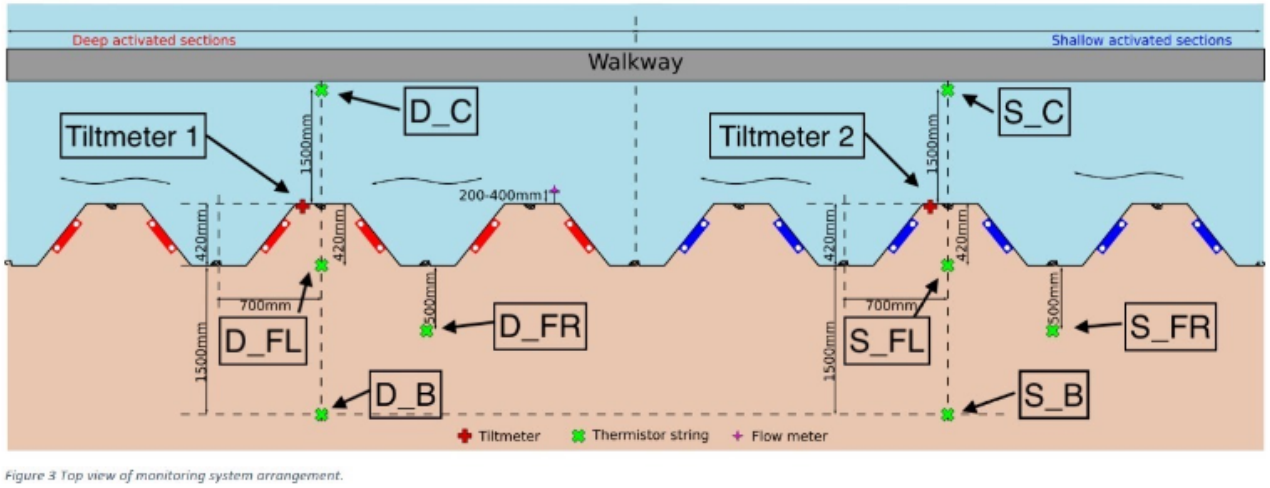

Figure 4.6: Schematic overview of the locations of the measurement devices (De Jong, 2020).

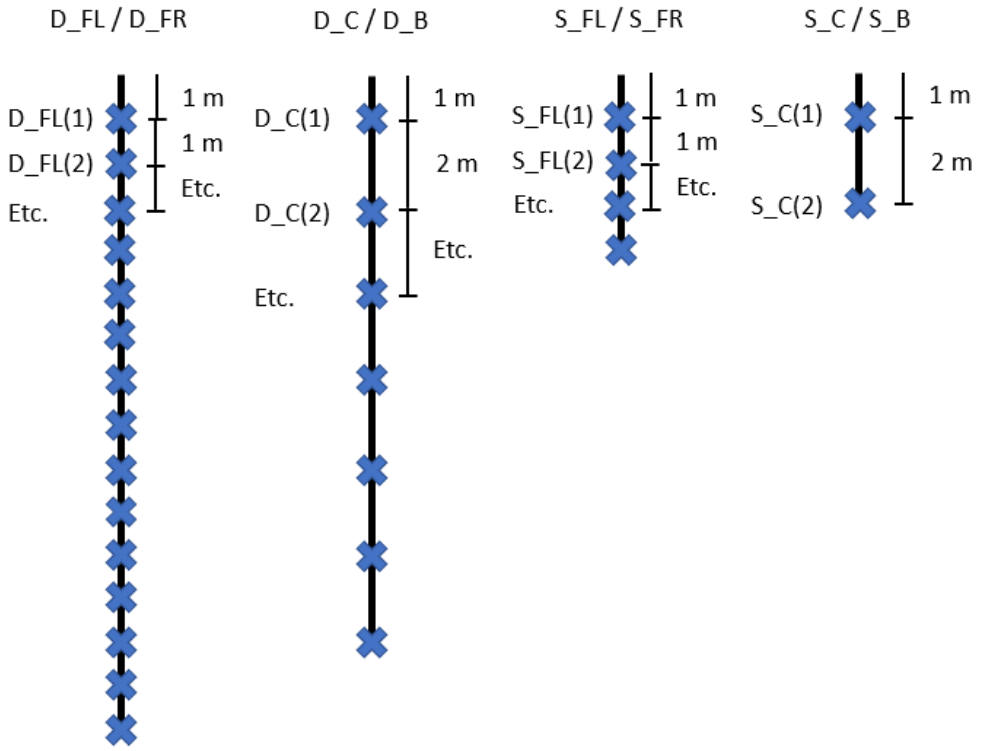

Figure 4.7: The thermistor strings used in the field test.

Table 4.1: Abbreviations of the thermistor location names.

Abbreviation	Full name
D_C	Deep canal
D_FL	Deep front left
D_FR	Deep front right
D_B	Deep back
S_C	Shallow canal
S_FL	Shallow front left
S_FR	Shallow front right
S_B	Shallow back

4.6 Analysis of the thermistor string data

This section contains the conclusion of the analysis of the data acquired from the field test for each phase. The the full analysis and graphs can be found in Appendix A. The locations of the thermistor strings as well as the abbreviations and information about the thermistor strings can be found in Figures 4.6 and 4.7; and Table 4.1.

Phase 1a: Single Shallow Side Activation

Figure 4.8 contains the temperature change of the subsurface in the shallow section of the test site. As a result of malfunctioning equipment, the sensors of S_FL at 3 and 4 metres depth have not registered any temperatures. Moreover, thermistor string D_B did not monitor any data. The temperatures picked up by the thermistor strings are very similar. At the start of phase 1, on October 26, the temperatures at both locations are 12 °C at the surface and 15 °C at 4 metres depth. The soil cooled uniformly down by approximately 4 °C. This is due to a combination dropping water and air temperatures; and the thermal activation of the shallow section.

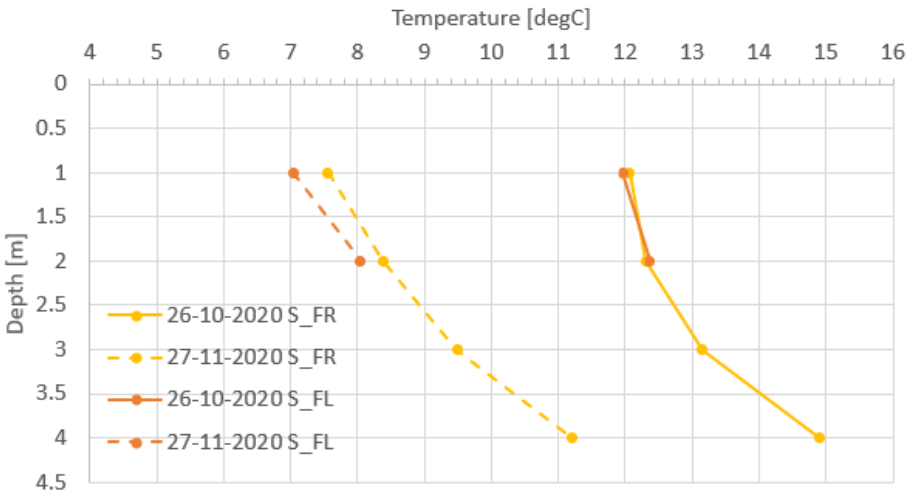

Figure 4.8: Temperature versus depth of the thermistor strings in the shallow section at the start and end of phase 1a.

Figure 4.9 contains the temperature changes in the deep (inactivated) section. All 3 datasets show a decrease in temperature in the upper 5 metres while below the temperature increases a little. The upper metres are influenced by cooling down air en water temperatures. The lower metres warm up most likely as a result of the high temperatures at 4 - 6 metres depth. This might be as a result of the temperatures migrating down through the soil but another possibility is that the steel pipes in which the thermistors are placed influence the temperature due to its high conductivity and low heat capacity.

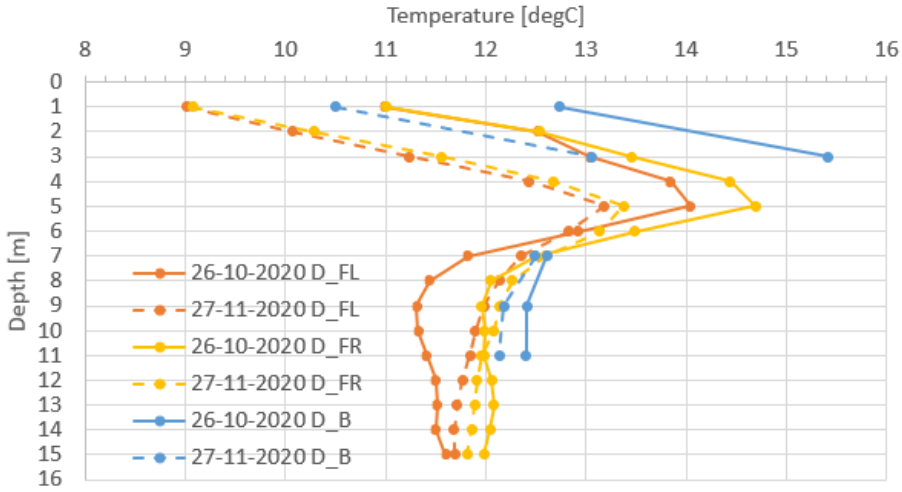

Figure 4.9: Temperature versus depth of the thermistor strings in the deep section at the start and end of phase 1a.

Phase 1b: Single Deep Side Activation

Figure 4.10 shows the temperature changes in the soil the deep section when the single deep loop is activated. Thermistor string deep front left shows a temperature decrease between 2 and 3 °C. 0.5 metres away from the sheet pile lies thermistor string deep front right. The temperature decrease monitored by this string is smaller by about 2 °C. Thermistor string deep back shows barely any temperature change. This thermistor is 1.5 metres away from the sheet pile.

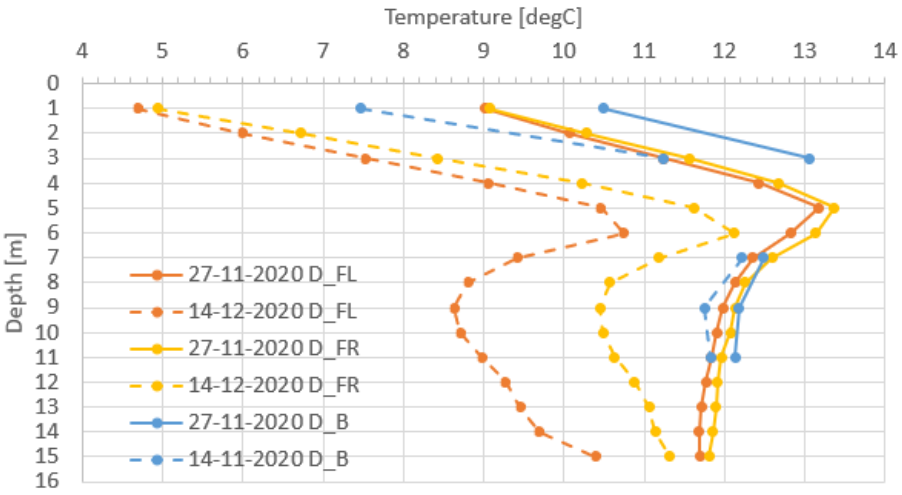

Figure 4.10: Temperature versus depth of the thermistor strings in the deep section at the start and end of phase 1b.

Figure 4.11 contains the temperature changes in the shallow section. The shallow loop was activated at the start yet the flow rate decreased linearly and became 0 l/min at December 7th. Therefore, the extracted temperature decrease is less but as a result of decrease water and air temperatures, this is not visible in the graph. The temperature sensed by the shallow front left thermistor string at the start of the phase is 0.5 °C lower than the temperature at shallow front right. Both temperatures decrease by approximately 2.5 °C in the top two metres and 1 °C below. This decrease is besides the heat extraction due to the changing water and air temperature.

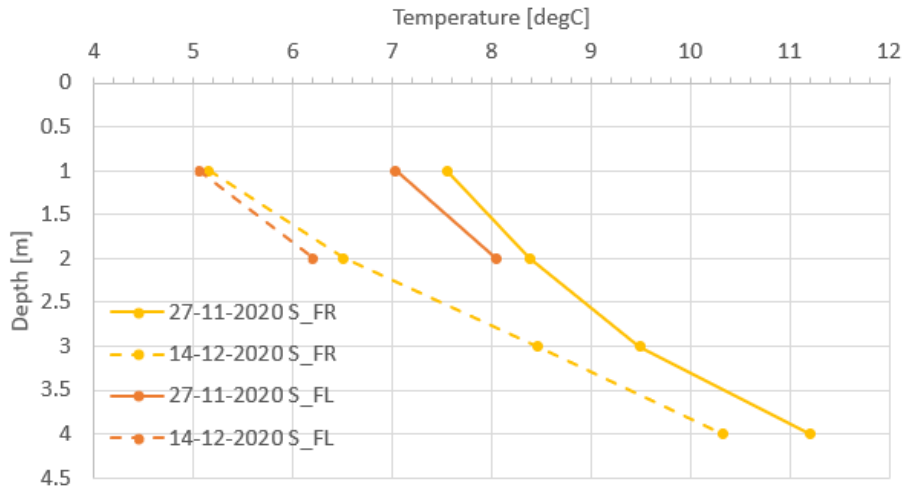

Figure 4.11: Temperature versus depth of the thermistor strings in the shallow section at the start and end of phase 1b.

Phase 2: Double Side Activation

Figure 4.12 shows the temperature changes in the subsurface in phase 2 in the deep section. Thermistor string deep front left monitored a temperature change of approximately 2 degrees below 4 metres and 1 °C above. Thermistor string deep front right, 0.5 metre away from the sheet pile, monitored the same relative temperature change. The thermistor string 1.5 metres from the sheet pile monitored a temperature decrease of approximately 1.5 degrees.

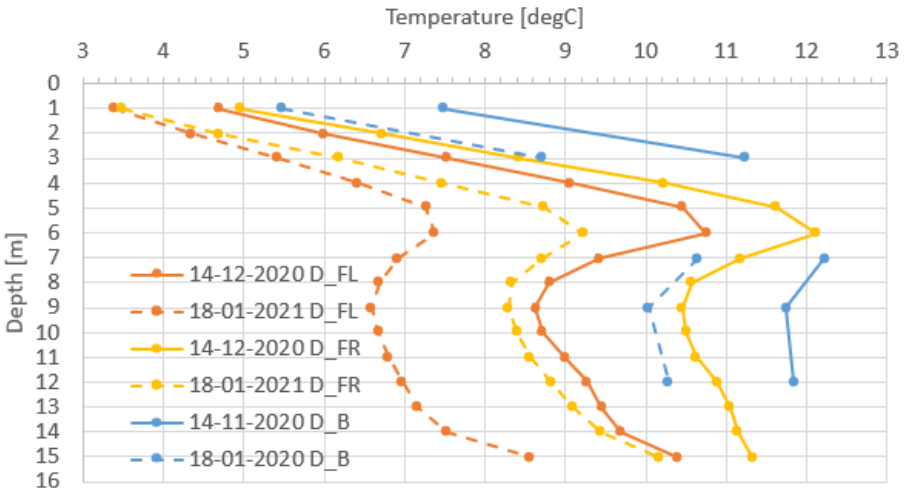

Figure 4.12: Temperature versus depth of the thermistor strings in the deep section at the start and end of phase 2.

Figure 4.13 shows the temperature change in the shallow section. Both thermistor string experienced the same temperature decrease of approximately 1 - 1.5 °C.

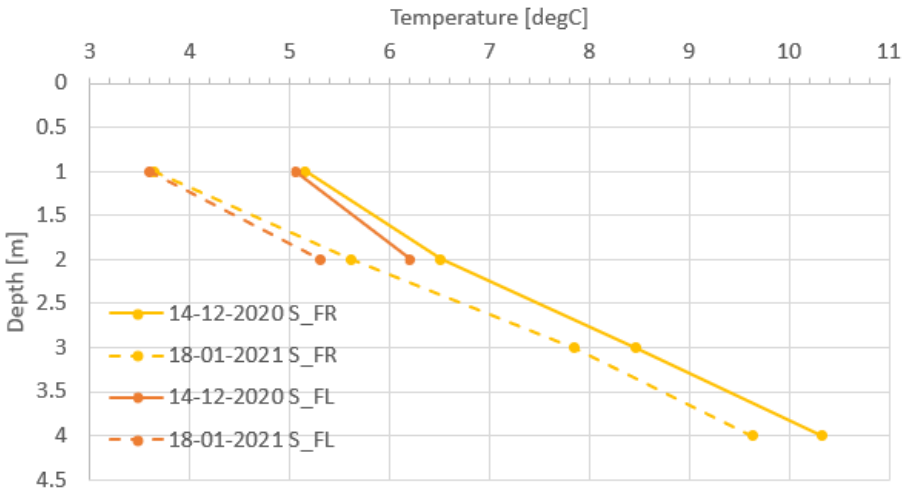

Figure 4.13: Temperature versus depth of the thermistor strings in the shallow section at the start and end of phase 2.

4.7 Analysis of the Inclinometer data

This section contains the analysis of the inclinometer data. Not all data is discussed in this section. The data not applicable to the activated section is added in Appendix A.

4.7.1 Phase 1a

Figure 4.14 shows the deformation of the upper 4 metres of the sheet pile. The measurements go 10 metres deep but, as the activation depth is 3 metres, this section experiences the largest impact. Indeed, the difference in deformation at 2 and 3 metres depth is already small and does continuously decrease. In the first few days of the phase, the heat pump turned on and off twice and a backfill of approximately 25 centimetres of sand was done. This results in a in- and decrease of the deformation in the first week. Afterwards, the deformations are less abrupt, increasing by approximately 0.5 millimetre to 3.25 millimetre before decreasing again. This might occur due to the following reasons: an in-situ measurement error, warm/cold days (radiation levels) or fluctuating canal/groundwater levels. Figure 4.15 shows the air temperature during phase 1a and Figure 4.16 the precipitation. Besides the influence from the sand backfill, the temperatures in late November/ early December were considerably warmer than the rest of the phase. At this point in time, a large amount of rain fell resulting in an increased saturation of the soil in the quay. This time periods overlaps with the large deformation, thereby making these phenomena possible causes of the increase and decrease of the distortion. Moreover, from November 9 on the air temperature increases by a few degrees. A few days later, an average precipitation of 3 to 4 millimetre fell every few days. Around this time the deformation of the sheet pile increases as well. At the end of the phase, both the temperature and the deformation decrease. These observations suggest the oscillations in deformation result from the air temperature.

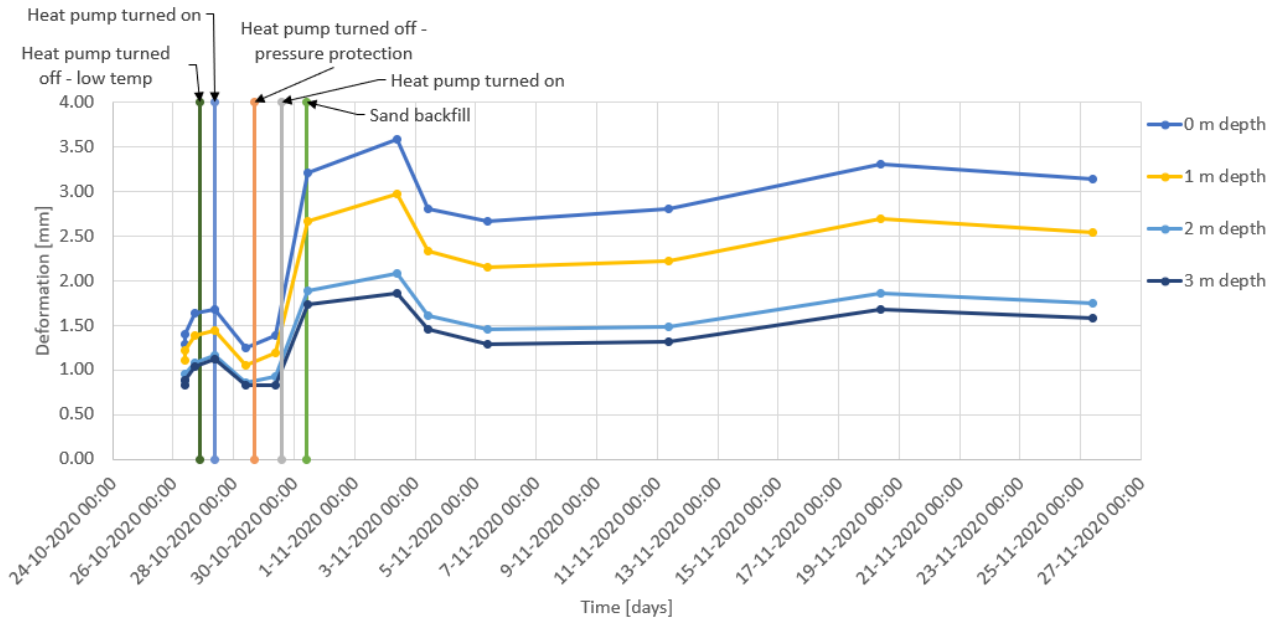

Figure 4.14: Deformation versus depth of the sheet pile wall in the shallow section in phase 1a.

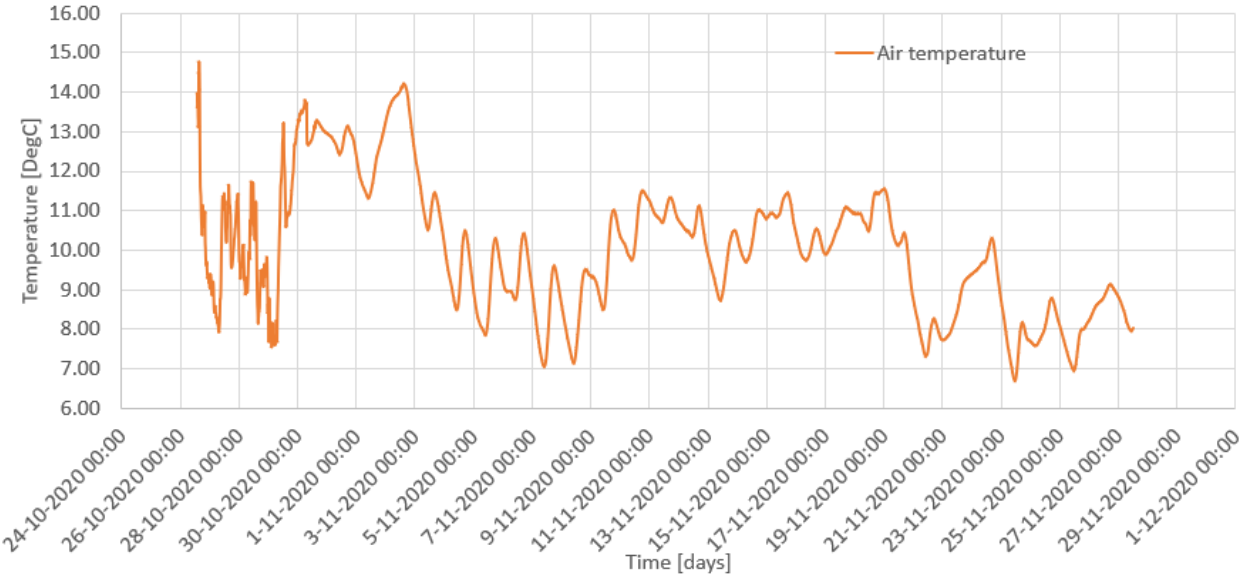

Figure 4.15: The air temperature in phase 1a.

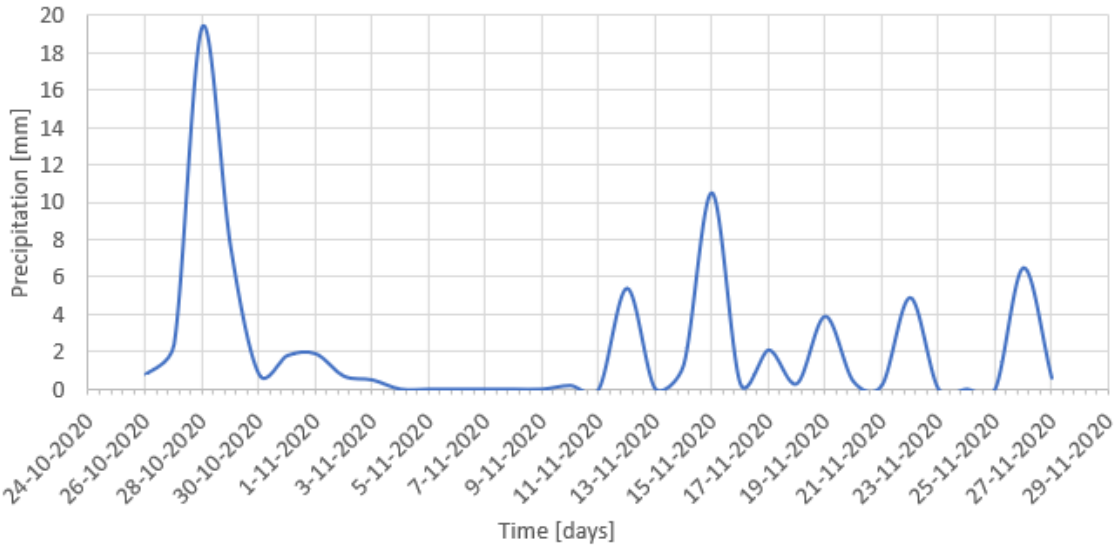

Figure 4.16: The daily precipitation in phase 1a.

Figure 4.17 shows the deformation of the sheet pile in the deep section in phase 1a. The shape of the graph is the same but the deformations are larger. The maximum deformation is approximately 6.5 millimetre after which this decreases to approximately 4 millimetre.

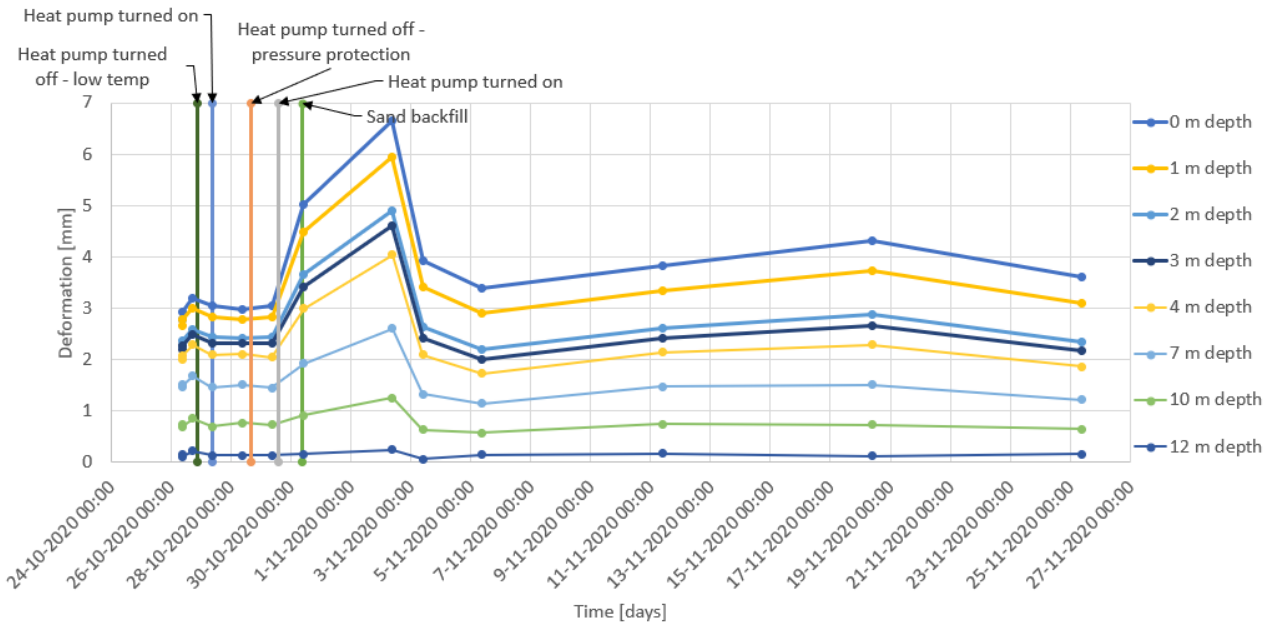

Figure 4.17: Deformation versus depth of the sheet pile wall in the deep section in phase 1a.

4.7.2 Phase 1b

Figure 4.18 shows displacement of the sheet pile in the deep section during the single side deep activation. As the whole length of the sheet pile is activated, the deformation at the first four metres is shown followed by the deformation every three metres. At the second measurement, the deformation into the canal has increased by almost 3 millimetres to 6 millimetre. The measurements following capture a small decrease in deforming which is followed by an increase. Figure 4.19 shows the air temperature in phase 1b. The trend of the two graphs is similar at the end of the phase, the deformation measurement at December 10 is smaller than the measurement prior. When the temperatures rise, from December 11 on, the deformation increases as well. The trend of the first two inclinometer measurements does not correspond to the temperature change. Figure 4.20 shows the precipitation in phase 1b. At the end of November a large amount of rain fell. This coincides with the increased deformation measured on December 3rd.

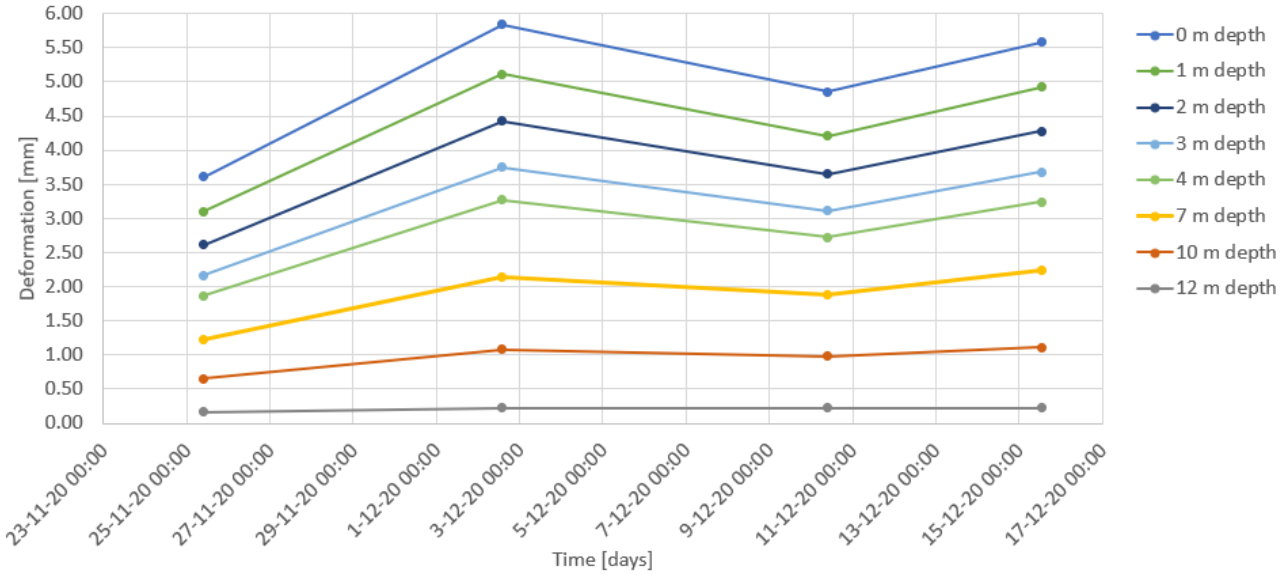

Figure 4.18: Deformation versus depth of the sheet pile wall in the deep section in phase 1b.

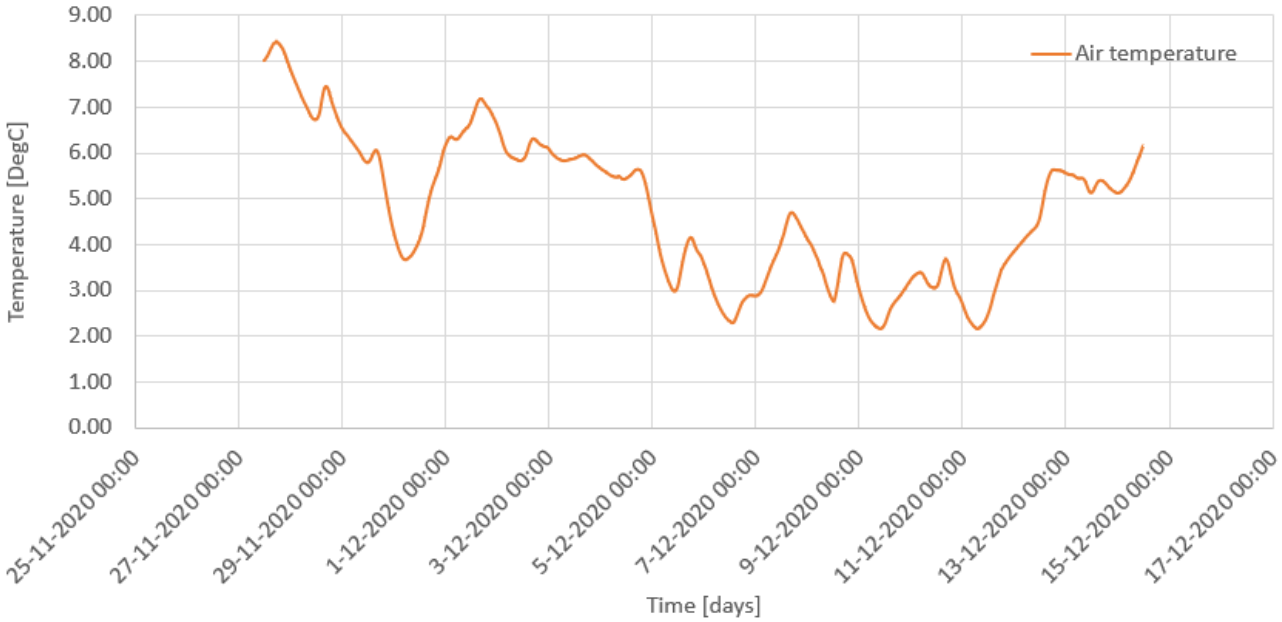

Figure 4.19: The air temperature in phase 1b.

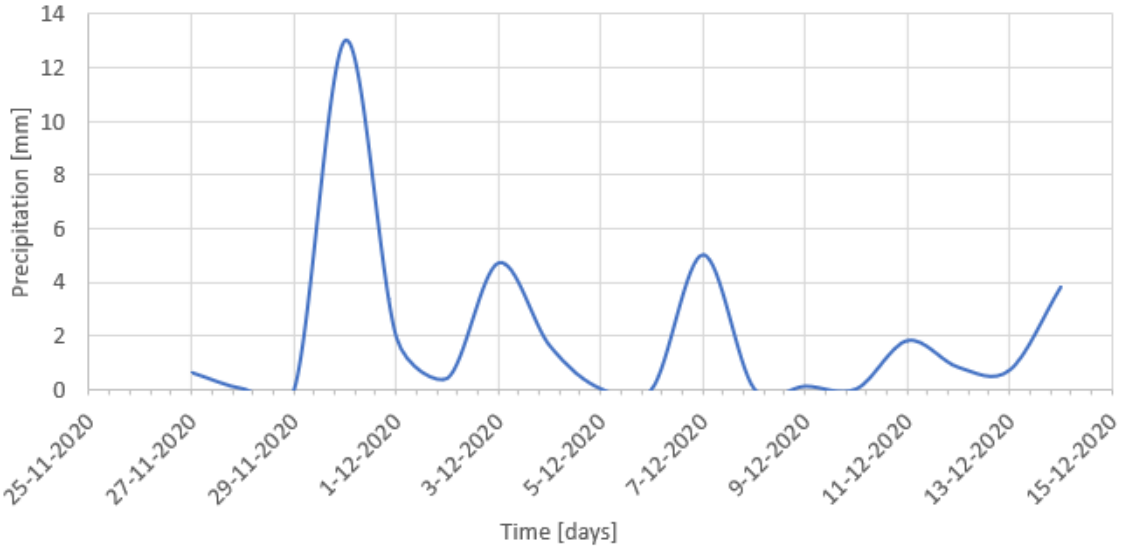

Figure 4.20: The daily precipitation in phase 1b.

Figure 4.21 shows the deformation of the sheet pile wall on the shallow (inactive) side. The maximum deformation is approximately 3 millimetre which increased slightly in the measurement performed on December 15th.

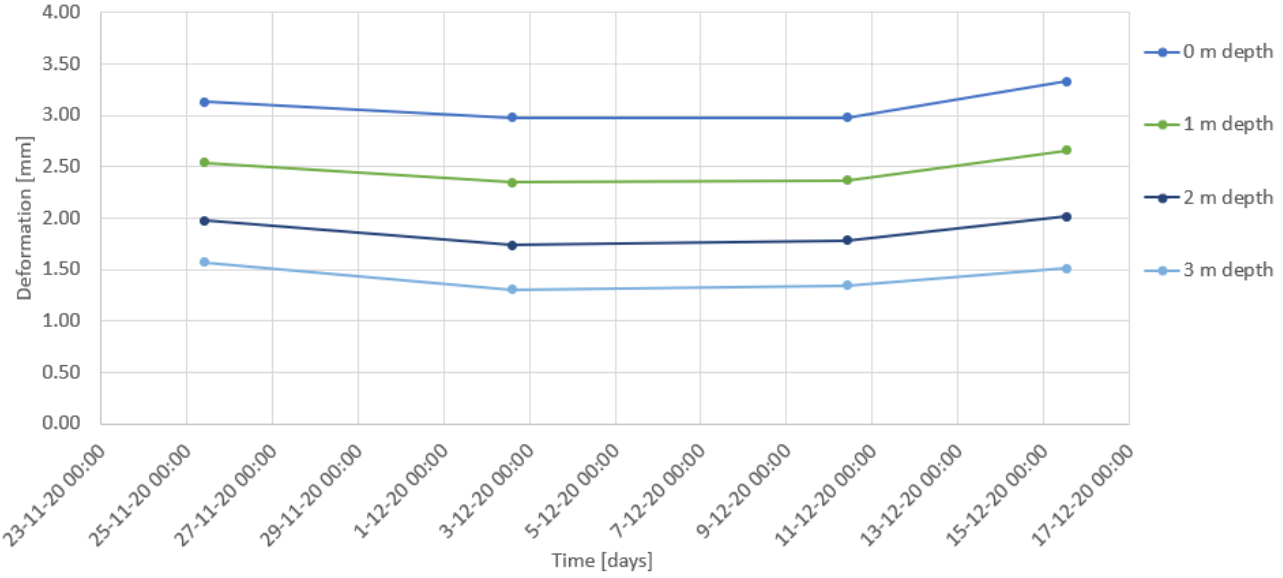

Figure 4.21: Deformation versus depth of the sheet pile wall in the shallow section in phase 1b.

4.7.3 Phase 2

The deformation visualized in Figure 4.22 are less constant than in the phase prior. In phase 2, two deep loops are activated. The deformation in this phase shows a variation between 4 and 6 millimetres. Again, the fluctuations in deformation can be correlated to the varying air temperature an precipitation, shown in Figure 4.23 and 4.24.

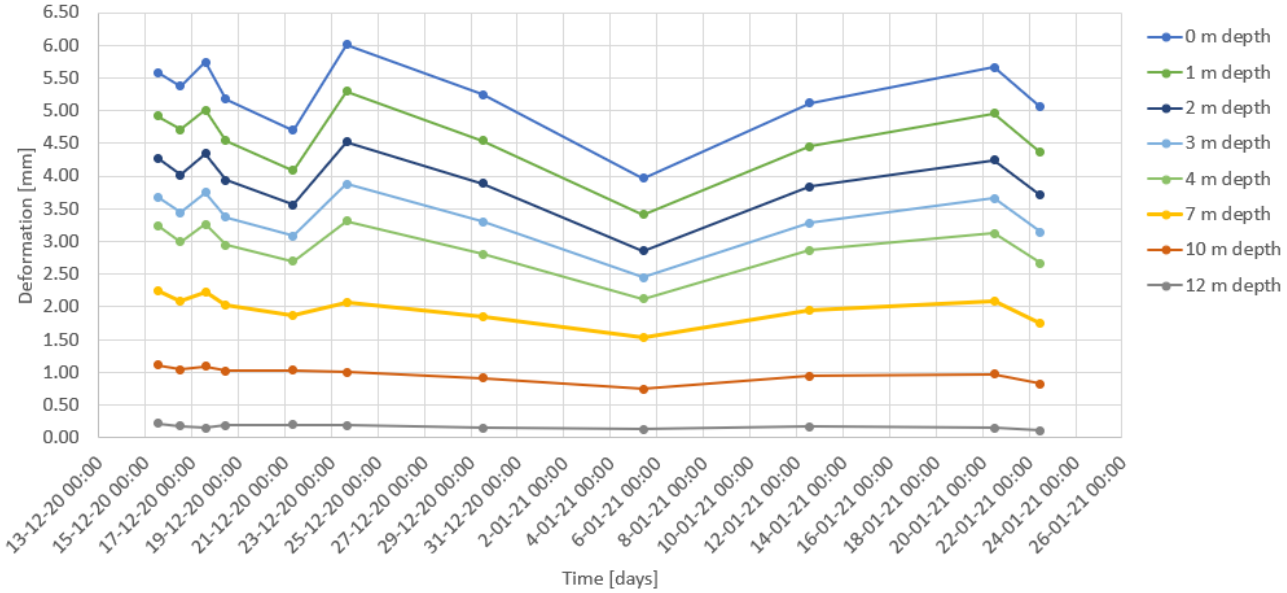

Figure 4.22: Deformation versus depth of the sheet pile wall in the deep section in phase 2.

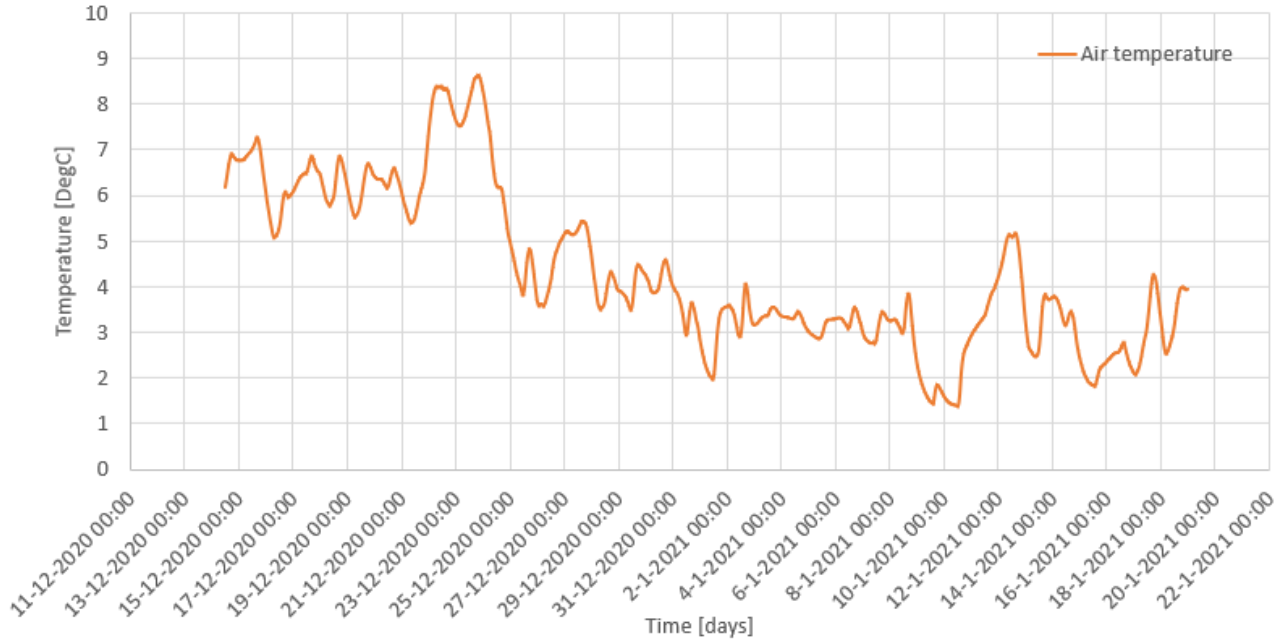

Figure 4.23: The air temperature in phase 2.

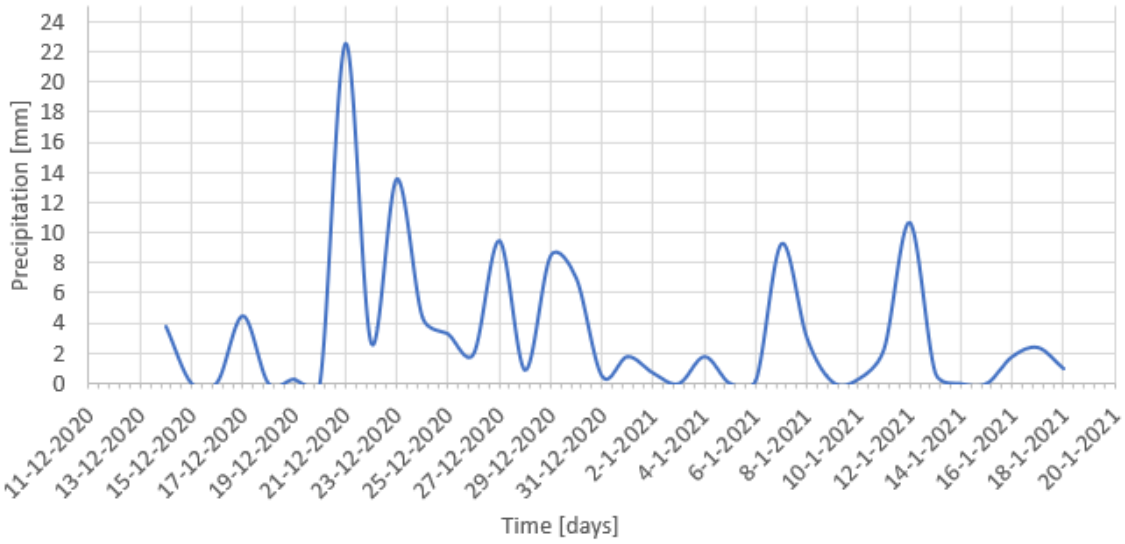

Figure 4.24: The daily precipitation in phase 2.

Figure 4.25 shows the deformation of the sheet pile wall in the shallow section. The decrease of deformation on December 17 is much larger than in the deep section (approximately 2 millimetres against 0.25 millimetre in the deep section). The drop on January 6th is the other way around. At the deep section this is 2 millimetre against 0.75 in the shallow section. Besides these two differences the deformations follow the same path even though they are smaller in the shallow section.

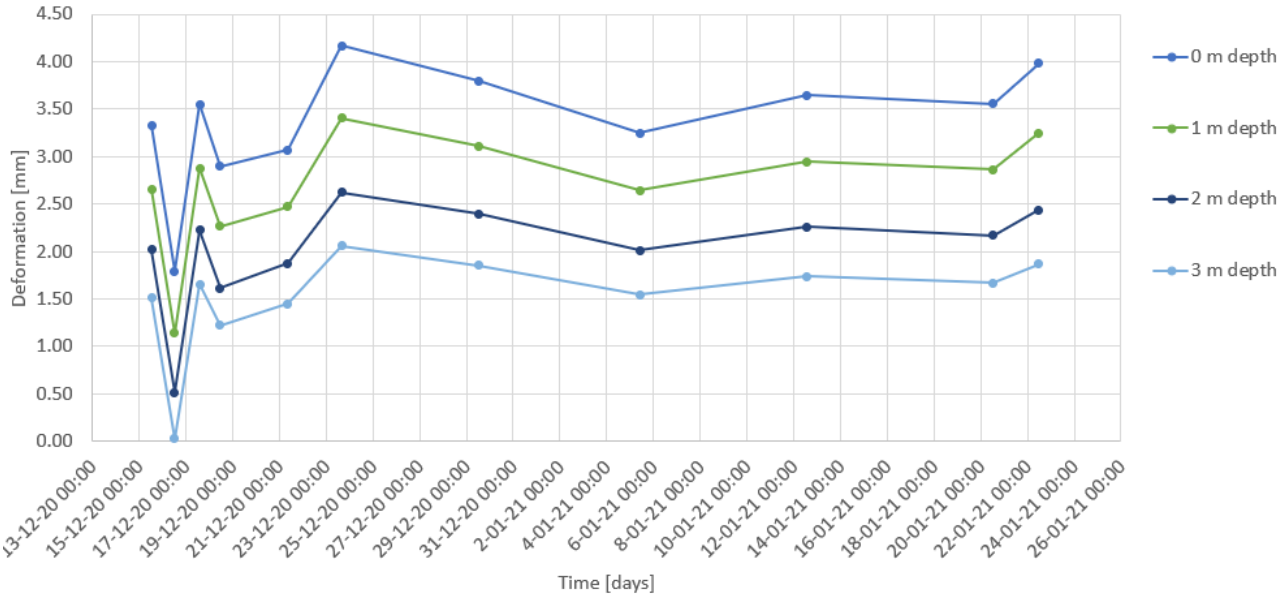

Figure 4.25: Deformation versus depth of the sheet pile wall in the shallow section in phase 2.

4.7.4 Determination of the Deformation Resulting From the Thermal Activation

By correcting for the difference in measuring depth and subtracting the maximum deformation of the thermally inactivate section from the thermally active section, the deformation resulting from the thermal activation is determined. Isolating this distortion gives a good idea of the order of magnitude of the influence of the thermal activation. It is difficult to determine the exact deformation as influences such as different ground surface level and saturation of the soil have a large impact on deformations, even on a sheet pile wall with the width of 7 metres.

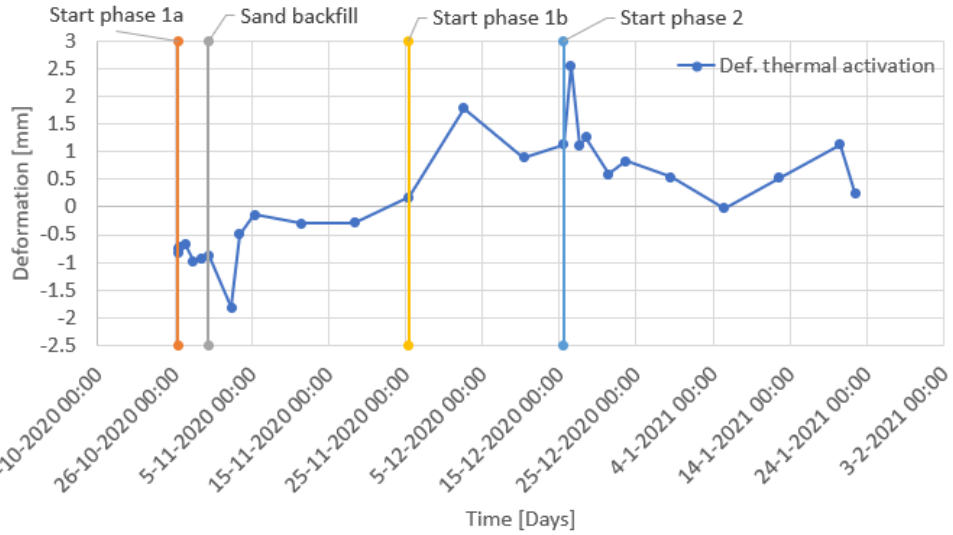

Figure 4.26: The maximum deformation resulting from the thermal activation (Phase 1a = single side shallow activation, phase 1b = single side deep activation, phase 2 = double side deep activation).

Figure 4.26 shows the thermally induced deformation. This graph shows that most of the measurements have deformation of slightly more than 1 millimetre or less. The negative deformation in phase 1a and the oscillations in deformation indicates there are more influences working on the sheet pile wall than the thermal activation. For a sheet pile wall, oscillating deformations of 1 millimetres are negligibly small.

4.8 Concluding remarks

Table 4.2 gives an overview of the temperature decrease measured in the subsurface. With the help of this data, research question 1 is answered, namely: 'What is the magnitude of temperature changes of the subsurface as a result of the thermal activation of the energy sheet pile?'. In all phases, one of the sections is active while the other is inactive. Assumed that the complete temperature decrease in the inactive section is the result of the ambient temperature, the difference in temperature between the activated and inactivated section is the temperature decrease resulting from the thermal activation. This means that in phase 1a and 1b the temperature decrease is 2 °C and in phase 2 1.5 °C. Table 4.3 shows the temperature decrease per week for each phase as a result of the thermal activation. A large temperature occurs in phase 1b, the single side deep activation. Phase 2, the double side deep activation, has a smaller average temperature decrease. This is the result of decrease in the previous phase as well as the the cooling down of the soil with a progressively smaller gradient. This effect is cancelled out by the averaging.

Table 4.2: Overview of the overall average temperature decrease per phase for each section.

Phase [-]	**Duration** [Weeks]	**Average decrease deep section** [°C]	**Average decrease shallow section** [°C]
Phase 1a: single side shallow	4	2	4
Phase 1b: single side deep	2	3.5	1.5
Phase 2: double side deep	4	2.5	1

Table 4.3: Overview of the weekly temperature decrease per phase as a result of the thermal activation.

Phase [-]	**Duration** [Weeks]	**Weekly decrease** [°C]
Phase 1a: single side shallow	4	0.5
Phase 1b: single side deep	2	1
Phase 2: double side deep	4	0.375

Based on the analysis of the inclinometer data research question 2, 'What is the response of the sheet pile wall to the temperature change?', can be answered. The total deformations as a result of the thermal activation are not larger

than 6 millimetres in the deep section. In the shallow section this is 4 millimetres. By subtracting the the deformation occurring in the inactivated section from the activated section, the deformation resulting from the thermal activation is determined. This lies in the range of 1 - 1.5 millimetre. This is shown in Figure 4.26. Influences working on the sheet pile wall such as radiation, canal and groundwater level; and a measurement error of 0.25 mm/m have an impact on this deformation as well. This analysis results in the conclusion that the sheet pile wall oscillates more or less 1 millimetre, which is negligible.

Chapter 5

Development of the Heat Conduction Model

This chapter contains methodological step 2 of this thesis and describes the investigations into the heat transfer packages of COMSOL multiphysics and the subsequent development of a heat conduction model that reassembles the in-situ conditions of the field test. This model is confined to the heat conduction, a mechanical analysis of the quay is not incorporated. The chapter starts with describing the basic principles of heat transfer. These principles stand at the base of the physics component of of a heat conduction analysis in COMSOL. The different types of heat conduction are investigated in Section 5.2 to define the differences between the heat transfer software packages and determine which of these packages is best fit to use in this problem. In Section 5.3 are the domain and material characteristics defined, i.e. the geometry, initial and boundary conditions; and material properties. This chapter is part of the effort to answer research question 4: 'Can an industry standard finite element method program capture the long-term thermal and mechanical behaviour of an energy sheet pile quay and the subsurface?'.

5.1 Principles of Heat Transfer

The heat transfer depends on three underlying physical mechanisms: conduction, convection and radiation (COMSOL Multiphysics, 2015). A good understanding of these mechanisms is necessary to understand the physics software packages in COMSOL and make a well substantiated choice when determining the most appropriate package. In the following section, the basic equations are explained while Appendix B contains the full equations specified to this situation.

5.1.1 Heat Conduction

Heat conduction is the transfer of heat without the movement of particles. For each different media, a different mechanism is responsible. For a fluid, the conduction occurs through oscillations of each molecule in a "cage" formed by its nearest neighbours; in metals mainly by electrons carrying heat and in other solids by molecular motion, which in crystals take the form of lattice vibrations known as phonons' (COMSOL Multiphysics, 2015). The heat conduction can be calculated using Fourier's law of heat conduction:

$$\mathbf{q}_{conduction} = -k\nabla T \tag{5.1}$$

where $\mathbf{q}_{conduction}$ is the conductive heat flux [W/m^2], k is the thermal conductivity [W/(m $\cdot$ K)] and ∇T the temperature gradient [K/m].

5.1.2 Heat Convection

Heat convection is the transportation of heat via fluid flow. This is a combination of heat diffusion and advection. The former is the dissipation of heat via the movement of particles from a high to a low temperature or the difference in density while the latter is the dissipation of heat governed by the velocity of the fluid (Snoeren, 2019). The term convection also refers to the transportation of heat from solids to liquids and is usually described by a heat transfer coefficient (COMSOL Multiphysics, 2015). The convection is described by Newton's law of cooling (Snoeren, 2019):

$$\mathbf{q}_{convection} = h\Delta T \tag{5.2}$$

where $\mathbf{q}_{convection}$ is the convective heat flux [W/m^2], h is the heat transfer coefficient [W/(m^2 $\cdot$ K)] and ΔT the temperature difference [K].

5.1.3 Radiation

Radiation is the transfer of heat via electromagnetic waves (Snoeren, 2019). This process is often neglected inside soils; therefore, this process will not be further elucidated.

5.2 Selection of the Most Suitable Heat Transfer Package for the Heat Conduction Model

In this section, an investigation is performed into the the predefined heat transfer packages in COMSOL Multiphysics. First, the principles of heat transfer are combined in a single situation. Thereafter, the packages for, respectively, heat transfer in soil, solids and fluids are investigated. In this section focusses only on the numerical component of a heat conduction model by analysing and comparing various physics packages, each with a different characteristics, after which it is decided which physics package is most applicable. The packages themselves are developed, and therefore verified, by COMSOL Multiphysics. Therefore, the verification is not done in this thesis.

5.2.1 Combining the Heat Transfer Principles

Combining these three physical mechanisms with the heat balance equation, while taking into account the laws of conservation of mass and momentum, the localized spatial heat balance equation in material frame is as follows (COMSOL Multiphysics, 2015):

$$\rho \frac{dE}{dt} + \nabla \cdot \mathbf{q} = \sigma : \mathbf{D} + Q \tag{5.3}$$

where ρ is the material density, E is the internal energy, σ is the Cauchy stress tensor, D is the strain rate tensor and Q is the exchanged heat rate. This formula describes 'that variations of internal energy in time are balanced by convection of internal energy, thermal conduction, radiation, dissipation of mechanical stress and additional volumetric heat sources' (COMSOL Multiphysics, 2015).

In this chapter, the modelling is performed using the advanced numerical method based simulation software COMSOL Multiphysics®. This program is a 'simulation platform that encompasses all of the steps in the modelling workflow — from defining geometries, material properties, and the physics that describe specific phenomena to solving and post processing models for producing accurate and trustworthy results' (COMSOL Multiphysics, 2015). Equation 5.3 is the equation used as basic formula for the heat transfer through media. Depending on the medium that transfers the heat, heat transfer principles and physical phenomena (e.g. transient fluid flow) are added or deleted. These equations are pre-defined in COMSOL Multiphysics thus not defined by the author.

The model builder in COMSOL Multiphysics provides a systematic way of creating a model. The assembling is as follows: the necessary physics packages are chosen after which the geometry is created and the materials are assigned. Thereafter, the initial and boundary conditions; and external influences, such as heat extraction, are assigned. Finally, before starting the computation, a mesh is created. COMSOL can be used to solve problems in various fields of physics and, as part of creating a heat conduction model to analyse the temperature changes in a quay, several heat transfer physics packages (called physics interfaces in COMSOL) for different media are investigated to determine the best package to analyse the problem. Moreover, groundwater and open water flow is investigated as this is influencing the energy extraction as well (Kürten et al., 2015). In addition, a glycol-water mixture flows through the loop system extracting or storing heat in the process. This flow in the canal, soil and loops affects the distribution of heat and; therefore, has to be incorporated into the calculation. Table 5.1 shows the investigated packages.

Table 5.1: Overview of the investigated physics package.

Component	Soil heat transfer	Solid heat transfer	Fluid heat transfer
Considered Packages	Heat transfer in porous media Heat transfer in solids	Heat transfer in shells Heat transfer in solids	Darcy's Law Free and porous media Heat transfer in pipes

The following analyses are conducted:

1. An investigation into the soil heat transfer packages.
2. An investigation into the solid heat transfer packages.
3. An investigation into the fluid heat transfer packages.

In the soil heat transfer investigation, the heat transfer in porous media and heat transfer in solids are analysed even tough, due to the name of the package, one is inclined to choose the former. The investigation continues with a analysis into the best applicable physics package for the sheet pile: either heat transfer in shells or heat transfer in solids. Next, the sheet pile is thermally activated by modelling the activation loops with the help of the heat transfer in pipes physics package. Finally, the groundwater flow is analysed with both the Darcy's law and free and porous media package.

Besides focussing on obtaining the most realistic solution, attention is paid to the complexity of coupling the heat exchange between the packages regarding possible unknown parameters but also the necessary computational power and time. Comparing the calculations as well as the computational load, the packages which simulate the reality as good as possible is used as baseline model to use for the validation of the field test.

Setup Used in the Investigation

In order to properly investigate and verify the workings of the soil, water and sheet pile components, an initial model is created. This model is used to assess the heat conduction through the soil and the sheet pile with and without energy extraction by means of a loop. The geometry is adjusted throughout the analysis to be able to compare two heat conduction packages. Before the adjustment, the model consists of 4 components: two block simulating the soil, a thin rectangular shaped block simulating the sheet pile and pipes modelling the loops welded onto the sheet pile - placed in the middle of the domain. In the adjustment, the domain simulating the sheet pile is removed, the soil blocks placed against each other and the lines of the pipes are placed exactly on the boundary between the two blocks. The model is shown in Figure 5.1, both blocks have a volume of 1 m^3 (i.e. all sides have a length of 1 metre) and the sheet pile has a thickness of 0.008 metre. The pipes have a diameter of 0.03 metre, a total length of 2.2 metre, a flow rate of ethylene glycol of 1e-4 m^3/s and a wall thickness of 0.003 metre.

As energy cannot be created nor destroyed, no energy will leave the model when all the sides are thermally insulated. As a result, it is possible to verify each calculation with a hand calculation. In addition, prior to each analysis, a hypothesis is drawn up which is then proved correct or invalidated.

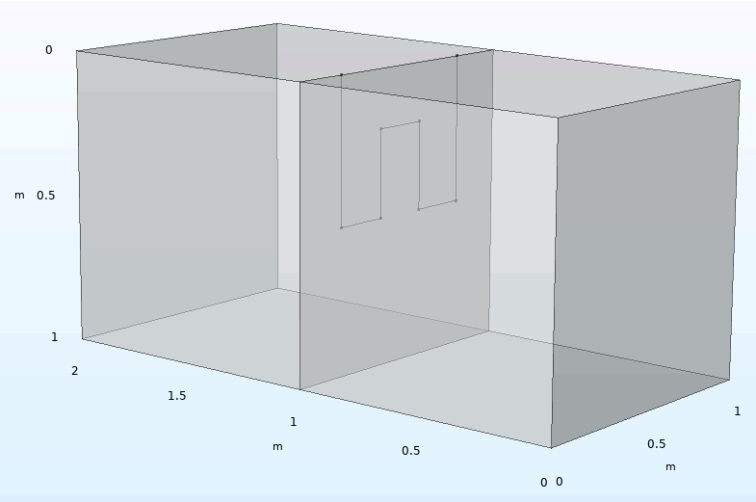

Figure 5.1: Basic heat conduction model 1 and 2 with two rectangular blocks and the pipes to extract energy.

Throughout the investigation, energy/temperature change is verified with by means of a hand calculation. The following equation is used:

$$Q = C_p \cdot m \cdot \Delta T \tag{5.4}$$

With Q being energy [J], C_p the heat capacity [J/(kg · °C)], m the mass of the analysed domain [kg] and ΔT the temperature change [°C].

5.2.2 Selection of the Best Soil Heat Transfer Package

Starting with determining the best applicable physics package for the soil, heat transfer in porous media and heat transfer in solids are analysed. Two different soil types are assigned the to the two soil domains, shown in Table 5.2. The thermal conductivity is kept equal, as this only governs the speed of the temperature change throughout the domain. By making the heat capacity two times larger, two times more energy is need to heat the domain up to the same temperature. In this case, if soil 1 cools down 6 °C, soil 2 will become 3 °C. The same happens when the density instead of the heat capacity is increased by a factor of 2.

Table 5.2: Thermal properties and settings basic heat conduction model 1.

Parameter	**Soil 1**	**Soil 2**
Density	1800 kg/m^3	1500 kg/m^3
Heat capacity	2400 J/(kg · K)	3500 J/(kg · K)
Thermal conductivity	2.4 W/(m · K)	2.4 W/(m · K)
Initial temperature	12 °C	0 °C

In this analysis, the computational time is 365 days after which the boundary between the two blocks is thermally insulated thereby separating the domains. Then, the analysis is run for another year allowing the temperature distribution in the blocks to converge to a single value.

It is expected that when the variables in Table 5.2 are used, the temperature of soil 2 will be about 25% cooler than temperature 1, as the density of soil 2 is lowered by 20% and the heat capacity raised by about 45% resulting in a 25% overall change.

Heat transfer in Porous media

After the calculation, the temperature of block 2 is 4.55 °C. The hand calculation, shown in Equation 5.5, results in a temperature of 4.5 °C, a 0.05 °C difference.

$$\Delta T_{domain\,2} = \Delta T_{domain\,1} \cdot \frac{C_{p,soil\,1} \cdot m_{soil\,1}}{C_{p,soil\,2} \cdot m_{soil\,2}} \tag{5.5}$$

$$\Delta T_{domain\,2} = (12 - 6.54) \cdot \frac{2400 \cdot 500 \cdot 1800}{3500 \cdot 500 \cdot 1500} = 4.5 \tag{5.6}$$

Heat Transfer in Solids

The same analysis with the heat transfer in solids package results in a temperature change of 5.47 °C of domain 1 (i.e. from 12 °C to 6.53 °C) and an increase of 4.51 °C. This is a difference of 0.01 °C which leads to the conclusion that in terms of heat conduction, there is no difference between both packages.

Determination of the Heat Transfer in Soil Package

Now that it is concluded that there is no difference in heat exchange, other aspects of the heat transfer packages are analysed. No nameable calculation duration difference is present as the calculations are very basic. Furthermore, regarding package properties, both heat conduction packages allow for a solid, fluid and porous media domain in which the latter two allow for the definition of a fluid flow. The governing equation is a combination of the governing equations of the solid and fluid equation (COMSOL Multiphysics, 2015) allowing for pores in the domain (defined based on the porosity of the soil) through which fluid can flow with a defined velocity.
To couple separate heat transfer packages (e.g. heat transfer in solids and heat transfer in porous media), the heat exchange must be coupled. As each heat transfer package contains the domain types necessary to solve a heat conduction problem in soil, water and a sheet pile, it is highly recommended to use one package for the whole analysis. Adding extra boundary conditions and dependent variables to couple demands extra computational power and as the analysis becomes more complex, mistakes are easily made.
To conclude, it does not matter which package is used as long as the correct domain type is defined (i.e. solid, fluid or porous media) and it is strongly recommended to use one package for the whole domain.

5.2.3 Selection of the Best Heat Transfer Package for the Sheet Pile Wall

COMSOL offers two suitable options for modelling the sheet pile:

1. Using a domain (i.e. with a volume) as sheet pile and use the domain type 'solids'.
2. Rather than using a domain for the sheet pile, a 'thin layer' boundary condition (as part of the heat transfer in porous media package) is assigned with the same characteristics as the sheet pile with volume in item 1.

Item 1 is the most obvious; however, in this situation, it is not the most convenient. The sheet pile is very thin compared to the soil domain, 8 millimetre and 2 times 5 metre, respectively. When it comes to meshing the domain, the necessary element size for the 8 millimetre domain is guiding, meaning that a fine mesh is assigned to the whole domain while a coarse mesh could be sufficient too. Therefore, if the sheet pile is modelled as a surface rather than a domain, the necessary element size can be based on the analysis in the soil domain. By means of defining a single layer material on to which the material type, thickness and amount of mesh elements is assigned, the surface is treated the same as a domain during a calculation.

To investigate if the different packages have different output, the analysis performed in the previous subsection with the two blocks with different soil types is repeated but this time with a sheet pile in between. In addition, to investigate if the different packages influence the heat extraction, the sheet pile is activated with the help of the heat transfer in pipes packages. Each computation is checked with a hand calculation.

The hypothesis for the first investigation, the heat exchange between two blocks of soil with different thermal properties and the sheet pile, is that it does not matter which of the packages is used to simulate the sheet pile. The steel of the sheet pile collides well; therefore, the thickness will not have much influence.

Analysis of two Different Blocks of Soil and Sheet Pile Without Heat Extraction

Using the data noted down in Table 5.2, the free heat exchange runs for 1 year after which the boundary between the two blocks is closed. Subsequently, the analysis is run for the timespan of another year so the temperature distribution converges to one temperature. Equation 5.5 is used as hand calculation with the parameters defined in Equation 5.6. It is expected that all three computation have the same result.

Heat Transfer in Porous Media - 'Solid' Sheet Pile Domain with a Volume The result of the analysis is that block 1 cooled down to 8.89 °C, i.e. $\Delta T_{domain\,1} = 3.11$, and block 2 warmed up to 2.58 °C. This is in accordance with the hand calculation.

Heat Transfer in Porous Media - Thin Layer Boundary Condition The heat transfer in porous media thin layer boundary condition resulted in the same temperatures as in the previous calculation.

Analysis of two Similar Blocks of Soil and Sheet Pile With Heat Extraction

In this investigation, the heat extraction via the loops is activated. All domains have the same initial temperature, 12 °C and the outer boundaries are thermally insulated. As a result, the energy extraction can be calculated by hand. Using Equation 5.4, the energy extracted from the soil and by the loops is calculated and if the amounts are equal, the computation is valid.

The hypothesis for this analysis is that it does not matter which of the two approaches is used in terms of energy output. However, with regards to computational time and power, is it expected the use of a thin layer boundary condition is more convenient.

Heat Transfer in Porous Media - 'Solid' Sheet Pile Domain with a Volume The temperature of the soil after a 10 days analysis is 10.24 °C, a ΔT of 1.76 °C. The temperature extracted can be seen in Figure 5.2. As a check to make sure the heat extraction works correctly, the following calculation has been done. The energy extracted from the soil is:

$$C_{p,soil}\left[\frac{J}{kg\cdot^{\circ}C}\right] * m_{soil}\,[kg] * \Delta T_{soil}\,[^{\circ}C] = Q_{soil}\,[J] \tag{5.7}$$

$$\left(2400\left[\frac{J}{kg\cdot^{\circ}C}\right]\cdot 2\,[m^3]\cdot 1800\left[\frac{kg}{m^3}\right] + 475\left[\frac{J}{kg\cdot^{\circ}C}\right]\cdot 0.008\,[m^3]\cdot 7850\left[\frac{kg}{m^3}\right]\right) * (12-10.24)\,[^{\circ}C] = 15232650\,[J] \tag{5.8}$$

And the energy extracted by the loops over 10 days is:

$$C_{p,glycol}\left[\frac{J}{kg\cdot^{\circ}C}\right]\cdot m_{glycol}\,[kg]*\Delta T_{glycol}\,[^{\circ}C]=Q_{glycol}\,[J] \tag{5.9}$$

$$2300\left[\frac{J}{kg\cdot^{\circ}C}\right]\cdot(2.2\,[m]\cdot 7.0684e{-}4[m^2]+1e{-}4\left[\frac{m^3}{s}\right]*864000\,[s])\cdot 1123\left[\frac{kg}{m^3}\right]\cdot(5-5.1378)\,[^{\circ}C]=15376177\,[J] \tag{5.10}$$

This means a difference of:

$$\Delta J=|15232650-15376177|/15232650\cdot 100=0.94\% \tag{5.11}$$

These small errors between the model and hand calculation prove the model is accurate.

Heat Transfer in Porous Media - Thin Layer Boundary Condition The same analysis has been performed using a thin layer boundary condition. The ΔT of the soil is: 1.55 °C. The energy change in the soil over 10 days is calculated as follows:

$$C_{p,soil}\left[\frac{J}{kg\cdot^{\circ}C}\right]\cdot m_{soil}\,[kg]\cdot\Delta T_{soil}\,[^{\circ}C]=Q_{soil}\,[J] \tag{5.12}$$

$$(2400\left[\frac{J}{kg\cdot^{\circ}C}\right]\cdot 2\,[m^3]\cdot 1800\left[\frac{kg}{m^3}\right])\cdot(12-10.45)\,[^{\circ}C]=13824000\,[J] \tag{5.13}$$

And the energy extracted by the loops over 10 days is:

$$C_{p,glycol}\left[\frac{J}{kg\cdot^{\circ}C}\right]*m_{glycol}\,[kg]*\Delta T_{glycol}\,[^{\circ}C]=Q_{glycol}\,[J] \tag{5.14}$$

$$2300\left[\frac{J}{kg\cdot^{\circ}C}\right]\cdot(2.2\,[m]\cdot 7.0684e{-}4\,[m^2]+1e{-}4\left[\frac{m^3}{s}\right]*864000\,[s])\cdot 1123\left[\frac{kg}{m^3}\right]\cdot(5-5.1223)\,[^{\circ}C]=14450036\,[J] \tag{5.15}$$

This means:

$$\Delta J=|13824000-14450036|/13824000\cdot 100=1.9\% \tag{5.16}$$

The error is 1% larger than in the solid sheet pile domain analysis yet this is still an acceptable difference.

Comparison Analyses Figure 5.2 shows the energy extraction in an analysis with a solid domain and a thin layer simulating the sheet pile. As one can see, the error is approximately 0.01 °C and the lines have the same gradient.

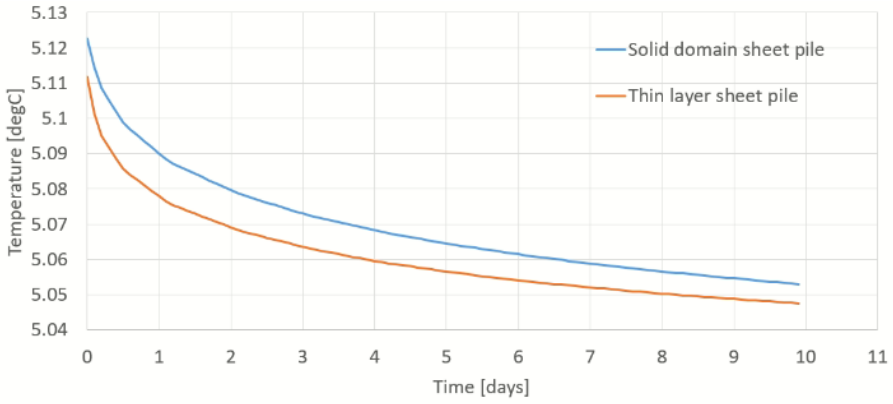

Figure 5.2: Comparison f the heat extraction between the solid (volumetric) domain and thin layer (area) sheet pile.

Determination of the Heat Transfer in the Sheet Pile Package

Based on the comparison of the extracted heat by means of a loop, the difference between modelling the sheet pile as a solid domain or thin layer is close to naught. Therefore, other important characteristics of both approaches are analysed: the necessary computational power and time. As already mentioned, simulating the sheet pile as volume raises the need for fine elements to mesh this thin domain. This governs the element size for the rest of the soil – which is considerably larger – resulting in a mesh with many elements, much more than necessary to reach conversion of the solution. By simulating the sheet pile as boundary, the element size is governed by the convergence of the outcome alone, most likely resulting in a coarser mesh thereby reducing the computational power and time needed. Concluding, it is advised to use the 'thin layer' boundary condition to model the sheet pile in a heat conduction analysis.

5.2.4 Selection of the Most Suitable Fluid Heat Transfer Package

Regarding the (subsurface) fluid flow, COMSOL offers multiple packages with their own specific characteristics. Two of these are Darcy's flow packages and, free and porous media package of which the former is most applicable to slow groundwater flow and the latter to fast groundwater flow. A third option exists, the porous media domain in the heat conduction in porous media package contains the option to specify a steady state flow in the soil. In addition, it is possible to select a 'fluid' domain to simulate the open water. As most of the soil in the Netherlands – and at the testing site – is fine grained, the groundwater flow is slow, making Darcy's law the most applicable to the situation. Analysing the outlet temperature in two analyses, one with Darcy's law package and one without, it is concluded that Darcy's law has little influence on the energy extracted. Yet, the computational time has doubled. Hence, Darcy's law package is not integrated in the model.

It is advised to use the possibilities for modelling open water and flow using the heat transfer in porous media. This is found to be quick and efficient and has the additional advantage that no extra dependent variable is introduced in the computation, making it a simpler model - reducing the chance of mistakes.

5.2.5 Conclusion

An overview of the advised physics packages is shown in Table 5.3. All of the corresponding governing equations can be found in Appendix B.

Table 5.3: Overview of the used physics packages in the baseline model

Component	Package
Soil	Heat transfer in porous media
Sheet pile	Thin layer boundary condition of heat transfer in porous media
Pipes	Heat transfer in pipes
Open water	Simulated as a fluid in heat transfer in porous media

5.3 Defining the Domain and Material Characteristics of the Heat Conduction Model

After analysing and defining the numerical component of the model, the material component is determined. The domains characteristics mean the input of the model which gives it the characteristics of the field test site, i.e. the geometry, thermal properties and the initial and boundary conditions. The objective is to develop a model closely resembles the soil stratigraphy of Zweth, but is also efficient with regards to the computational time and necessary power.

5.3.1 Investigation and Description of the Geometry

Besides using the most applicable and efficient physics packages, the level of detail in modelling the geometry is of importance too. This part of the analysis sets out to investigate the necessary level of detail of the geometry to end up with good results retrieved as efficient as possible. The two aspects that are investigated in this subsection are the following:

1. The need for modelling the soil layers
2. The need for modelling the shape of the sheet pile

The model that is used can be seen in Figure 5.3. The canal is 3 metres deep and two sheet piles are modelled, with a total width of 1.4 metres. The brown domains are soil. The investigation is carried out in the aforementioned order and, if found to be of importance to the results, the model is updated.

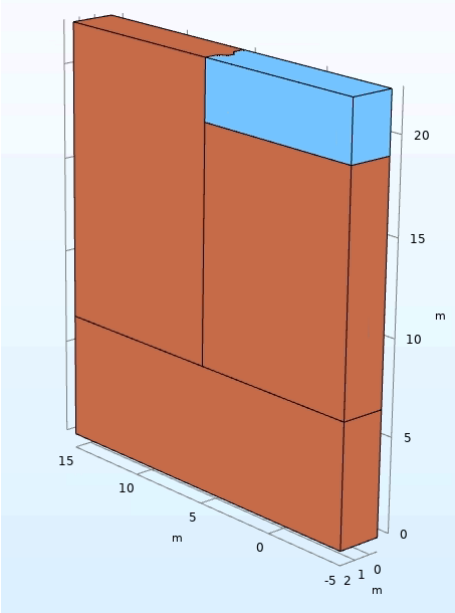

Figure 5.3: A picture of the model used for the analyses described hereafter. The blue domain simulates the water is the canal and brown the soil.

Modelling Soil Layers Separately

In this analysis of 100 days, the thermal properties of the soil are averaged to find out how much influence this has on the extracted heat. The properties can be found in Table 5.4. The hypothesis is as follows: it is expected that the averaging of the soil layers will not have a large effect on the extracted heat. This expectation is based on the fact that the thermal properties of the different soil types are not that different as can be seen in Table 5.5.

Table 5.4: Averaged thermal properties

Parameter	Soil averaged properties	Steel
Density	1520 kg/m^3	7850 kg/m^3
Heat capacity	2118 J/(kg · K)	475.15 J/(kg · K)
Thermal conductivity	1.51 W/(m · K)	44.5 W/(m · K)
Initial temperature	12 °C	12 °C

Figure 5.4 shows the result of the analysis. As can be seen, the difference between the two outcomes is close to naught. This proves the hypothesis to be correct, resulting in adapting the separate soil layers as one with averaged thermal properties.

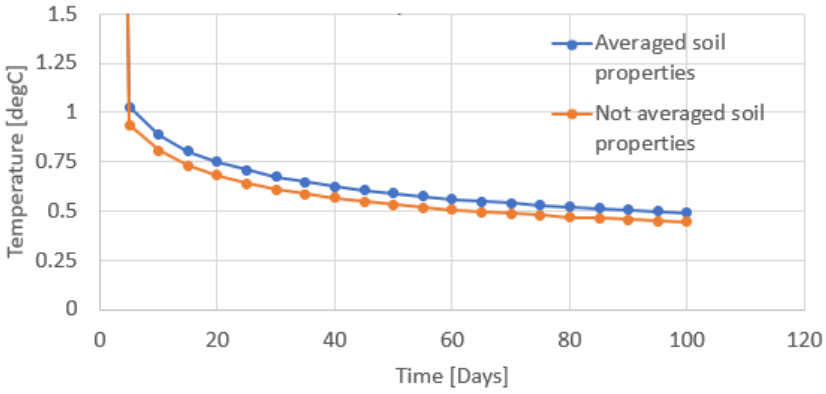

Figure 5.4: The result of the analysis in which the averaged thermal properties are compared to non-averaged properties.

Analysis Shape of the Sheet Pile

One of the most distinguished features of the sheet pile is its shape and this provides the possibility to use it to extract energy from the water as a result of the turbulent flow. However, in the model used, turbulent flow is incorporated. Therefore, the need for modelling the shape of the sheet pile might not be there thereby providing the opportunity to simplify the geometry. A 100 days analysis with two deeps loops is performed to test the hereafter mentioned hypothesis. The thermal properties noted in Table 5.4 are used.

Four analyses have been performed: a bulged sheet pile geometry analysis with and without flow; and a flat sheet pile geometry analysis with and without flow. The shapes can be found in Figure 5.5. It is expected, based on the earlier mentioned lack of turbulent flow, the bulged shape of the sheet pile does not result in a significantly different amount of heat extracted - provided that the distance between the loops is respected.

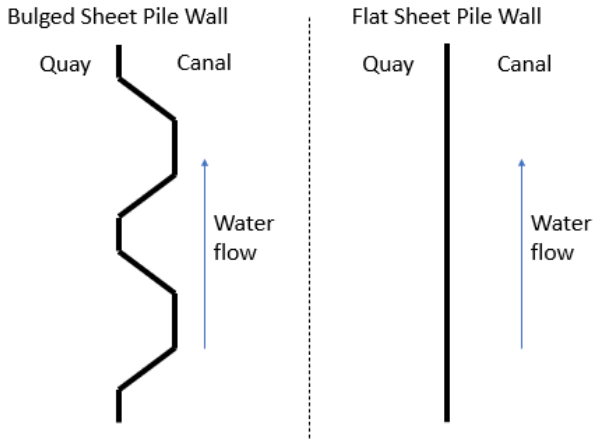

Figure 5.5: Top view of the bulged and flat shape of the sheet pile.

Figure 5.6 shows the result of the analyses. The bulged and flat flow; and the two no flow calculations lie on top of each other showing the shape of the sheet pile does not influence the performance. The 'heat pump out temperature' is the temperature of the glycol-water mixture coming out of the heat pump into the loops attached to the sheet piles.

As a result of this calculation, it is found – based on the extracted heat – that it is not necessary to model the shape of the sheet pile. However, as the distance between the loops has to be respected (otherwise the loops have more influence on one another), the width of the domain has to be enlarged thereby making, most likely, the analysis slower. In addition, this model might extended with turbulent flow and; therefore, having sheet pile with bulges is a future investment.

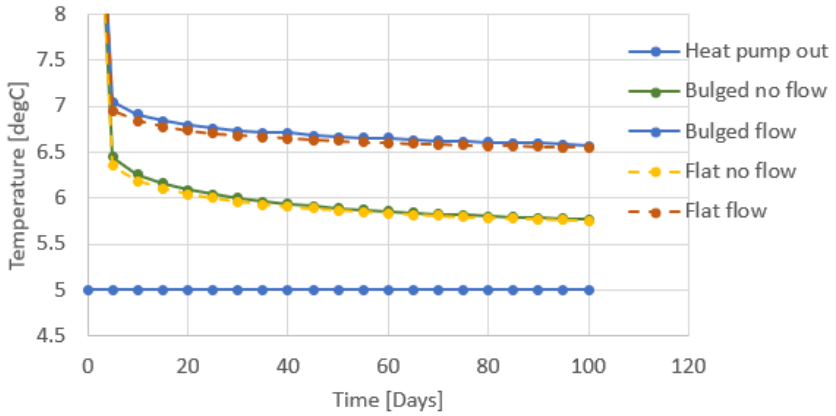

Figure 5.6: The result of the analysis in which the shape of the sheet pile is analysed.

Concluding Remarks for the Geometry Investigation and Development

Based on the performed research, it is found that it is – in this this situation – not necessary to have separate soil layers and a bulged shaped sheet pile. However, it has to be noted that the thermal properties of the different soil types influence the temperature regeneration during the summer. Therefore, a non-averaged stratigraphy could prove important for a multiple year analysis. With regards to the shape of the sheet pile, as it is necessary to keep the spacing between the loops the same, the width of the domain has to be enlarged significantly. In this particular situation, 'unfolding' the sheet pile would result in an increase from 8.4 to 13.6 metres width. Independent from this domain volume increase stands the mesh element size. Even though a less detailed domain could result in a coarser mesh, the coarseness is governed by the convergence of the results and might not change. Hence, the analysis could prove to need more computational power thereby cancelling out the initial gains from simplifying the geometry.

Based on the analysis of the mechanics of a heat conduction simulation, the geometry of the baseline heat conduction is as follows. As can be seen in Figure 5.7, the depth of the model is 16 metres (x-direction), the width of the sheet pile wall is 8.2 metre (y-direction) with an additional 3 metres added to the deep section to prevent influence from the boundary conditions and the height is 22.3 metre (z-direction). The canal is 1.8 metres deep and has a continuous flow of 0.01 m/s in negative y-direction. In accordance with Figure 4.4, the shallow loops are located on the right side of the sheet pile wall when standing on the quay facing the canal. The soil thermal parameters are based on a CPT performed nearby and averaged. These averaged values can be found in Table 5.6 as well as the properties of the steel and glycol-water mixture running through the loops.

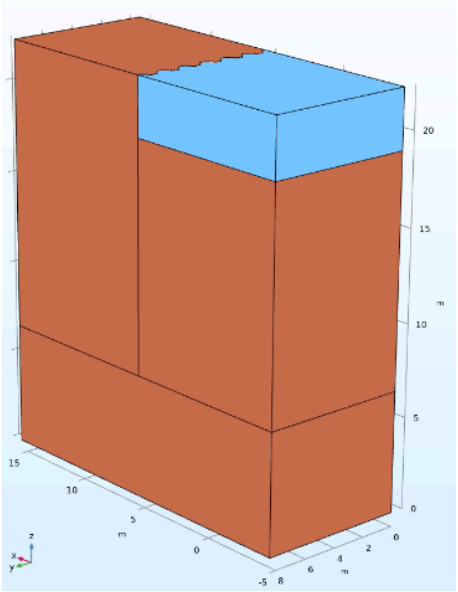

Figure 5.7: Geometry of the baseline heat conduction model. The brown domains simulate soil while the blue domain simulates the canal.

The vertical line normal to the x-direction is the boundary on which the sheet pile is projected. This sheet pile is of the type ZZ 17-700 and made of steel. With the loops incorporated into the sheet pile by welding them on the sheet pile, the whole sheet pile acts as a heat sink. The shank space of one welded loop is 0.3 metre. The loops in the shallows section reach to a depth of 3 metre while the deep loops cover the whole depth - approximately 15 metres.

5.3.2 Mesh Convergence

In order to obtain an accurate computation, the coarseness of the mesh needs to be investigated. This is related to the size of the elements in the mesh and can influence the results when changed. Hence, the optimal element size has to be defined so the results are accurate and the mesh is not unnecessarily fine. All parameters are fixed and only the mesh size is varied. Starting with the mesh of the sheet pile, the amount of elements can be defined instead of the element size. As the area of the sheet piles is fixed, the element size changes automatically when the amount of elements is altered. Starting with 1 element, the sheet pile wall is divided into an increasing number of elements. The deviation of the outlet temperature of the shallow activation loop is compared with each previous output by means of the mean square error (MSE).If two subsequent mesh refinements do not change the MSE substantially, one can assume convergence is achieved. The optimal amount of elements is found to be 55.

Continuing with the domain, COMSOL offers the possibility to use predefined meshes with different element sizes. The options are: very coarse, coarse, normal, fine, finer and extremely fine. Convergence is accomplished by using a finer mesh. In addition, coarser meshes result in low-quality elements.

5.3.3 Boundary Conditions of the Model

This section contains the explanation of which physics packages and boundary conditions are applied where in the model. All the theoretical background of the boundary conditions is taken from COMSOL Multiphysics (2015) and COMSOL Multiphysics (2017).

Heat Transfer in Porous Media

Figure 5.8 show the boundary conditions of the model. The figure on the left hand side is depicted from the same point of view as Figure 5.7. The picture on the right is viewed from the opposite direction. The boundaries on which the air temperature work are depicted in yellow. These are the top of the quay and water and the sheet pile in contact with the air. The heat flux boundary condition from the surrounding soil in the quay is shown in purple and the heat flux boundary condition from the soil under the canal in green. These boundary conditions are based on the measurements of thermistor strings D_C and D_B. To model the temperature of the water correctly, the measured water temperature is imposed as temperature boundary condition on the boundary from where the flow originates, shown in red. On the other side of the water domain is a open boundary (in brown) present so the heat dissipates. The bottom of the domain has a fixed temperature of 12 °C. Finally, on the boundary of the water in contact with the rest of the canal thermal insulation is applied.

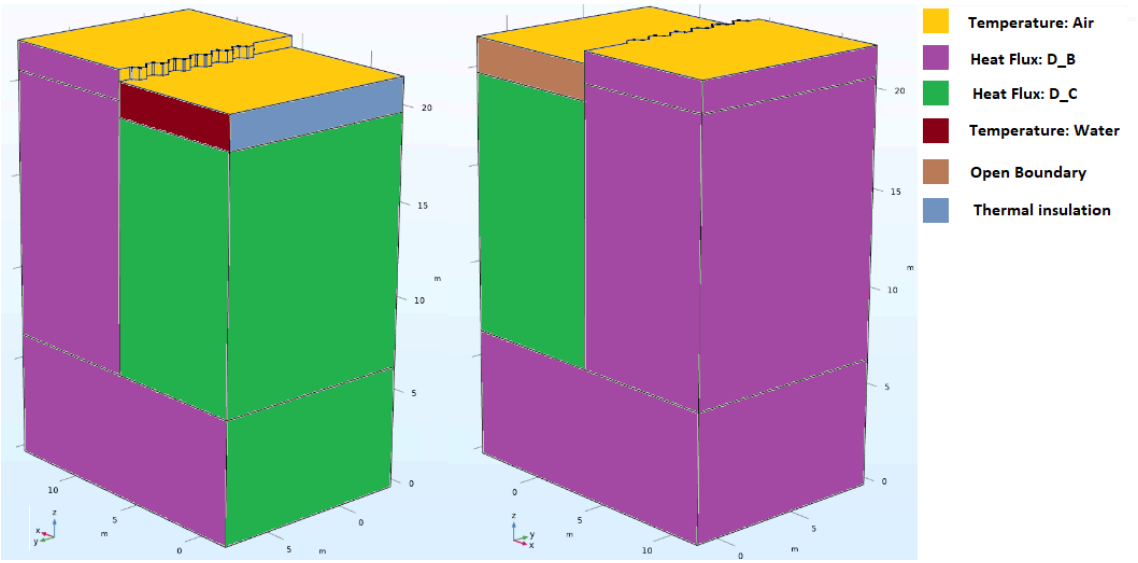

Figure 5.8: Overview of the boundary conditions applied to the 'heat Transfer in Porous Media' package.

Open Boundary / thermal insulation One of the two basic boundary conditions is the inward heat flux , in COMSOL known as an 'Open Boundary'. The heat can flow into or out of the domain. Equation 5.17 gives the analytical expression.

$$-\mathbf{n}\cdot\mathbf{q} = q_0 \tag{5.17}$$

Where **n** is the vector normal to the surface, **q** is Fourier's conductive heat flux vector [W/m^2] and q_0 is the inward heat flux [W/m^2]. Usually, the inward heat flux is the sum of several heat transfer mechanisms. One special type of open boundary condition is when:

$$q_0 = 0$$

such that no heat loss is allowed. This is called thermal insulation and is used in case of symmetry.

Heat Flux When a heat flux is applied to a surface, it is thermally influenced by an external heat source, thus simulating the transfer of thermal energy from a heat source to a heat sink. The flux works both ways, it can either warm or cool the material. In this model, a convective heat flux is used. The function is given as:

$$q_0 = h\cdot(T_{ext} - T) \tag{5.18}$$

Fixed Temperature This boundary condition is a constraining type and prescribes either a single temperature or a changing temperature by means of a function to a boundary.

Thin Layer This boundary condition is used to model the sheet pile. A solid material can be considered a boundary when their thickness is considerably thinner than the adjacent domains. The thickness of the sheet pile is assigned as parameter so this is used in the calculation. Three approaches can be chosen: thermally thin, thermally thick and the general approach. The thermally thin approach assumes the layer very conductive while the thermally thick assumes the opposite. The general approach can be used for a multilayer material with both the aforementioned conductivities. As steel is highly conductive, the thermally thin approach is used. The governing equation is:

$$d_s\rho C_{p,s}\frac{\partial T_{soil}}{\partial t} + \nabla_t\cdot\mathbf{q}_s = d_s Q_s + q_0 \tag{5.19}$$

with:

$$\mathbf{q}_s = -d_s k\nabla_t T \tag{5.20}$$

Where d_s is the thickness of the layer [m], ρ is the density of the material [kg/m^3], C_p is the heat capacity [J/(kg $\cdot$ K)], T_{soil} is the temperature [K] and q_s the conductive heat flux [W/m^2], Q_s is the heat source and q_0 the inward heat flux [W/m^2].

Heat Transfer in Pipes

As the 'heat transfer in pipes' package is based on assigning pipe properties to dimensionless lines, the boundary conditions are assigned to points rather than surfaces. Two conditions are applied to both activation loops: at the entrance of the pipes is the temperature of the inflow set and at the exit of the pipe systems is a heat outflow boundary condition assigned. The temperature at the inlet can either be a fixed temperature or a temperature based on a function. The boundary conditions are defined as follows:

Wall Heat Transfer The wall Heat Transfer boundary condition is used to model heat exchange across a pipe. Three different components of the pipe are identified: the internal film resistance, the wall layer and the external film resistance. The film resistance coefficient captures features such as: thermal conductivity, density, external velocity from sources other than the pipe material. The wall layer is used to define the thermal conductivity and wall thickness of the pipe. This boundary condition accounts for the heat transfer between the sheet pile and pipes from the pipes point of view. The radial heat transfer from the surroundings is defined as:

$$Q_{wall} = (hZ)_{eff}(T_{soil} - T_{pipes}) \tag{5.21}$$

Where Q_{wall} is the wall heat transfer [W/m], $(hZ)_{eff}$ is an effective value of the heat transfer coefficient [W/m$^2\cdot$ K], T_{soil} the temperature of the soil [K] and T_{pipes} the temperature of the pipes [K].

Pipe Properties "The Pipe Properties node is used to define the pipe shape, flow resistance, and surface roughness" (COMSOL Multiphysics, 2017).

5.3.4 Definition of the Material Properties

The thermal properties of a material describe the ability to retain and conduct heat. Three properties are assessed in this paragraph: the heat capacity, thermal conductivity and thermal diffusivity. At the end of the paragraph, a table (Table 5.5) is added containing the established values for each material.

Heat Capacity The heat capacity of a material is the amount of heat required to raise its temperature 1 degree (Andersland and Ladanyi, 1994). The heat capacity can be calculated by summing the heat capacity of the different constituents with respect to the amount of material present. Equation 5.22 shows the equation to calculate the heat capacity C.

$$C = \frac{1}{m}(c_s m_s + c_w m_w + c_i m_i + c_a m_a) \tag{5.22}$$

Where C is the heat capacity [kJ/ (kg · K)], m is the total mass [kg] and the subscripts s, w, i and air stand for solids, water, ice and air. Total saturation and unfrozen conditions are assumed simplifying the equation to:

$$C = \frac{1}{m}(c_s m_s + c_w m_w) \tag{5.23}$$

Thermal Conductivity Thermal conductivity is a measure for the ability of a material to transfer heat. Generally, heat transfer is the highest in solids, then liquids and finally gasses. As soil comprises both solids and liquids and usually has a site specific ratio, the thermal conductivity is determined using a theoretical approach described by Andersland and Ladanyi (1994). Equation 5.24 shows the main equation to calculate the thermal conductivity.

$$k_{soil} = (k_{sat} - k_{dry})K_e + k_{dry} \tag{5.24}$$

Where k_{soil} is the thermal conductivity [W/(m · K)], k_{sat} the saturated thermal conductivity [W/(m · K)], k_{dry} the dry thermal conductivity [W/(m · K)]and K_e the Kersten number [-]. The saturated and dry thermal conductivities are calculated as follows:

$$k_{sat} = k_s^{1-n} k_w^n \tag{5.25}$$

$$k_{dry} = \frac{0.137\rho_d + 64.7}{2700 - 0.947\rho_d} \pm 20\% \tag{5.26}$$

where k_s^{1-n} is the thermal conductivity of the solids present in the soil [W/(m · K)], k_w^n the thermal conductivity of water [W/(m · K)], n the porosity [-] and ρ_d the dry density [kg/m^3]. The formula for the Kersten number varies for course-grained and fine-grained soil:

$$K_e = logS_r + 1.0 \;\; (S_r > 0.1) \tag{5.27}$$

$$K_e = 0.7logS_r + 1.0 \;\; (S_r > 0.05) \tag{5.28}$$

Where S_r is the saturation [-]. Fully saturated soils are assumed. Therefore, the Kersten number is equal to 1 and Equation 5.24 simplifies to:

$$k_{soil} = k_{sat} = k_s^{1-n} k_w^n \tag{5.29}$$

Thermal Diffusivity The thermal diffusivity is the ratio between the thermal conductivity and the rise in temperature as a result of this conductivity. The rise in temperature is dependent on the heat capacity and the bulk density of the soil (Andersland and Ladanyi, 1994). Consequently, the equation is:

$$\alpha = \frac{k}{C * \rho} \tag{5.30}$$

where α is the thermal diffusivity [m^2/s], k is the thermal conductivity [W/(m · K)], C is the heat capacity [kJ/(kg · K)] and ρ is the density [kg/m^3].

Overview Thermal Properties Table 5.5 shows the thermal properties of the materials present in the subsurface. These are based on Andersland and Ladanyi (1994), which contains a table in which the thermal properties of a selection of dry materials are presented. These materials include peat, clay, sand. Table 5.5 contains the fully saturated properties based on the Equations 5.23, 5.29 and 5.30.

Table 5.5: Thermal properties of soil types and other components

Material	**Porosity** (n) [-]	**Density** (ρ) [**kg/m^3**]	**Heat capacity** (C_p) [**MJ/(m^3 · K)**]	**Thermal conductivity** (k_u) [**W/(m · K)**]	**Thermal diffusivity** [**m^2 / s**]
Water	-	1000	4.16	0.56	$1.34 \cdot 10^{-4}$
Peat	0.6	1100	3.20	1.25	$6.78 \cdot 10^{-5}$
Silty Clay	0.6	1500	3.50	0.80	$1.60 \cdot 10^{-4}$
Sandy Clay*	0.4	1800	3.10	2.00	$1.60 \cdot 10^{-4}$
Clay	0.6	1400	3.30	0.90	$1.70 \cdot 10^{-4}$
Sand	0.33	1800	3.00	2.59	$1.60 \cdot 10^{-4}$
Steel	0	7850	3.73	44.50	$1.19 \cdot 10^{-2}$

* = The sandy clay consists mostly of sand which has a much higher thermal conductivity than clay. Therefore, there is a large difference with the thermal conductivity of silty clay and clay.
Averaging these thermal properties results in:

Table 5.6: Averaged thermal properties

Material [-]	**Density** [**kg/m^3**]	**Heat Capacity** [**J/(kg · K)**]	**Thermal conductivity** [**W/(m · K)**]
Soil averaged properties	1520	2118	1.51
Steel	7850	475.15	44.5
Glycol-water mixture (20/80)	1024	3833	0.50
Open water	1000	4216	0.56

5.4 Concluding Remarks

This chapter is part of the effort to answer research question 4: 'Can an industry standard finite element method program capture the long-term thermal and mechanical behaviour of an energy sheet pile quay and the subsurface?'. An investigation into the different heat conduction packages that COMSOL offers is carried out. Based on this, the most applicable packages have been selected. Moreover, an investigation into the level of detail necessary for the material component of the model to obtain reliable data has been carried out to make the computation as optimal as possible. The heat conduction model, in combination with the geotechnical stability model described in the next chapter, is validated in Chapter 7, after which the research question is answered.

Chapter 6

Development of the Geotechnical Stability Model

This chapter contains the investigation into the Thermo-Hydro-Mechanical (THM) analysis and the development of the geotechnical stability model in PLAXIS. This is methodological step 3 and is part of the endeavour of answering research question 3: 'Can an industry standard finite element method program capture the long-term thermal and mechanical behaviour of an energy sheet pile quay and the subsurface?'. The research into the workings of the THM analysis is performed to get a better gasp the influence of the thermal component of the computation. A good understanding of this is vital to interpret the computations correctly and compare these to the field test data. This chapter starts with the principles of heat transfer, fluid flow and deformation. Thereafter, an investigation into the workings of the mechanics is undertaken, followed by the description of the material component of the model - described in Section 6.2. This results in a geotechnical stability model. The chapter is finished with concluding remarks.

6.1 Principles of Heat Transfer, Fluid Flow and Deformation

To properly interpret the THM analysis in PLAXIS, a good understanding of the basic principles is necessary. This section holds the basic principles of heat transfer, fluid flow and deformation of the soil.

6.1.1 Heat Transfer

The heat transport is based on conduction, convection and radiation; described in the previous chapter.

6.1.2 Saturated Water Flow

The flow of water in saturated soil is described using Darcy's law. This formula is:

$$Q = -k \cdot A \cdot i \tag{6.1}$$

Where Q is the total discharge [m^3/s], k the hydraulic conductivity [m/s], A the area of the soil domain [m^2] and i the hydraulic gradient (dh/dl) [-].

6.1.3 Deformation

The way a soil deforms in a finite element calculation is based on the constitutive model chosen for the soil. The constitutive model is the relationship between stress and strains. Terzaghi's principle gives a definition of stress and the strain is the change in soil volume as a result of this.

$$\sigma_{tot} = \sigma' + u \tag{6.2}$$

$$\epsilon = \frac{V}{V_{ini}} \tag{6.3}$$

Where σ_{tot} is the total stress [kPa], σ' the effective stress [kPa], u is the pore pressure [kPa], ϵ is the strain, V is the soil volume and V_{ini} the initial volume [-].

6.2 Investigation of the Mechanics of a Thermal-Hydro-Mechanical Analysis

In order to properly model and interpret the behaviour of the soil and sheet pile under thermal loading, a good understanding of the mechanics is indispensable. This section contains an investigation into the mechanics. It starts with the explanation of the basic model used. Secondly, the time-dependent modelling of a Hydro-Mechanical analysis is investigated. The thermal component is added to the model once we have a good understanding of the HM analysis. This section is finished with an overview of conclusions and recommendations for a Thermal-Hydro-Mechanical (THM) analysis.

6.2.1 The Definition of Governing Equations in PLAXIS

In agreement with the heat conduction model, the geotechnical stability model is defined using PLAXIS, an industry standard finite element program. This program allows for the engineer to model the geometry, define initial and boundary conditions, the material properties and the staged construction. Based on the goal set for each staged construction, e.g. a plastic analysis, the program uses pre-defined governing equations. Therefore, these do not have to be defined by the engineer. Appendix B contains the governing equations for the thermal, saturated fluid flow and deformation analysis.

6.2.2 Setup Used in the Investigation

As a starting point for investigating the mechanics of the Thermal-Hydro-Mechanical analysis, a simple model is assembled. It consists of sand modelled with the constitutive model HSsmall. The length and type of sheet pile (named: ZZ 17-700) as well as the parameters of the sand (named: Sand Top Layer) can be found in Appendix C. The model is plain-strain. This model is only used in the investigations. To answer the main and research questions a different model, based on the investigations, is developed and described in Section 6.3. The geometry is constructed in three stages:

1. The domain consists of sand on which a k0 procedure is applied to determine the in-situ stresses.
2. a sheet pile is placed after which the sand is excavated on one side. The excavation does not have a horizontal bottom, close to the sheet pile the canal is less deep. The height difference is bridged by a slope.
3. The water domain is added which is necessary to model the temperature of the soil under the canal realistically. The water is treated like a solid in order to reproduce the thermal behaviour. However, since the mechanical behaviour of water cannot be represented by a solid, special mechanical and thermo-mechanical parameters are chosen to rule out the solid like behaviour of the water. The characteristics of this material can be found in Table 6.1 and contains the improvements resulting from the following investigation.

A horizontal phreatic line is added and applies to the whole domain. The phreatic line lies 20 centimetres below the surface, in both the soil and water domain. A picture of the model is shown in Figure 6.1.

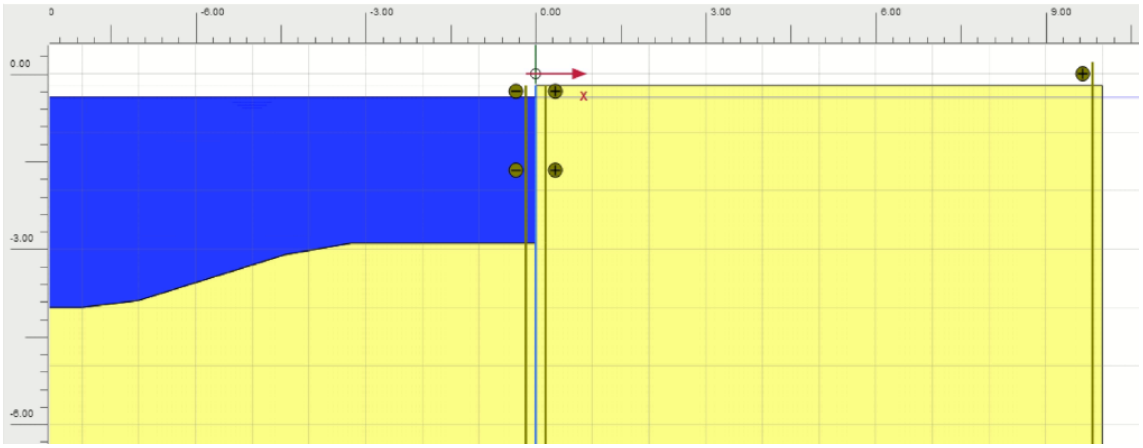

Figure 6.1: A picture of the setup of the test model for a plain-strain THM analysis.

Table 6.1: Strength and thermal properties of the water.

Parameter	Value
Volumetric weight γ/γ_{sat}	10/10 kN/m^3
Stiffness E'	1 kN/m^2
Poisson's ratio ν	0.499
Heat capacity C_p	418.6E3 kJ/(t · K)
Thermal conductivity λ_s	2 kW/(m · K)
Density ρ_s	0.01 t/m^3
Thermal expansion coefficient α_s	0 1/K
Thermal resistance R	0.1340 m^2·K/kW

Two chosen values deserve an additional explanation: the thermal conductivity and thermal expansion coefficient. The former is assumed 2 kW/(m · K) because the water in the canal has a small but continuous velocity, thereby keeping its temperature rather than cooling down as a result of the energy extraction. By means of thermal boundary conditions, the water domain is forced to take its realistic temperature. The thermal expansion coefficient is set to zero. The water domain is considered infinitely large; therefore, the shrinkage/expansion of the water is zero as it levels out over an infinitely large area. Moreover, if the domain changes volume, it causes stresses on the soil and sheet pile instead of flowing around them.

6.2.3 Investigation of the Time-Dependent Hydro-Mechanical Analysis

The investigation is started with a non time-dependent analysis which serves as a benchmark calculation and to see whether the settings are correct. The deformation of the tip of the sheet pile with and without the water domain is 0.044 and 0.046 millimetre, respectively. These deformations are very small as the sheet pile is long and the domain consists of sand. This situation is chosen for sake of simplicity, as mechanical failure of the sheet pile and soil do not pose a risk.

A time-dependent analysis, simulating a time span of 30 days and without a water domain, results in a maximum sheet pile deformation of 0.029 millimetre. As verification, a 1000 days time-dependent analysis resulted in a deformation of 0.044 millimetre in which the sheet pile distortion looks the same. This is in line with expectations as there is no consolidation or other time dependent influence which alters the state of the soil. With the water domain, the maximum deformation is 0.023 millimetre, a difference of 0.006 millimetre resulting from stabilizing influence from the water on the sheet pile. An overview is given in Table 6.2. The deformations are so small that they could be considered zero. This is expected as the sheet pile is embedded along 12 metres by very stiff sand.

In the analysis, the domain simulating the water changes slightly in volume. In order to fix the volume of the water domain, Poisson's ratio is set to 0.499, the highest value possible. To prevent deformations it is important to let the water domain end at the same height as the phreatic line. By setting the volume weight of the water to 10 kN/m^3, buoyancy is prevented from happening by cancelling out the up- and downward pressures out. Figure 6.2 shows the result of the analysis, amplified 20000 times.

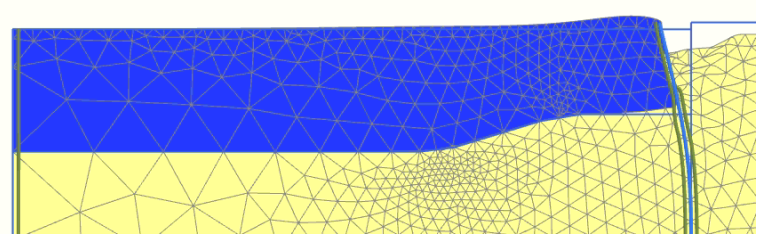

Figure 6.2: Deformation of the water domain with a volumetric weight of 10 kN/m^3. The maximum soil deformation is 0.065 millimetre and the picture is scaled up 20000 times.

Table 6.2 provides an overview of the analyses made. Compared to the initial time-dependent analysis, the absolute errors are in the order of thousandth decimals - which are acceptable differences. Moreover, running the same calculation for 1000 days results in the same error margin proving the correctness of the analysis.

Table 6.2: Maximum deformation of the top of the sheet pile.

Analysis	**Time [Days]**	**With water [mm]**	**Without water [mm]**
Non-time dependent; Benchmark	-	0.044	0.046
Time-dependent; initial	30	0.037	0.049
Time-dependent; initial	1000	0.037	0.044
Time-dependent; improved	30	0.047	0.049
Time-dependent; improved	1000	0.042	0.044

The improved time-dependent analysis results in a larger deformation than the benchmark and initial analyses. Yet, these deformations are still close to negligible. As a result, these improvements are incorporated.

6.2.4 Investigation of the Time-Dependent Thermal-Hydro-Mechanical Analysis

With the HM analysis verified, the thermal component is activated in the computation. To develop a better understanding of the thermal component the following learning objectives have been formulated and are explored with the verified basic HM model.

- Learning objective 1 - Interpretation of the movement of the sheet pile
- Learning objective 2 - Sensitivity analysis of the thermal properties
- Learning objective 3 - Required level of detail of the model

Item 1 continues the previous analysis: interpreting and understanding the mechanics and; consequently, identifying issues and solving those issues. Now that a basic single soil type THM model is assembled, additional investigations are performed such as a sensitivity analysis on the thermal properties and a investigation of the behaviour of different soil types under thermal loading.

By adding a thermal line load to the model, the sheet pile is thermally activated over the whole length. A constant temperature of 2 °C is applied, while the soil domain is initially uniformly 12 °C. As no ambient temperature is applied the default boundary condition, which is a closed boundary, works on the soil surface. The boundary conditions at the sides are closed as well and at the bottom of the geometry the temperature is fixed at 12 °C.

As a result of the thermal activation, large expansions of small volumes of soil occur - both with and without a water domain. Figure 6.3 shows this at the interface between the water, soil and sheet pile. Additional investigation shows this location is subjected to a large thermal gradient, as at t=0^+ the temperature changes in the direct vicinity from 12 to 2 °C. This is remedied by ramping the temperature of the sheet pile. In case of domain consisting of sand, the necessary amount of time required differs per situation: when the water domain is present, the ramp up needs a minimum of 1 hour (=0.0416 days) to avoid deformations. When no water domain is present, this minimum ramp duration has to be 1.5 hour. This change is due to the colliding effects of the water. The unrealistically high thermal conductivity cools down the canal bottom quickly, thereby reducing the thermal gradient faster from multiple directions than when no water is present. When another soil type is present, this ramping up time is different. Therefore, it is advised to investigate this for each new calculation.

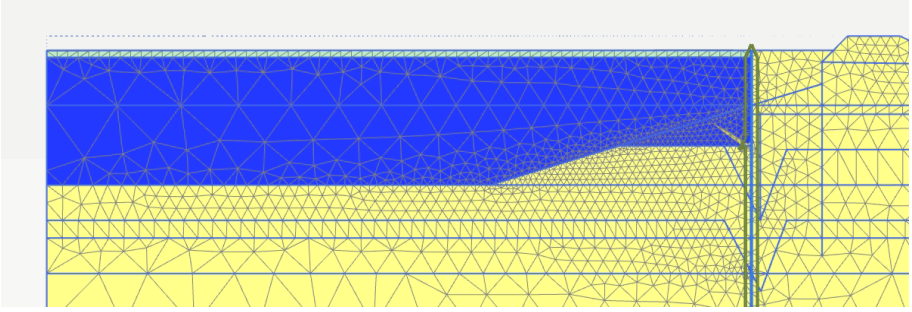

Figure 6.3: Deformation of the soil at the water-soil-sheet pile interface of 12 metre. The picture is amplified by 0.2.

Activating the thermal component results in the deformation shown in Table 6.3. The close to similar results between a HM and THM, in which a line boundary condition with a temperature of 12 degrees is used, shows that the boundary has no influence other than a temperature change of the soil and sheet pile in the computation. The difference between the HM and (2 °C) THM analysis is a factor 10. This deformation is large, but within an acceptable range. In addition, the numerical behaviour of the analysis is working as supposed. Therefore, this outcome is deemed acceptable.

Table 6.3: Maximum deformation of the sheet pile.

Analysis	**Temperature [°C]**	**With water [mm]**	**Without water [mm]**
Non-time dependent Benchmark	-	0.044	0.046
Time-dependent HM	-	0.047	0.049
Time-dependent THM	12	0.038	0.038
Time-dependent THM	2	4.6	4.0

Learning Objective 1 - Interpretation of the behaviour of the Sheet Pile

Interpretation of the movement of the Sheet Pile Key to interpreting the behaviour of the sheet pile is understanding the movement as a result of the thermal loading. Analysing the THM simulation in the basic model in PLAXIS, the following sheet pile behaviour is identified:

Table 6.4: Deformation of the sheet pile at various intervals. Negative x is towards the canal and negative y is into the soil.

Time [days]	$\mathbf{u}_{x,top}$ **[mm]**	$\mathbf{u}_{y,top}$ **[mm]**	$\mathbf{u}_{x,bottom}$ **[mm]**	$\mathbf{u}_{y,bottom}$ **[mm]**
1	$-3.6 \cdot 10^{-3}$	-0.025	$-0.3 \cdot 10^{-3}$	-0.015
2	-2	-1.5	-0.05	0.2
5	-2.5	-1.65	-0.1	0.05
10	-1.6	-1.85	-0.06	-0.075
20	-1.8	-2.1	-0.1	-0.26
30	-2.05	-2.3	-0.12	-0.46

The data in Table 6.4 shows that the sheet pile moves upward at first after which it sinks almost 0.5 millimetre. In horizontal direction, the sheet pile moves back and forth and at t = 30 days the deformation is 2.05 millimetre into the canal.
Resulting from making the sheet pile a heat sink, the soil cools down and, consequently, shrinks. Theoretically, with the adjacent soil retreating, the active and passive forces working on the sheet pile decrease. In addition, as the soil in the quay cools down it is expected to shrink and the water in the canal has a Poisson's ratio of 0.499 (i.e. a fixed volume), one would expect that the sheet pile experiences little pressure from the soil in the quay as it retracts. However, as shown in Table 6.3, a deformation of 4.6 millimetre results from thermal loading. This is due to the soil shrinking but not holding its original shape - it still pushes on the sheet pile.

As the water is highly conductive hence cools down fast, the cold is quickly spread out in horizontal direction resulting in a relatively large volumetric strain in the whole canal bottom. In the quay, the thermal conductivity is much lower, thereby limiting the volumetric strain to the vicinity of the sheet pile. This is pictured in Figure 6.4.

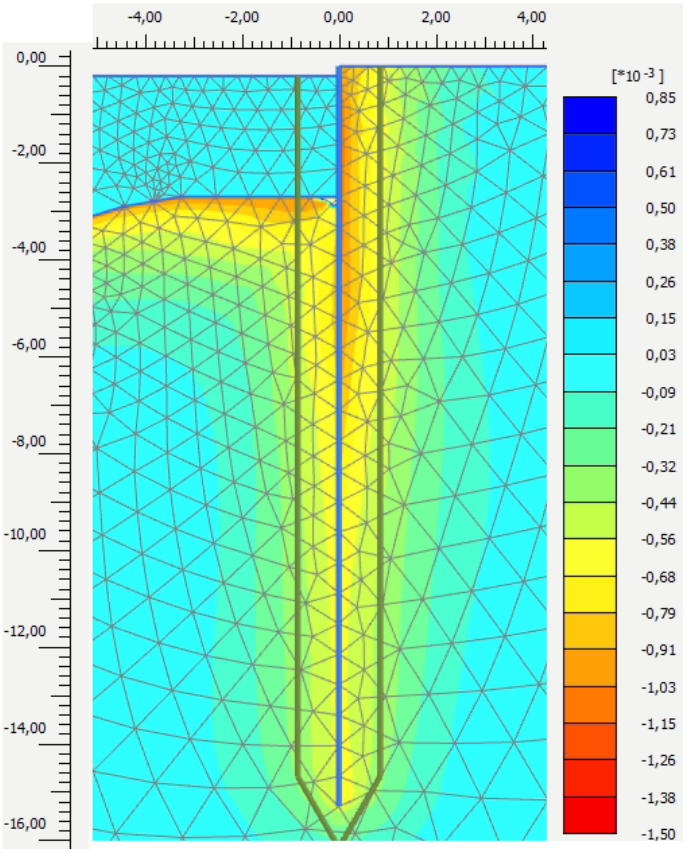

Figure 6.4: The strains of the soil as a results of the thermal activation at t = 30 days.

Analysing the change in volumetric strain over time, the strain gets progressively larger with time but gives no explanation for the direction movement of the sheet pile. Instead, the forces on the sheet pile are explored to explain the behaviour.

Interpretation of the Forces on the Sheet Pile Three forces are working on the sheet pile: an axial force, a shear force and a bending moment. The axial force is the force working on the sheet pile in the longitudinal direction on the sheet pile. The shear force is the force working perpendicular on the sheet pile. The bending moment is the reaction of the sheet pile on an external force or moment causing bending. As can be seen in Table 6.5, the axial forces are the only forces that notably change over time. At t = 1 day, the large positive force works on the lower part of the sheet pile which gets progressively smaller while the negative forces working on the top become more negative. This is shown in Figure **??**. The sheet pile capacity can be found in Table 6.6.

Table 6.5: The forces working on the sheet pile.

Time [days]	**Axial force (min - max) [kN/m]**	**Shear force(min - max) [kN/m]**	**Bending moment (min - max) [kNm/m]**
1	-10.72 - 40.44	-12 - 16	-1.6 - 30.8
2	-11.42 - 31.9	-12 - 16	-1.6 - 31.4
5	-14.5 - 15.5	-12.5 - 16	-1.7 - 32.7
10	-21.2 - 0.2	-12 - 16	-2 - 33.6
20	-30.5 - 0	-12 - 16	-2.2 - 34
30	-37.45 - 0	-12 - 16.5	-2.4 - 34

Table 6.6: The characteristics of the sheet pile type ZZ 17-700.

Value	Unit	Wall	Single	Double
Elastic resistance moment	cm^3	1735	1207	2415
Moment of inertia	cm^4	36425	25367	50735
Weight	kg/m	104.7	73.3	146.6
Coating surface	m^2/m	2.82	1.97	3.94
Steel cross section	cm^2	132.8	92.99	185.98

The negative axial force working on the top of the sheet pile indicates that the top layer soil layers transfers force to the wall while the positive force on the sheet piles show that the deeper layers resist the movement of the wall. At the top, the soil sinks more than the wall and at the bottom of the wall vice versa. With thermal activation, the whole package shrinks and sinks more than the wall, causing the soil to hang on the wall everywhere.

Concluding Remarks Two aspects of the sheet pile behaviour are studied: the movement and the forces in a sand domain. The positive and negative forces on the sheet pile result from the soil pulling and pushing. As a result of the thermal activation, the soil pulls uniformly due to the negative strain it experiences. When soils have a lower volumetric weight, the aforementioned extension occurs less distinct, and with a volumetric close to that of water, the behaviour does not show at all.

Learning Objective 2 - Sensitivity Analysis Thermal Properties

It's well known among engineers that the outcome of any model is only as good as the input. Therefore, having a feel for realistic parameters and the way they react is vital for a good analysis. This section holds a sensitivity analysis for three thermal parameters: heat capacity, thermal conductivity and the thermal expansion coefficient. Each parameter is varied by 25% to investigate the influence on the maximum sheet pile deformation and the heat flux from the sheet pile on the soil in direct contact.

The following hypothesis is defined for this analysis: it is expected that the thermal expansion coefficient has the most influence on the deformation of the sheet pile and the thermal conductivity influences the temperature change in direct vicinity of the sheet pile the most - thereby changing the soil volume. The heat capacity, which indicates the amount of energy necessary to raise the temperature of 1 kilogram of soil by 1 degree, governs the overall temperature change of the soil and is a very important parameter in the analysis of how much energy can be extracted but less so in a stability analysis. Concluding, the expectation order is, from most to least influence: thermal expansion coefficient, thermal conductivity and thermal capacity.

Sensitivity of the Heat Capacity Table 6.7 contains the sensitivity analysis for the heat capacity of the sand. With the variation of 25%, the deformation varies approximately 0.2 millimetre and the heat flux range shifts 0.7 - 0.75 W/m^2. This translates to a 4% deformation and an 8% heat flux change.

Table 6.7: Results of varying of the heat capacity by 25%.

Percentage	Value [kJ/(t · K)]	Deformation sheet pile [mm]	Heat flux [W/m^2]
100	1667	4.685	8.9 - 10.25
125	2083.75	4.489	9.6 - 11
75	1250.25	4.857	8.2 - 9.5

Sensitivity of the Thermal Conductivity The analysis of the thermal conductivity is displayed in Table 6.8. The variation in the deformation as a result of raising and lowering the thermal conductivity is 0.215 and 0.250, respectively. The heat flux range is 0.4 - 0.6 W/m^2 higher when the thermal conductivity is 25% higher and 1.95 - 2 W/m^2 lower when lowering the conductivity. Two additional analyses are performed because a non-linear increase is identified. The thermal conductivity (2.59 W/m^2) is increased and decreased by 50% and shown in Figure 6.5. As this graph shows, the heat flux increases linearly with increasing thermal conductivity, except at a conductivity of 2.59 $W/(m \cdot K)$. This explains the aforementioned observations.

Table 6.8: Results of varying of the thermal conductivity by 25%.

Percentage	Value [W/(m · K)]	Deformation sheet pile [mm]	Heat flux [W/m^2]
50	1.295	4.129	6.5 - 7.6
75	1.94	4.435	7.25 - 8.4
100	2.59	4.685	9.2 - 10.4
125	3.24	4.900	9.6 - 11
150	3.885	5.053	10.8 - 12.1

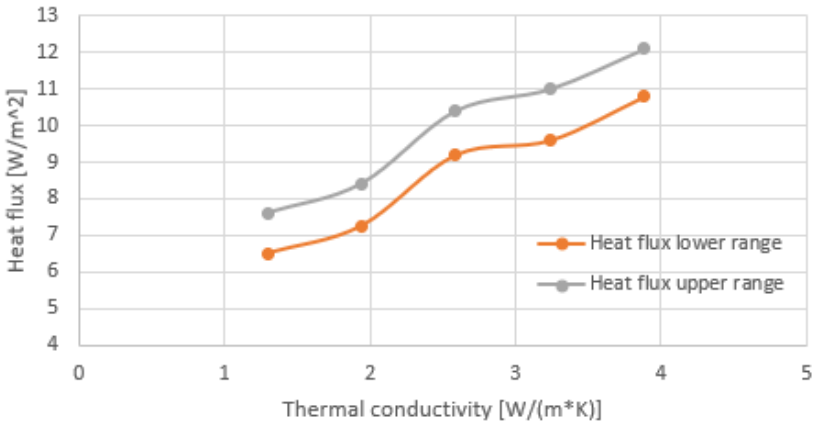

Figure 6.5: The heat flux from the sheet pile on the soil with increasing thermal conductivity.

Sensitivity of the Volumetric Thermal Expansion Coefficient Table 6.9 holds the values acquired in the sensitivity analysis for the thermal expansion coefficient. At the start of this analysis, the expectation that this variable has the largest influence on the sheet pile deformation is taken as hypothesis. The values confirm expectations: an approximate 1 millimetre change occurs when the thermal expansion coefficient is altered by 25%. The heat flux as a result of the thermal activation does not change. This can be easily explained by the fact that the thermal expansion coefficient does not influence the amount of energy that soil can absorb or conduct.

Table 6.9: Results of varying of the volumetric thermal expansion coefficient by 25%.

Percentage	Value [1/K]	Deformation sheet pile [mm]	Heat flux [W/m^2]
100	0.1e-3	4.685	8.9 - 10.25
125	0.125e-3	5.547	8.9 - 10.25
75	0.075e-3	3.685	8.9 - 10.25

The aforementioned hypothesis in which the expected order of influence on the deformation is: the thermal expansion coefficient, thermal conductivity and thermal capacity (from high to low) is proven correct. Furthermore, the relation between the deformation and the thermal properties; and the heat flux and thermal properties is more or less linear.

Averaging Thermal Properties Building on the observation that the averaging of the soil properties has little influence on the temperature behaviour in the soil, this analysis is extended to the geotechnical stability model in PLAXIS 2D. Up to this moment, the whole soil domain consists of sand. If other soil types are introduced, the behaviour of the sheet pile and the temperature change is different. The updated model consists of peat up to a depth of 5 metres. Below that, there is a 5 metre clay layer and the lowest part of the stratigraphy consists of sand.

Two analyses are performed, one in which the different soil types have individual thermal properties and one in which these properties are averaged. In contradiction to the analysis in Chapter 5, this research considers the mechanical behaviour as well. Only the thermal properties are investigated.

Based on the aforementioned findings in the sensitivity analysis, it is expected that averaging the thermal properties has an effect on the behaviour and performance of the sheet pile. As is found, the thermal expansion coefficient has an influence on the distortion of the sheet pile and, to a lesser extend, the thermal conductivity governs the temperature change in the soil influencing the expansion/shrinkage indirectly. Table 6.10 shows the outcome of the analyses.

Table 6.10: Results of the investigation into averaging thermal properties in a THM analysis.

Type	**Max. deformation [mm]**	**Max. axial force** [kN/m]
Non-averaged	4.53	-30.2
Averaged	5.83	-50

It's clear that the non-averaged and averaged thermal properties result in different deformations and axial forces. Therefore, it is concluded that it is necessary to define the thermal properties for each layer separately - proving the hypothesis to be correct.

Table 6.11: Averaged thermal properties

Parameter	**Value**
Density	1.52 t/m^3
Heat capacity	2311 kJ/(m $\cdot$ K)
Thermal conductivity	0.0016 kW/(m $\cdot$ K)
Volumetric thermal expansion coefficient	$3.37 \cdot 10^{-4}$ 1/K
R	5.06 m^2 $\cdot$ K/kW

Learning Objective 3 - Required level of detail of the model

As part of the investigation into the workings of the thermal component of the computation, the required level of detail for the initial temperature distribution of the soil is investigated. The hypothesis is that it has to be as detailed as possible, as the temperature changes induce volumetric changes, thereby loading the sheet pile.

Two types of thermal boundary conditions to simulate thermal activation of the sheet pile are investigated: a constant temperature and a constant heat flux. These two differ in the way that the line on which the boundary condition works is a constant temperature and it (in this case) cools down its surroundings. The heat flux boundary condition simulates a heat sink or source,the former in this investigation, and extracts energy with a fixed rate from the surroundings. Therefore, the latter boundary condition is much more susceptible to initial amounts of energy in the soil. Based on the analysis of the soil temperature distribution described in Chapter 4, an initial temperature distribution is modelled and compared to an initial overall 12 °C domain. It is determined this has noticeable influence. In addition, a boundary condition working as ambient temperature on the soil is investigated as well. This condition, simulating the air temperature, works on all outer boundaries of the simulated soil. Consequently, this works on the bottom of the canal too if water is not simulated. To investigate the impact of the air temperature, the presence of water and climate is investigated as well. This computation's initial temperature distribution is based on the analysis in Chapter 4. Table 6.12 holds the maximum deformation of the sheet pile for all different combinations.

Table 6.12: Averaged thermal properties

Sheet pile boundary condition [-]	**Climate boundary condition** [-]	**Water present [mm]**	**No water present [mm]**
Temperature	No	3.9	3.6
Temperature	Yes	3.9	3.8
Heat flux	No	4.7	3.7
Heat flux	Yes	4.6	4.0

According to expectations, the initial conditions have considerable influence, just like the presence of a water domain and the climate boundary condition. The difference in deformations are the largest when a heat flux is applied on the sheet pile. Therefore, it is advised to use the a water domain and climate boundary condition in all computations.

6.2.5 Concluding Remarks for a Thermal-Hydro-Mechanical Analysis

In this section the following conclusions have been drawn:

- The water domain is necessary to control the temperature in the soil in direct contact with the canal. By assigning a (unrealistically) high thermal conductivity to the material a uniform temperature is achieved.
- Make the water domain 10 kN/m^3 so buoyancy is cancelled and the soil underneath the canal isn't loaded. The water domain needs to consist of a very soft (E = 1 kPa) material to minimize stabilizing effects of the soil on the sheet pile. To prevent settlement and loads on the sheet pile due to shear, the material in the water domain needs to have a fixed volume with a fixed volume (i.e. Poisson's ratio = 0.5).
- Use a ramp up for the temperature in the thermal activation dependent on the presence of a water domain and the volumetric weight of the soil.
- The presence of water domain has a positive influence on the temperature in the soil and; therefore, the strains. Adding the water domain makes it possible to give the soil under and adjacent to the canal a different temperature than the air temperature.
- Thermal expansion coefficient has the largest influence on mechanics of the sheet pile.

6.3 Defining the Domain and Material Characteristics of the Geotechnical Stability Model

This section contains the description of the material component of the model. It starts with the description of the staged construction and geometry, followed by the investigation into the mesh convergence. Next, the applied boundary conditions are described and finally, the material properties are defined.

6.3.1 Description of the Staged Construction and Geometry

This section holds the description of the phasing in PLAXIS, displayed in Figure 6.6.

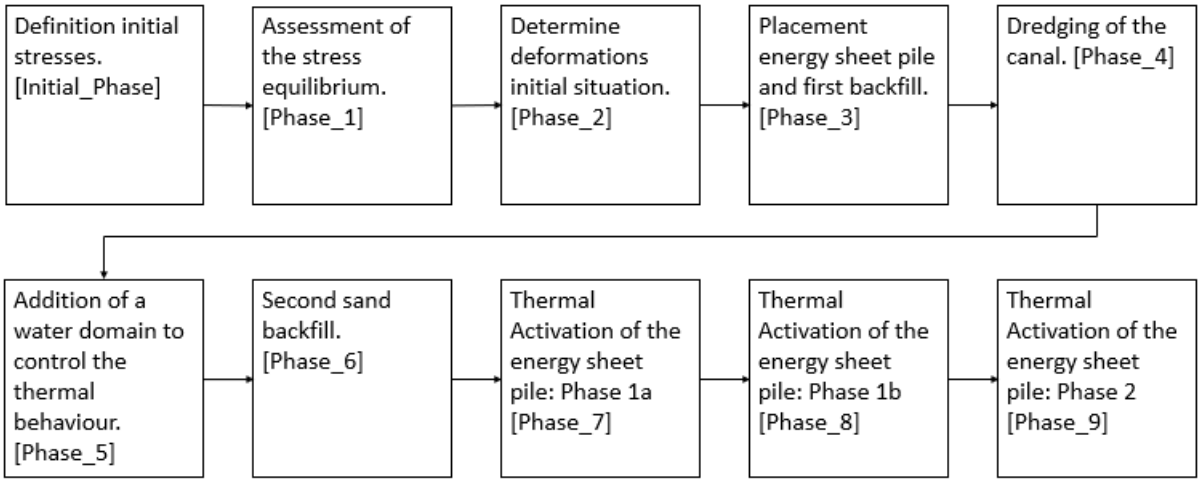

Figure 6.6: Overview of the staged construction.

Definition of the Initial Stresses

The staged construction consists of eight phases in which the geometry is constructed and assessed. The first three phases is a 'K0 procedure'. The K0 procedure generates the initial effective stresses, pore pressures and state parameters and uses these to calculate the horizontal stresses, hence the name of phase. However, this phase is only applicable to a levelled ground surface, which is not the case here, thus raising the need for an extra phase to determine the horizontal stresses. The constitutive soil model for the whole domain is HSsmall. More information about the settings and parameters can be found in Section 6.3.4.

Assessment of the Stress Equilibrium

The first plastic calculation, named the '0-step', calculates the in situ initial deformations (without loads) thereby determining whether the horizontal forces are in equilibrium. The top sand layer, consisting of sand, fails because

current wooden sheet pile is not modelled. The absence of the sheet pile results in a vertical slope. To deal with this, the sand layer is assigned to have a cohesion of 5 kN/m^2.

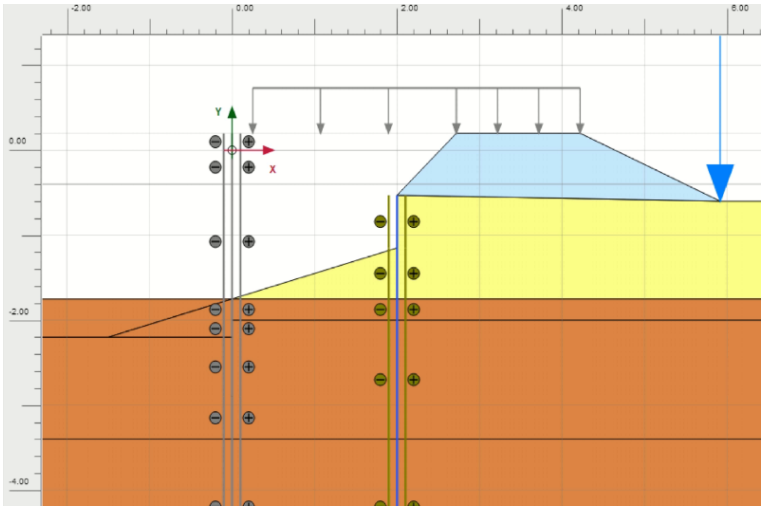

Figure 6.7: The initial situation of the quay

Determining the Deformations in the Initial Situation

A second deformation calculation is performed in which the original situation is modelled. A wooden sheet pile serving as bank protection of the current quay is included as well as the characteristic load of the adjacent road. The cohesion of the sand behind the sheet pile is reset to zero. Figure 6.7. Figure 6.7 shows the initial situation. After this stage the displacements and strains are set to zero.

Placement of the Energy Sheet Pile and First Backfill

The first phase after the initial situation is the placing of the energy sheet pile approximately two metres away from the current quay in the canal. The space between the quay and energy sheet piles is filled with sand and a characteristic load is applied. A deformation assessment is carried out to prove this situation is stable.

Dredging of the Canal

After resetting the displacement and small strain to zero, the dredging of the canal bottom adjacent to the sheet pile to a depth of NAP -2.2 metres is modelled. The result can be seen in Figure 6.8. After this stage the displacements and strains are set to zero.

Addition of the Water Domain

The water domain is activated to the computation of which the surface lies 0.8 metres below the ground surface. After this stage the displacements and strains are set to zero. In addition, a uniform temperature distribution of 12 °C throughout the whole domain is simulated.

Second Sand Backfill

A second sand backfill is added. A layer of 0.25 metres is added behind the sheet pile wall. After this stage the displacements and strains are set to zero. The initial temperature distribution based on the analysis of the thermistor strings in Chapter 4.

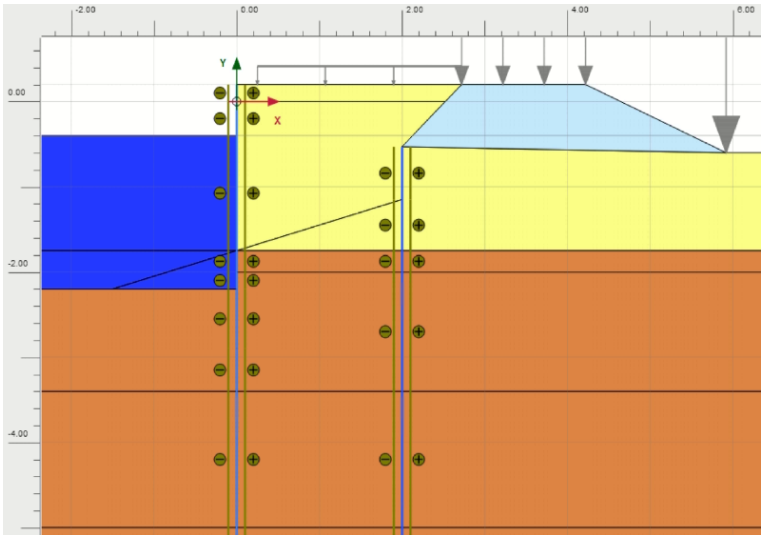

Figure 6.8: The situation after the energy sheet pile has been placed with the energy sheet pile at the utmost left and the wooden sheet pile at the toe of the dike.

Thermal Activation of the Energy Sheet Pile: Phase 1a

A fully coupled transient thermo-hydro-mechanical (THM) calculation is performed. The shallow section of the energy sheet pile wall is activated and lasts for 32 days. The temperature distribution, defined in the previous phase, is the initial condition after which the sheet pile spreads a temperature variation over time. The hydraulic assessment consists of a pore pressure calculation based on the phreatic level for each time step. Parallel to both calculations, a mechanical analysis of the sheet pile and soil is performed. All the stresses induced by the soil, temperature and pore pressures on the soil and sheet pile are assessed.

Thermal Activation of the Energy Sheet Pile: Phase 1b

Phase 1b is simulated in which the single side deep activation is modelled. This phase lasts for 17 days.

Thermal Activation of the Energy Sheet Pile: Phase 2

Phase 2 in which the double deep side is activated is simulated in this stage. This phase lasts for 36 days.

Geometry

The geometry in PLAXIS 2D has a total width of 30 metres, with the energy sheet pile located at x = 0 metres. The depth goes to -30 metres and the stratigraphy is based on the soil profile described in Chapter 4. Two sheet piles are present, the pre-existing wooden sheet pile wall and the energy sheet pile wall. The wooden sheet pile is 6 metres deep and the energy sheet pile wall 15.5 metres. Figure 6.9 shows the geometry of the PLAXIS 2D model.

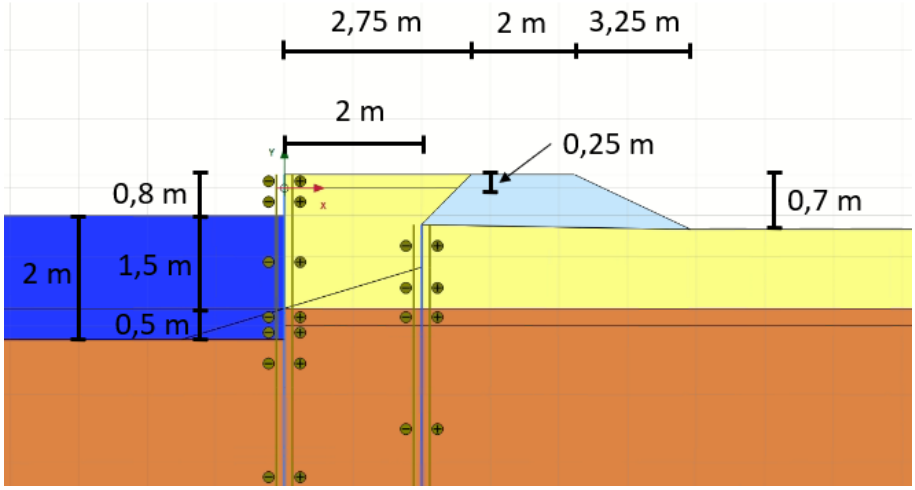

Figure 6.9: The geometry of the PLAXIS 2D model.

6.3.2 Mesh Convergence

As proper use of a finite element program dictates, the mesh convergence has to be analysed to ensure a correct output. Like COMSOL, PLAXIS has predefined choices for mesh coarseness. The options are: very coarse, coarse, medium, fine and very fine. To assess which coarseness is necessary, the temperature has been measured 0.1 metres behind the sheet pile at a depth of NAP -1.65 metres. Figure 6.10 shows three tested coarsenesses: coarse, medium and fine. As can be seen, the medium and fine mesh output are practically the same; therefore, one can state convergence has been achieved with the medium mesh coarseness.

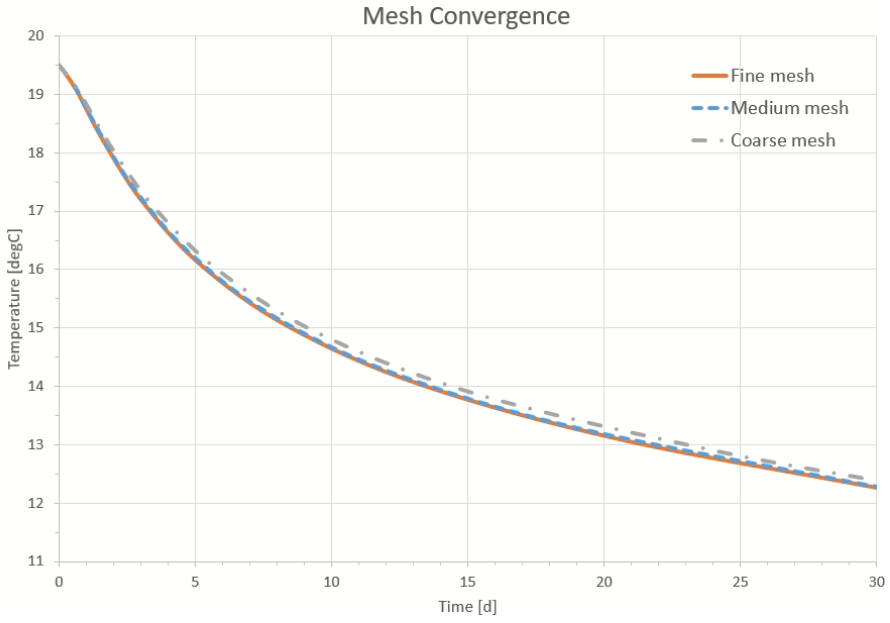

Figure 6.10: The output of the three mesh coarsenesses that have been tested.

6.3.3 Boundary conditions of the Model

Two types of boundary conditions have been assigned: thermal and hydraulic conditions. This section gives an overview of both.

Thermal Boundary Conditions

To predict the deformation of the sheet pile wall as accurately as possible, a temperature distribution and behaviour that is as close to reality as possible is essential. Therefore, the following boundary conditions are applied.

Thermal insulation The verticals of the model, left and right, are thermally insulated.

Temperature The bottom of the model has a uniform fixed temperature of 12 °C which is activated throughout the calculation. At a depth of approximately NAP -6 metres, a fixed temperature of 12 °C is set as well. This condition is only activated when the initial temperature distribution is defined, as it is the boundary of the heat penetration under influence of the climate. This boundary condition is also used to control the colliding characteristics of the sheet pile as well, by fixing the temperature at 12 °C until the THM analysis is started. In addition, in this analysis the temperature change of the sheet pile as a result of the thermal activation is modelled with the help of this boundary condition.

Convection This boundary condition is used to transfer heat or cold from a medium to the adjacent material. This is applied in this model as climate condition, which is used to let the air temperature influence the soil temperature as happens in the field test. Convection allows for a time dependent increase or decrease of the temperature by means of the functions outlined in Section 6.3.4.

The convection boundary condition requires a heat transfer coefficient. This coefficient is the proportional constant between the heat flux and thermodynamic driving force for the heat flow (i.e. the temperature difference). Therefore, the value is defined as follows:

$$h = \frac{q}{\Delta T} \tag{6.4}$$

Where h is the heat transfer coefficient [kW/m^2/K], q is the heat flux [kW/m^2] and ΔT the temperature difference [K].

Hydraulic Boundary Conditions

While determining heat conduction model, described in Chapter 5, the aim of modelling the (ground)water flow is motivated by the desire to predict the temperature extraction as precisely as possible. In the determination of the baseline geotechnical stability model, the focus lies on the loads induced by the pore pressures rather than the temperature change. Therefore, the pore pressures are based on the phreatic level only.

Seepage The account for the possibility of groundwater entering or exiting the model due to changes in density, the left and right hand side have open boundary conditions named seepage. This condition allows water to flow freely in and out the model.

Closed At the bottom of the model a closed boundary condition applied. No water is allowed to flow in or out the model.

6.3.4 Definition of the Strength and Thermal Properties

This section contains the definition of the strength and thermal properties used in the soil stability model. First, the used material model for the soil is discussed. Subsequently, the role of water in soil behaviour is elucidated, the thermal properties of the materials are defined and finally the thermal functions are described. The explanation of the material models and drainage type are based on Brinkgreve (2019) lectured at Delft University of Technology.

Material Model - HSsmall Model

A constitutive model, otherwise known as a material model, aims to describe the mechanical behaviour of soil in a relationship between stress and strain. The hardening soil (HS) model is based on the idea that the stress-strain relationship in a drained triaxial test can be approached by a hyperbolic function. In addition, it's based on hardening plasticity in combination with the Mohr-Coulomb failure behaviour. The model is characterized by stress-dependent stiffness behaviour, a hyperbolic stress-strain relationship in axial compression, shear and compaction hardening and elastic unloading/reloading. In addition, an improved version, the hardening soil small strain (HSsmall) model, includes a small-strain stiffness relation which provides the ability to model the high small-strain stiffness to low large-strain stiffness.

The HSsmall model has thirteen model parameters, four of which are reference stiffness parameters:

1. E_{50}^{ref} = the secant stiffness from triaxial test at reference pressure;
2. E_{oed}^{ref} = the tangent stiffness from oedometer test at the reference pressure;
3. E_{ur}^{ref} = the reference stiffness in unloading/reloading;
4. G_{0}^{ref} = the reference shear stiffness at small strains;

Other parameters are:

5. $\gamma_{0.7}$ = the shear strain at which G has reduced to 72.2%;
6. m = the rate of stress dependency in stiffness behaviour;
7. p^{ref} = the reference pressure;
8. ν_{ur} = Poisson's ratio in unloading/reloading ($-d\epsilon_3/d\epsilon_1$);
9. c' = is the cohesion;
10. ϕ' = the friction angle;
11. ψ = the angle at which the grains, of which the soil consists, dilate when the soil shears;
12. R_f = the failure ratio q_f/q_a;
13. K_0^{NC} = the stress ratio $\sigma_{xx}'/\sigma_{yy}'$ in 1D primary compression.

The HSsmall model has the following advantages and possibilities compared to Mohr-Coulomb:

- Better non-linear formulation of soil behaviour in general (both soft soils and harder types of soil);
- Distinction between primary loading and unloading/reloading;
- Memory of pre-consolidation stress;
- Different stiffnesses of different stress paths based on standard tests;
- Well suited for unloading situations with simultaneous deviatoric loading (excavations);
- Large stiffness at small strain levels (vibrations) (HSsmall only).

However, it also holds some limitations and disadvantages:

- No peak strength and softening;
- No accumulation of strain or pore pressure in cyclic loading;
- No secondary compression;
- No anisotropy;
- The model has difficulties to account for very soft soils where the ratio $E_{50}^{ref}/E_{oed}^{ref} > 2$.

Plates

Two plates are defined in the model, one used to model the existing wooden sheet pile and the other for the energy sheet pile. The properties of these structures are added to Appendix C as well.

Drainage Type

Water plays a large role in soil behaviour. The degree of saturation can influence the strength, both negatively and positively. Moreover, identifying how soil and the water in it will react when loaded is of key importance for modelling as accurately as possible. This subsection contains the description of drained and undrained behaviour of soil as well as the possible manners to distinguish the different behaviours.

Terzaghi's effective stress principle divides the total stress in a soil in effective stresses and pore pressures ($\sigma = \sigma' + p$). The effective stress is the stress soil grains transfer to each other and the pore pressure is the water pressure in the pores. When the soil is loaded, the extra stress is initially carried by the water resulting in an excess pore pressure. Over time, this excess pore pressure will dissipate thereby returning to a balanced pore pressure. This phenomenon is called consolidation.

Drained Behaviour Depending on the type of soil, the reaction to this loading will either be drained or undrained. The most important factor that determines this reaction is its permeability and grain size distribution. Big grained soil with large pores allow for a relatively high groundwater flow allowing excess pore pressures to dissipate quickly resulting in the complete extra load being carried by the grains. Consequently, drained soil behaviour is seen in large grained soils such as sand.

Another factor which influences the behaviour type is time. When the stability or settlement over a long time is analysed, it is assumed a new equilibrium of effective stress and pore pressure has been achieved. This means no excess pore pressures in the soil are considered, making the behaviour of soil drained.

Undrained Behaviour Arising from the definition of drained behaviour, undrained behaviour occurs in soils with a small permeability. Due to its small pores, water is unable to flow resulting in the water being locked into the soil.

Resulting from this locked-in water, the external loading of the soil is both carried by the water as well as the grain skeleton. The isotropic part of the load is added to the pore pressures and as water cannot sustain shear stresses, these extra induced stresses are carried by the grains. However, water can have an indirect effect on these stresses. During undrained loading, the change in pore water pressure can change the effective stress and thereby changing the undrained shear strength of the soil. Depending on the amount of over-consolidation, this might results in a soil with decreased strength. During consolidation, this strength will return to its original value or might even be higher due to the extra confining stress from the additional load.

Another consequence of undrained behaviour is the inability of soil to experience volumetric strain due to drainage. This is especially relevant to this research project as thermal loading is expected to change the temperature of the soil, making the ground water expand or contract. Therefore, this load could induce volumetric strain and give engineers an extra challenge.

Applied Strength and Thermal Functions

This subsection contains the description of the chosen material model, drainage type and thermal functions applied in the geotechnical stability analysis. Each soil layer is assigned its own material model and drainage type. Table 6.13 gives an overview of these for clarity.

Material Model The choice of material model influences the outcome of the stability analysis significantly. In the calculation of the settlement behind a sheet pile, small strains of the soil are very common. Therefore, the need to focus on this rises. The HSsmall model is able to consider these strains as well as the very stiff behaviour of soil that comes with it. Hence, all soil types are assessed with this model.

Drainage Type As is explained, the choice of drainage type is primarily dependent on the permeability and the considered time range. As the emphasis lies on the short term reaction of the soil, the drainage type is defined on the permeability solely. As sand is a large grained soil, this is calculated according to the drained method. The other present soil types, peat, clay, silty clay and sandy clay, are calculated according to the undrained method.

Table 6.13: Overview of the assigned material properties.

Material	Material Model	Drainage type
Sand, top layer	HSsmall	Drained
Peat	HSsmall	Undrained
Clay, Weakly Silty	HSsmall	Undrained
Clay, Strongly Sandy	HSsmall	Undrained
Clay	HSsmall	Undrained
Sand	HSsmall	Drained
Water	LE	Drained

Thermal Functions The following descriptions are based on (PLAXIS, 1994). The thermal function describes the variation of the temperature over time. PLAXIS offers 3 ways to specify a function: as a harmonic, a linear and by means of a table. Only the table function is used in this thesis. This table can either be defined in the thermal functions window or be imported as a .txt file. In both cases, the table consists of two columns, the first column is the time in days and the second column holds, depending on the type of function, the ΔTemperature [K] (temperature function), the ΔHeatFlux [kW/m^2] (heat flux function) or the ΔHeatTotalFlux [kW/m^3] (heat total flux function).

Thermal Properties

The heat capacity and thermal conductivity are used as input parameters in PLAXIS as well. These are described in Section 5.3.4. In contrast to COMSOL, the thermal properties in PLAXIS apply to the solids only, rather than a mixture

of grains and water. Therefore, the variables in Table 6.1 differ from the variables in Table 5.5.

Thermal Expansion Coefficient This parameter describes how much the material expands (or elongates) when the temperature increases. It is, formulated differently, the stain per unit of temperature. The values, displayed in Table 6.14, are based on the thermal expansion coefficients of the minerals described in Delage (2013).

Vapour Diffusion Coefficient This parameter controls the diffusion of vapour in the material. If the vapour is not considered, this parameter is set to zero.

Thermal Diffusion Enhancement Factor The dependence of the temperature on the mass flux of vapour is controlled by this parameter. If the vapour is not considered, this parameters is set to zero.

Unfrozen Water Content The unfrozen water content is a percentage of water in liquid state in the soil. This option can be used in case of permafrost, freezing, thawing and other situations where frozen soil is present. Long lasting and deep soil frost is uncommon in the Netherlands - especially in the western part. Hence, the unfrozen water content is assumed to be 0.

Table 6.14: Thermal properties of soil types and steel (1/2).

Material	**Heat capacity** (C_s) [kJ/(t · K)]	**Thermal conductivity** (λ) [kW/(m · K)]	**Density** (ρ_s) [t/m^3]	**Volumetric thermal expansion coefficient** (solids) [1/K]
Water*	$4186 \cdot 10^2$	2	0.01	0
Peat	2909.09	0.00125	1.10	0
Silty Clay	2333.33	0.00080	1.50	$1.02 \cdot 10^{-4}$
Sandy Clay	1722.22	0.00200	1.80	$1.02 \cdot 10^{-4}$
Clay	2357.14	0.00090	1.40	$1.02 \cdot 10^{-4}$
Sand	1666.66	0.00259	1.80	$1 \cdot 10^{-4}$
Steel	475.16	0.04450	7.85	$11.00 \cdot 10^{-4}$

*= the water has a very high thermal conductivity to simulate convection in the material.

Table 6.15: Thermal properties of soil types and steel (2/2).

Material	**Vapour diffusion coefficient** (D_v) [m^2/day]	**Thermal diffusion enhancement factor** (f_{Tv}) [-]	**Unfrozen water content** [%]
Water	0	0	0
Peat	0	0	0
Silty Clay	0	0	0
Sandy Clay	0	0	0
Clay	0	0	0
Sand	0	0	0
Steel	-	-	-

6.4 Closing Remarks

This chapter is part of the effort to answer research question 4: 'Can an industry standard finite element method program capture the long-term thermal and mechanical behaviour of an energy sheet pile quay and the subsurface?' The mechanics of a Thermal-Hydro-Mechanical analysis are investigated as well as several learning objectives. Based on this research, a geotechnical stability assessment model is developed. Together with the heat conduction model, developed in Chapter 5, research question 4 is answered in the next chapter - based on these models.

Chapter 7

Validation of the Developed Models

In this chapter the heat conduction model and the geotechnical stability model are validated using the in-situ measured temperature and deformation of the sheet pile in the field test. The chapter is started by giving a short recap of the test setup and the definition of the initial and boundary conditions. Subsequently, the validation is started by comparing both the heat conduction model and geotechnical stability model to the field test data. After this, several parameters are subjected to a sensitivity analysis and calibrated. After this calibration, the validation is finished by giving an overview of the adjustments and the corresponding improvements. After the validation a 4 year analysis using the geotechnical stability model is done to see the effects of the thermal activation on a sheet pile wall over a long time. Finally, research question 3 is answered: 'Can an industry standard finite element method program capture the long-term thermal and mechanical behaviour of a sheet pile and the subsurface?'.

7.1 Overview of the test setup, Initial and Boundary Conditions

The following phases are validated in this chapter:

- Phase 1a: 27-10-2020 – 27-11-2020; Single side shallow activation, colour code: blue
- Phase 1b: 27-11-2020 – 14-12-2020; Single side deep activation, colour code: purple
- Phase 2: 14-12-2020 – 18-01-2020; Double side deep activation, colour code: purple and green

Originally, phase 1a and 1b were combined into one phase. However, due to technical difficulties, the shallow and deep loop activation were split. The different loops with their colours can be seen in Figure 7.2. An overview of the locations of the monitoring setup is given in Figure 7.1. In the validation, the location of the monitoring device is elucidated for each graph.

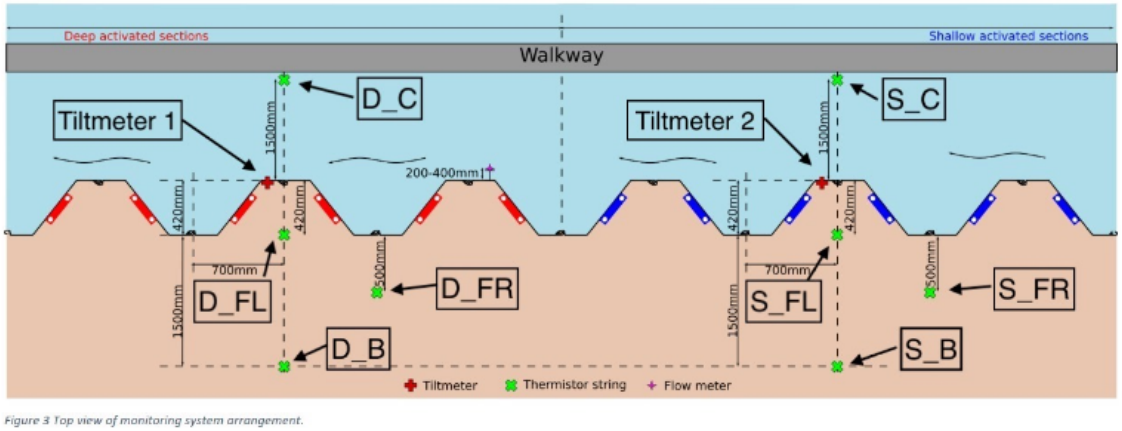

Figure 7.1: Schematic overview of the locations of the measurement devices (De Jong, 2020)

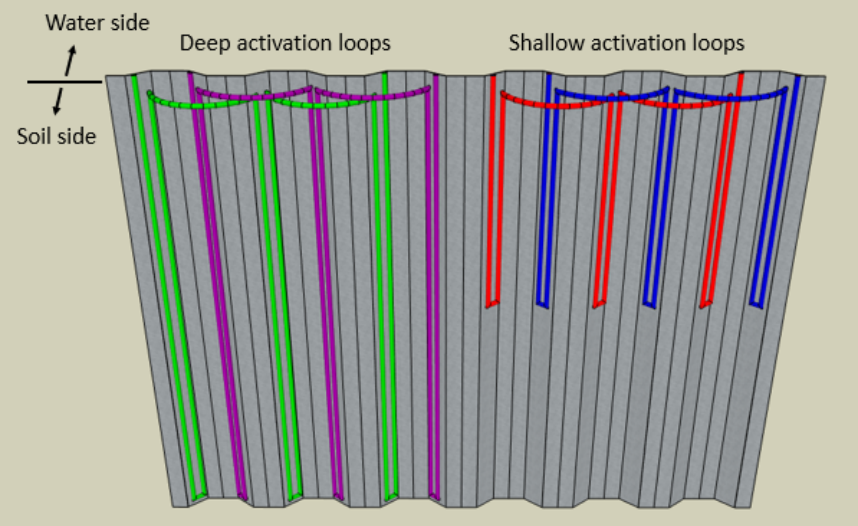

Figure 7.2: Overview of the set-up with the shallow activation on the right hand side and the deep activation on the left hand side.

Initial and Boundary Condition Heat Conduction Model

The initial and boundary conditions applied in the model are based on the data acquired from the field test. In phase 1a, the deep loops are not activated and; therefore, display the natural temperature distribution. Moreover, the thermistor string at the back in the quay (thermistor string D_B in Figure 7.1) lies far enough away to experience little influence of the heat extraction. As a result, this dataset is used as boundary condition in the quay. The same applies to thermistor string D_C, this dataset is used for both the initial and boundary conditions. Phase 1b and 2 continue with the solution of the calculation prior. An overview of the initial and boundary conditions for phase 1a is as follows:

- Initial condition quay = D_FL;
- Heat flux from quay = D_B;
- Initial condition canal = D_C;
- Heat flux from canal = D_C;
- Air temperature = D_B(1);
- Water temperature = Bovelander (2020);
- Flow velocity canal water = 0.01 m/s parallel to the sheet pile wall;
- Flow velocity ground water = 10^{-7} in the same direction as the canal.

The flow conditions in the loops in the different phases are shown in Table 7.1. This is an approximation, the flow rate which is, especially in phase 1a, not constant thereby making it difficult to model. This simplification of the flow rate means there will be a guaranteed error between the numerical approach and the measured data. The measured flow rate and the simplifications are shown in Figure 7.3.

Table 7.1: Flow rates of the activated loops per phase.

Phase	**Flow rate blue loop [l/min]**	**Flow rate purple loop [l/min]**	**Flow rate green loop [l/min]**
1a	7.5	0	0
1b	0	7.5	0
2	0	2.8	2.8

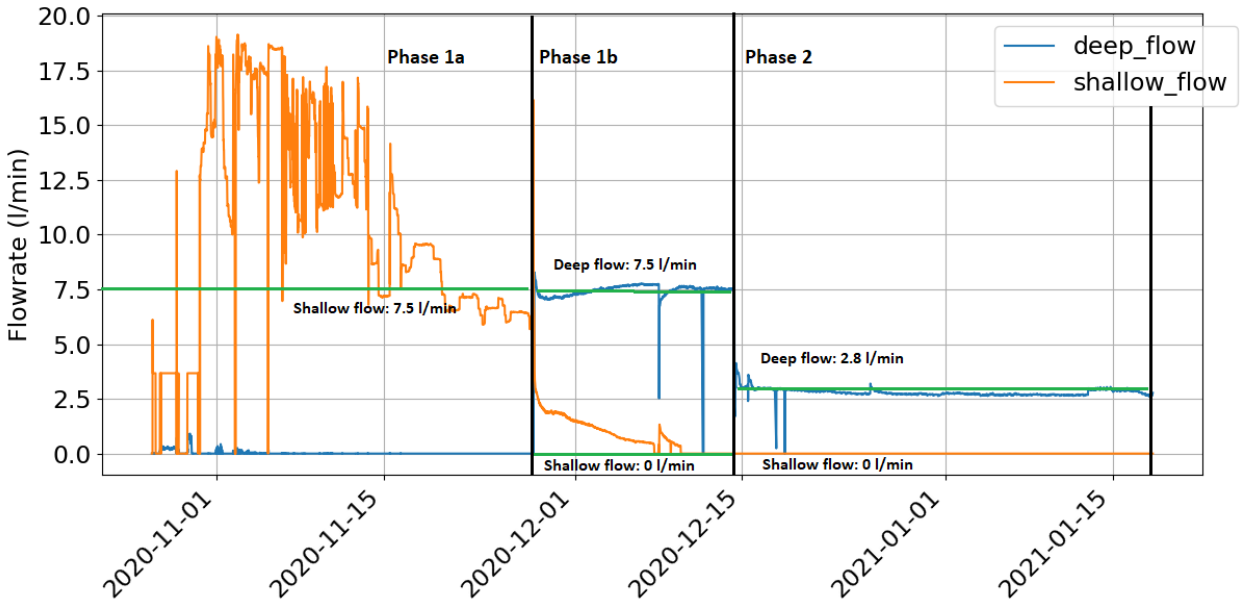

Figure 7.3: The flow rate through the deep and shallow loops in phase 1a, 1b and 2; and the approximated flow rate used for the numerical approach.

Initial and Boundary Condition Geotechnical Stability Model

Based on the numerical approximation performed in COMSOL, the temperature change of the sheet pile as a result of the thermal activation is determined. Investigations show that, independent from the temperature change in the soil, the temperature of the loops does not change after an equilibrium is found. This results in the following temperatures:

Table 7.2: Temperatures of the sheet pile as a result of the thermal activation.

Phase	**Activation type [Deep/Shallow]**	**Temperature [°C]**
1a	Shallow	3
1b	Deep	2
2	Deep	1.5

In addition, the following initial and boundary conditions are defined:

- Initial condition quay = D_FL
- Initial condition canal = D_C
- Air temperature = D_B(1)
- Water temperature = Bovelander (2020)

7.2 Validation of the Heat Conduction Model

This section contains the validation of the heat conduction model. The data used to validate is the temperature of the soil measured by the thermistor strings and the in- and outlet temperatures of the heat pump. Not all in-situ measured and numerically approached temperatures are analysed in all phases. In phase 1a, the thermistor strings in the deep and shallow section are analysed. The data from the deep section serves as initial temperature of the soil after which the natural temperature decrease is assessed. The data collected in the shallow section is compared with the numerically approached temperatures to check the energy extraction from the soil. In phase 1b is the deep section assessed as only one deep loop is activated. In phase 2 both deep loops are activated. Therefore, the data from the deep section is only compared. All phases include an analysis of the numerically determined and the measured heat extraction.

7.2.1 Phase 1a: Single Side Shallow Activation

Figure 7.4 shows the locations of the thermistor strings in the deep section. Encircled in red is the thermistor of which the data is used as to validate the natural temperature change in the soil. Starting with Figure 7.5, thermistor string D_FL is used.

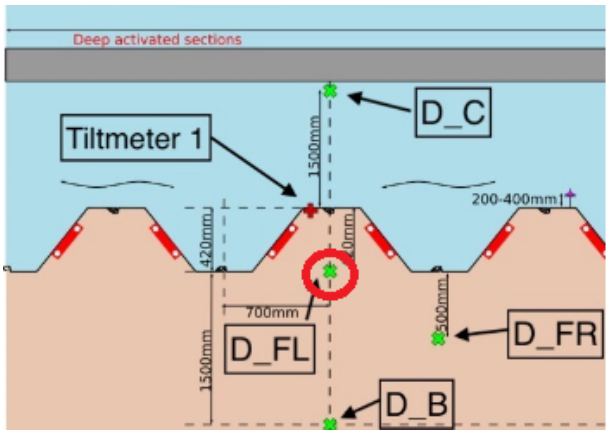

Figure 7.4: Location of thermistor string D_FL. The spacing between sensors is 1 metre and the thermistor is 15 metres deep.

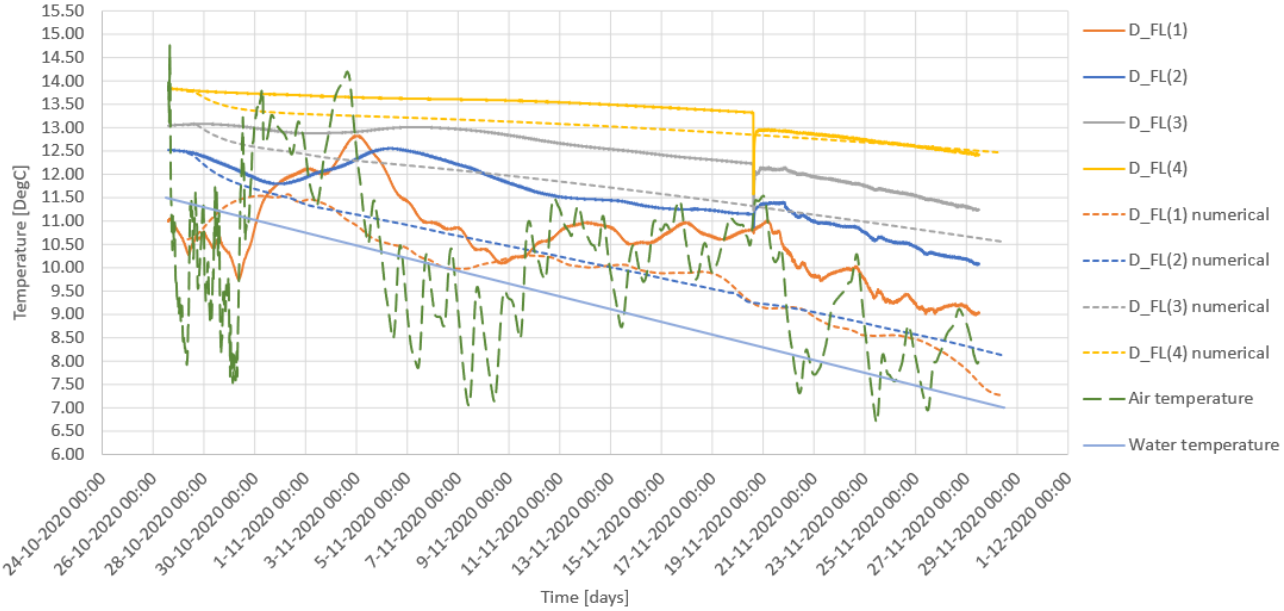

Figure 7.5: Comparison of field test data of thermistor string D_FL and baseline heat conduction model in the (un-activated) deep section. (1/2)

Figure 7.5 shows the data of the first four thermistors of D_FL acquired in the field test and the numerically approached temperature. The air temperature and the water temperature are plotted as well so that the ambient influence can be compared. Generally, the numerically obtained temperatures are lower than the measured temperatures. This difference decreases with depth. The two thermistors closest to the surface (D_FL(1) and D_FL(2)) seem to be governed by the water temperature as they are more or less an offset of the line. The lack of radiation added to the model could also have some influence in the low numerically approached temperatures.

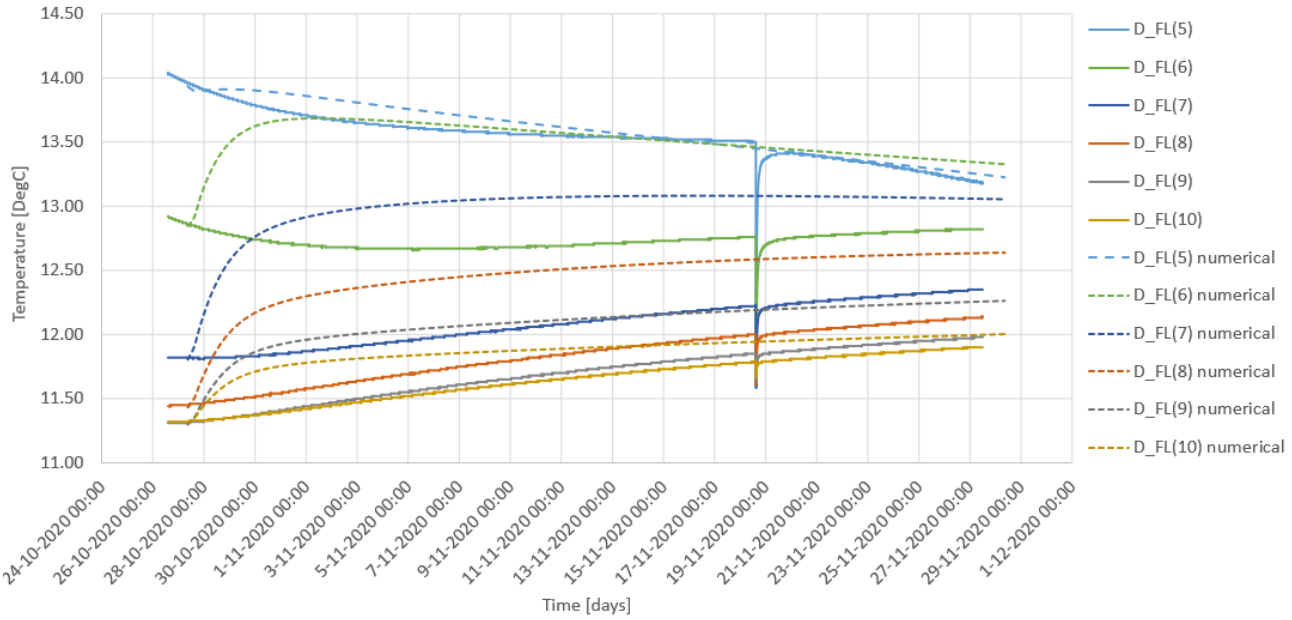

Figure 7.6: Comparison of the field test data of thermistor string D_FL and baseline heat conduction model in the (un-activated) deep section. (2/2)

Figure 7.6 shows the data of thermistors D_FL(5) to D_FL(10), which lie at a depth of 5 to 10 metres. In this graph, the general trend shows an overestimation of the temperatures acquired in the numerical analysis. This is a result of the way the initial conditions are defined. The initial temperature distribution in the quay is based on the data from thermistor string D_FL, located very close to the sheet pile. The initial temperatures underneath the canal is based on thermistor string D_C, which is located 1.5 metres away from the sheet pile. Visualised in Figure 7.7, the left picture shows a gradient between the horizontal isothermal contour line of 15 °C lying mostly under the canal while the picture on the right shows an initially steep gradient which eventually balances out equally on both sides of the sheet pile. The blue arrow shows the area in which the overestimated temperatures in Figure 7.6 lie. The last five thermistors, D_FL(11) to D_FL(15) all converge around 12 °C, which is according to expectations (Sedighi et al., 2015).

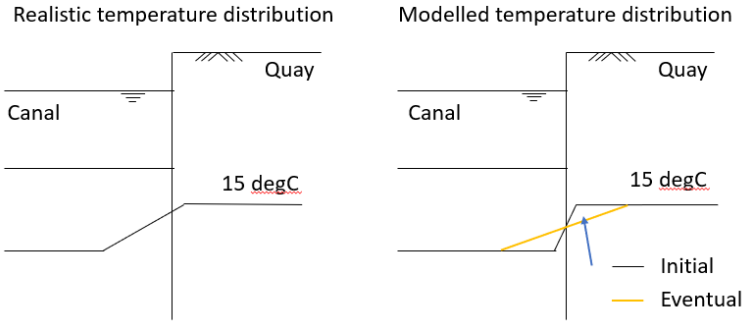

Figure 7.7: Left: the natural isothermal contour; right: the modelled is thermal contour line and its eventual position.

Figure 7.9 shows the in-situ measurements and the numerical approach of the temperature of thermistor string S_FL - which is encircled in Figure 7.8. This thermistor string lies closest to the sheet pile on the activated (shallow) side. As one can see, the general trend of the numerical results is negative and more or less parallel to the in-situ measurements. The calculated values for S_FL(1) and S_FL(2) are in correspondence with the measured values. It is expected that the calculated values for S_FL(3) are too cold and should lie in the middle between S_FL(2) and S_FL(4). However, the sensors in the string don't work. Therefore, no comparison data is available which is why S_FL(3) and S_FL(4) are not analysed.

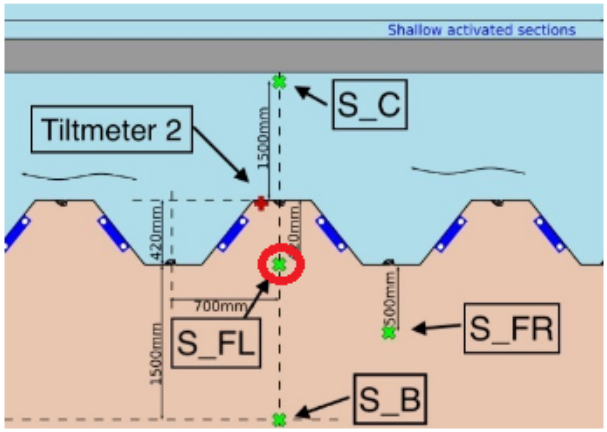

Figure 7.8: Location of thermistor string S_FL. The spacing between sensors is 1 metre and the thermistor is 4 metres deep.

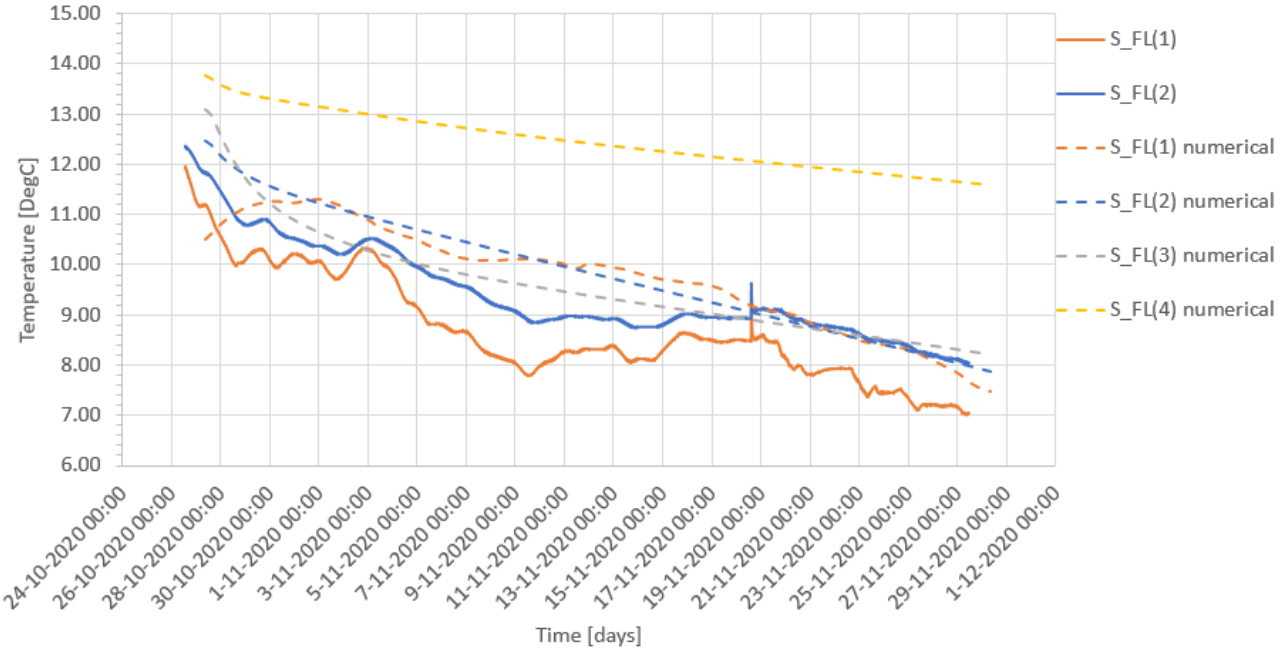

Figure 7.9: Comparison of the field test data of thermistor string S_FL and baseline heat conduction model in the (activated) shallow section.

Figure 7.10 shows the heat pump performance in which the dotted lines represent the computed in- and output. In the first half of November, the heat pump did not run optimally - too much heat was being extracted. This cooled the liquid too much resulting in the heat pump shutting down. In addition, the flow rate in the loops was oscillating, resulting in high and low temperatures being alternately extracted. In the second half of the month, after adjusting the power, the in-temperature converged to approximately 3 °C and the out-temperature to 0 °C. It is clear that the temperatures obtained with the numerical approach decrease gradually while the actual temperatures do not. This is most likely due to the heat pump turning on and off to ensure the water-glycol mixture does not reach sub-zero temperatures. Another explanation could be that in the field test less energy has been extracted in the first two weeks allowing for a larger yield in the weeks afterwards.

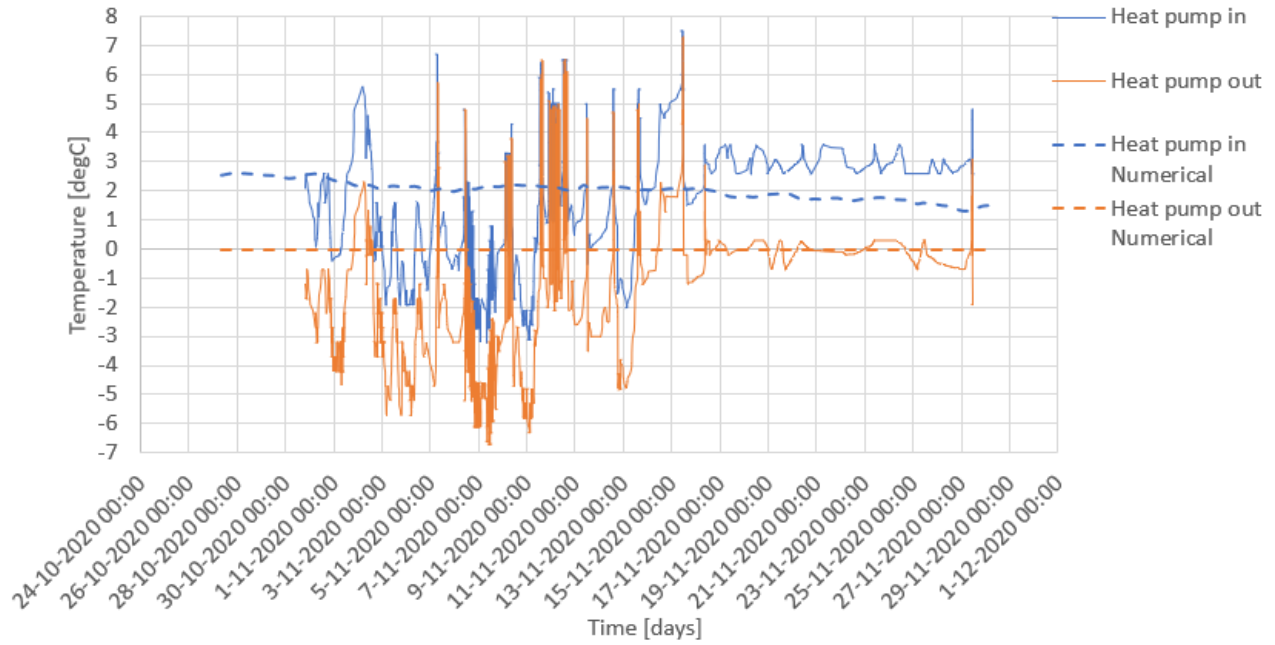

Figure 7.10: Comparison of the temperature going in and out the heat pump - measured and calculated.

7.2.2 Phase 1b: Single Side Deep Activation

In this phase, only one single deep loop is activated - the purple coloured loops in Figure 7.2. Again, thermistor string D_FL is used to validate the data. The location is shown in Figure 7.4. In this analysis, the solution of phase 1b is used as initial condition.

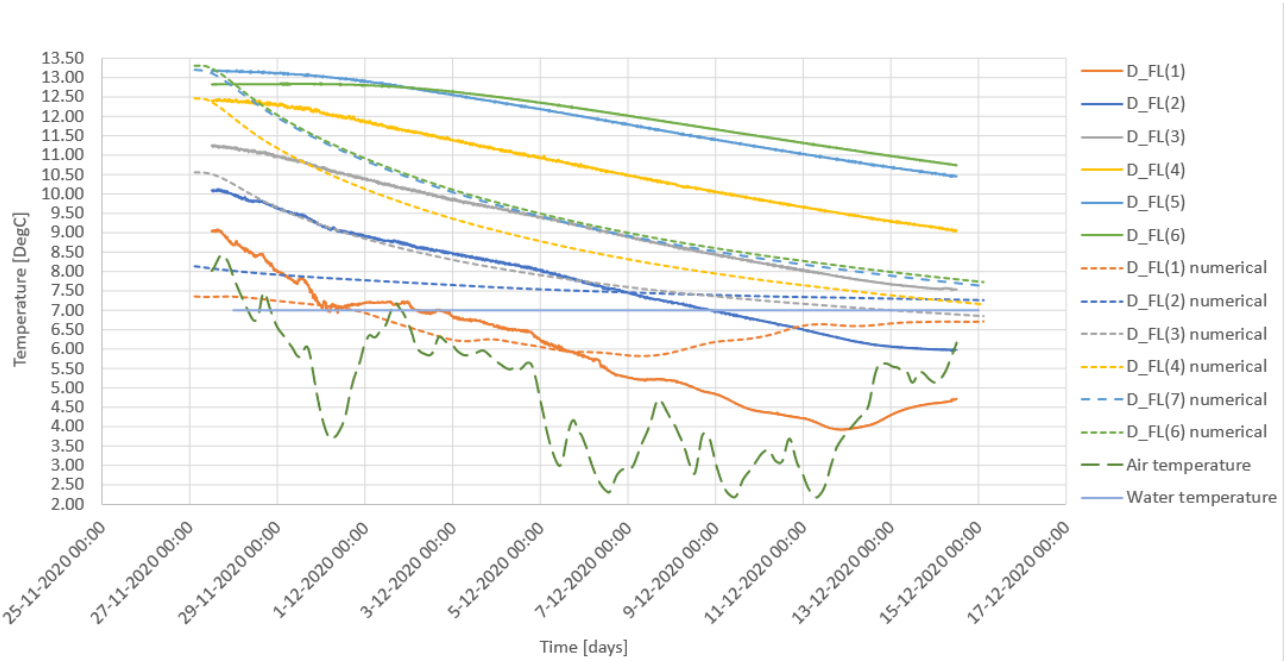

Figure 7.11: Comparison of the field test data of thermistor string D_FL and baseline heat conduction model in the (activated) deep section. (1/2)

The sensor closest to the top, D_FL(1), follows the the in-situ measured temperature more or less, but after one week the numerically determined temperature diverges and becomes too warm - clearly influenced by the water temperature. As already determined, this temperature has a large influence on the adjacent soil. It is most likely that this

temperature has a large influence on the fluid in the thermistor string and this cancels the temperature decrease resulting from the heat extraction. Deeper down, where the water temperature has little influence, the temperature is too cold. A possible explanation for this is that the soil has a heat capacity that is too low and; therefore, contains not enough energy to have temperatures remain at the test site level.

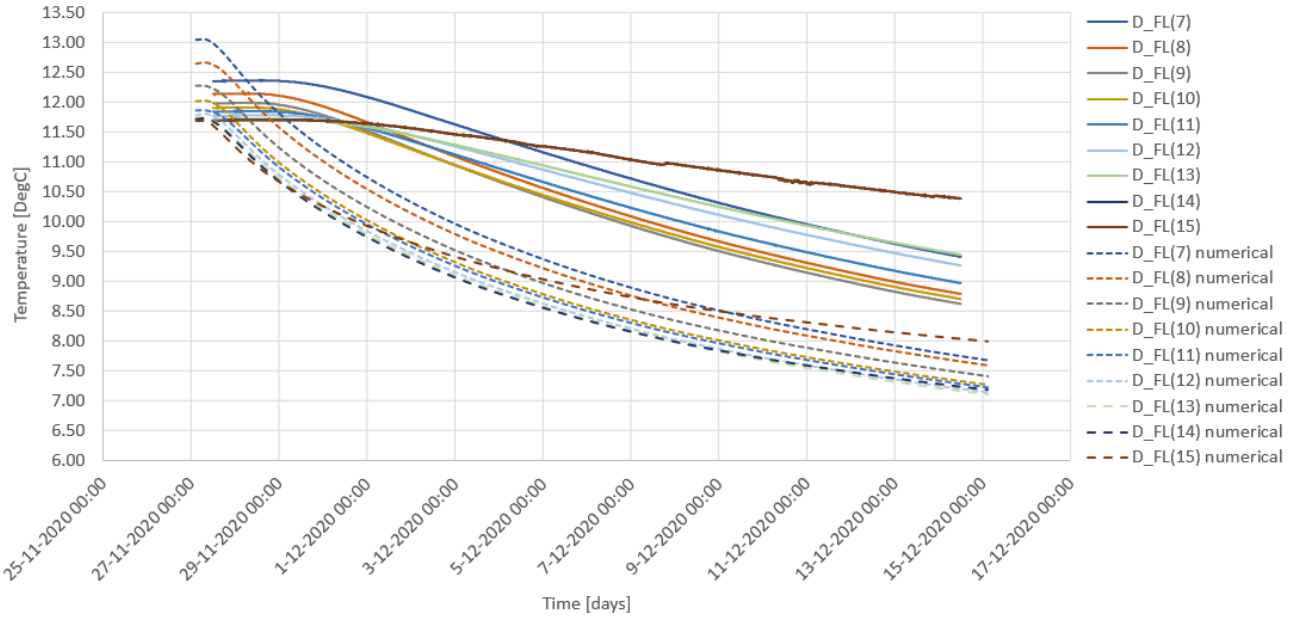

Figure 7.12: Comparison of the field test data of thermistor string D_FL and baseline heat conduction model in the (activated) deep section. (2/2)

Figure 7.12 shows the numerical and in-situ data of thermistor sensors 7 to 15 metres depth of string D_FL. In this graph is the temperature at the end of the calculation too low as well. Moreover, the final temperature is at all depths more or less 7.5 °C, which is 0.5 °C higher than the water temperature. The soil temperatures at the start of the analysis show a close fit to the measured temperatures.

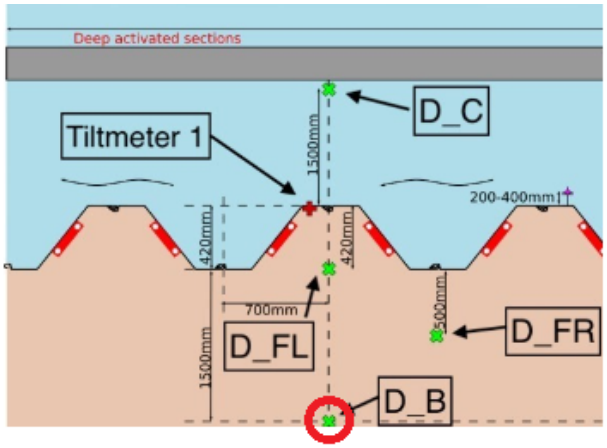

Figure 7.13: Location of thermistor string D_FL. The spacing between sensors is 1 metre and the thermistor is 15 metres deep.

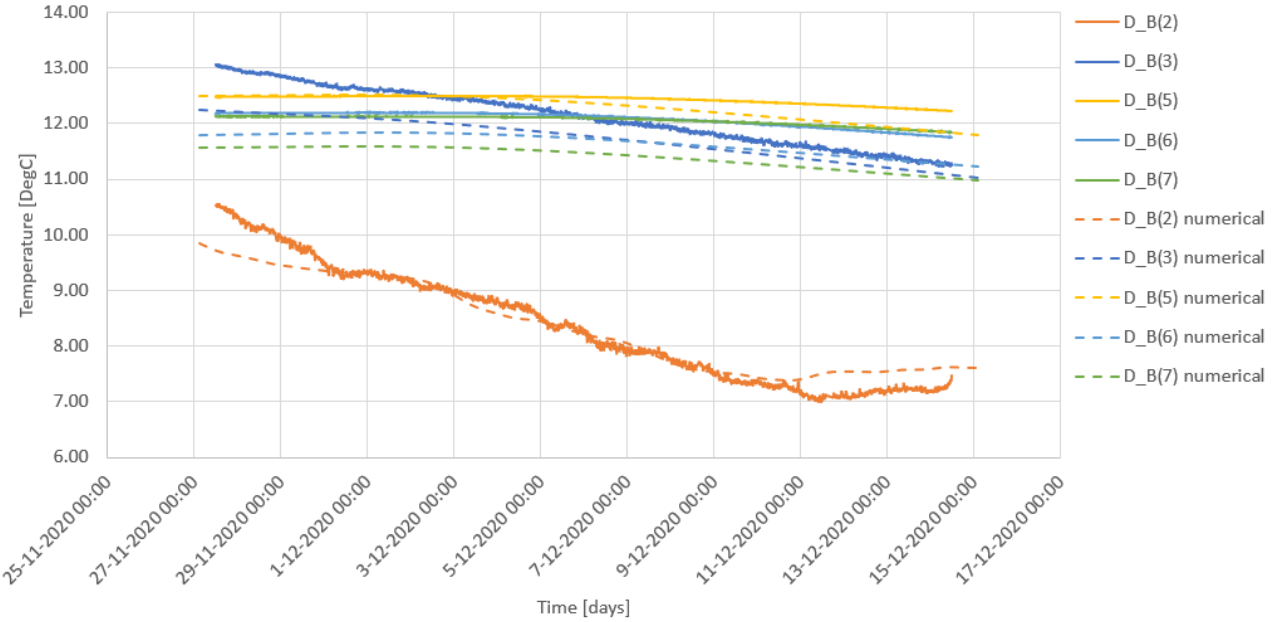

Figure 7.14: Comparison of the field test data of thermistor string D_FL and baseline heat conduction model in the (activated) deep section. (2/2)

Figure 7.14 show the data of thermistor string D_B, encircled in Figure 7.13, and the numerical approach. D_B(1) is missing in the legend and graph because this particular sensor is placed outside of the soil and; therefore, measures the air temperature. The thermistor string lies 1.5 metres away from the canal and thereby less affected by the water temperature and thermal activation. Moreover, this thermistor string has not a 1 but 2 metres spacing between the sensors, as shown in Figure 4.7. D_B(2) is the sensor lying 1 metre below the surface and the numerical data shows a very good fit. The sensors below, all with a 2 metres spacing, have approximately the same temperatures. The numerical approach lies within the same bandwidth, even though the two deepest numerically determined temperatures are 0.5 °C colder. Overall, all temperatures shown coincide with the model.

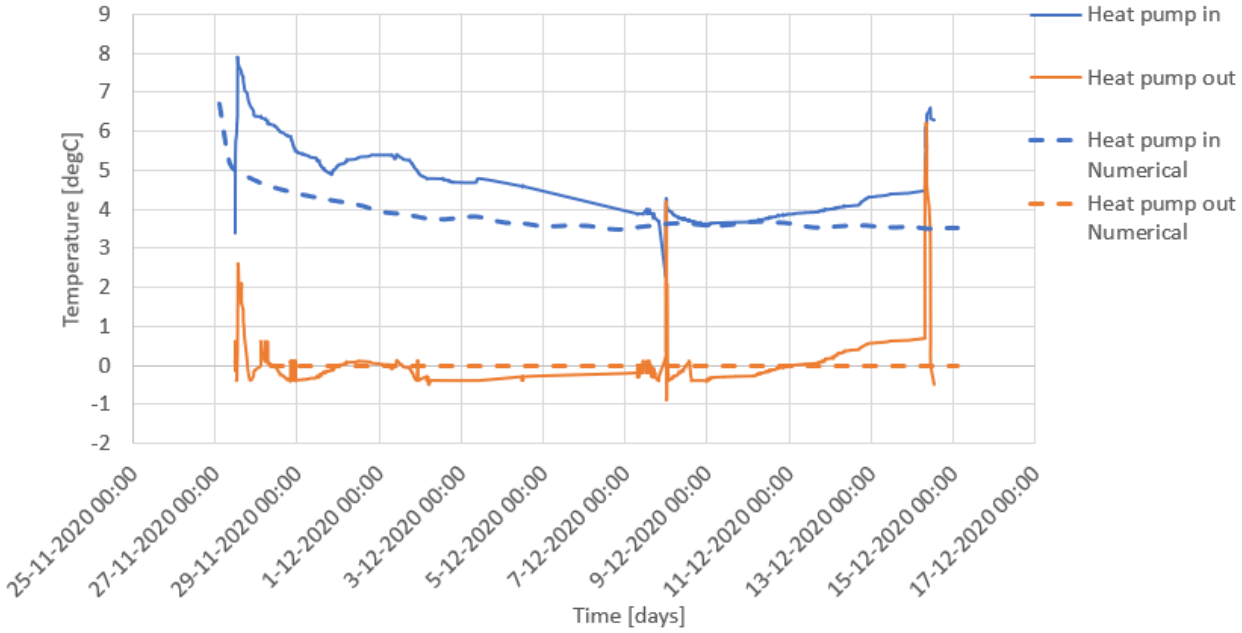

Figure 7.15: Comparison of the temperature going in and out the heat pump - measured and calculated.

Figure 7.15 shows the temperature of the glycol-water mixture going in and out of the heat pump, and the numerical approach. 'Heat pump in' is when the fluid comes out of the loops into the heat pump and 'heat pump out' is the temperature after heat has been extracted. This latter temperature is constant at more or less 0 °C. Therefore, the temperature in the heat conduction model is fixed at 0 degrees too. As can be seen, the numerical approach is generally lower than the in-situ measured temperature. The water is fixed at 7 °C – warmer than the 'heat pump in' temperature – this cannot be the limiting influence. As mentioned earlier, it might be possible that the heat capacity of the soil is too low. This causes the soil to cool down too fast and as the temperature difference decreases, the exchange decreases as well.

7.2.3 Phase 2: Double Side Deep Activation

In this phase, the two deep loops are activated. These are the purple and green loops, shown in Figure 7.2. This means, the deep loops are used for validation.

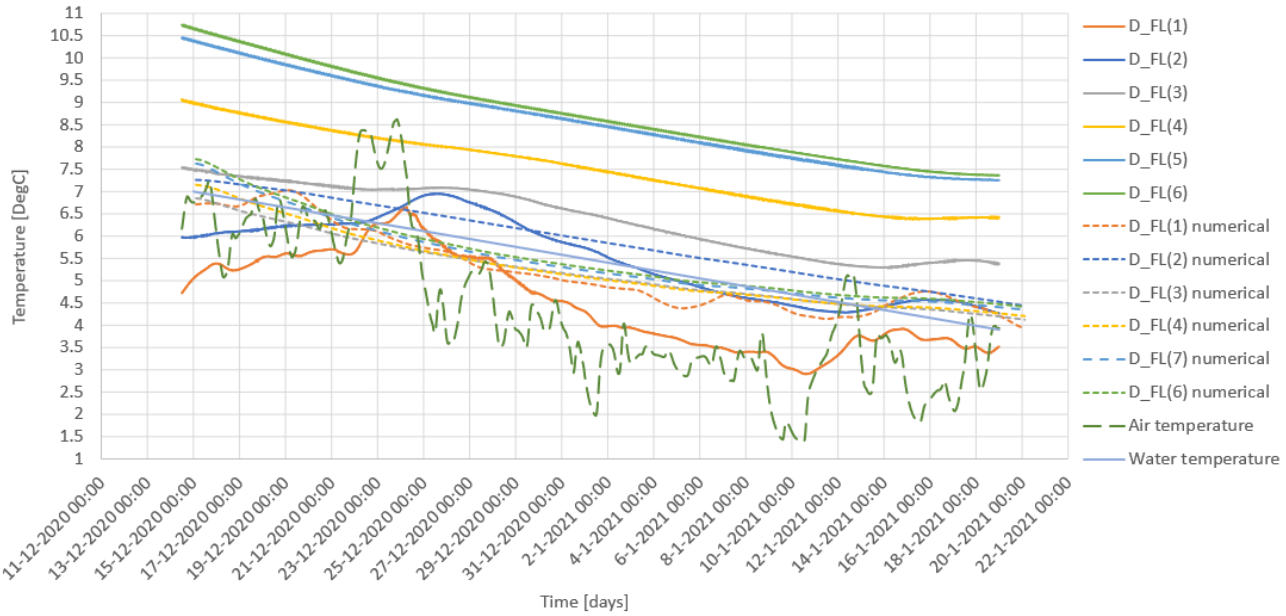

Figure 7.16: Comparison of the field test data of thermistor string D_FL and baseline heat conduction model in the (activated) deep section. (1/2)

Figure 7.16 shows the numerical data of phase 2 and the thermistor string data of D_FL, encircled in Figure 7.4. The data resulting from the numerical analysis clusters around the line indicating the temperature of the water, which cools down from 7 to 4 °C. In agreement with the previous phase, the in-situ measured temperatures are higher. In addition, the temperature differ by more or less 1 °C per metre.

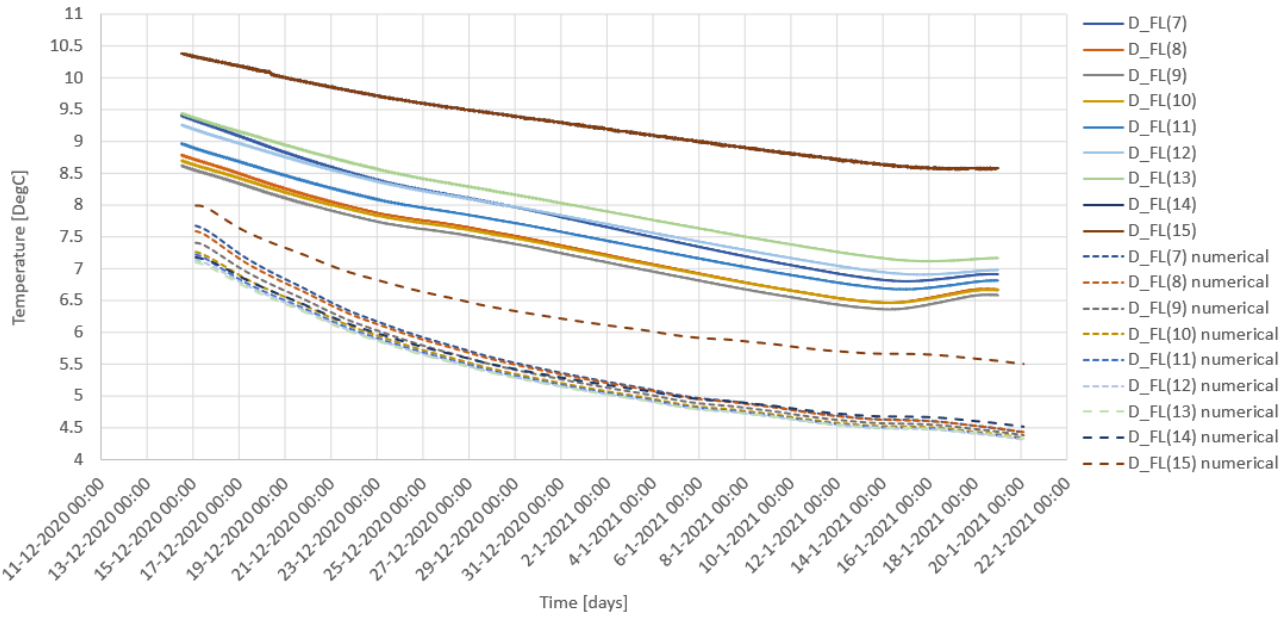

Figure 7.17: Comparison of the field test data of thermistor string D_FL and baseline heat conduction model in the (activated) deep section. (2/2)

The bottom sensors in Figure 7.17 show the same behaviour of the temperature distribution as previously mentioned. The numerically determined data follows the same trend as the water temperature but 0.5 °C higher. On average, the in-situ measured temperatures are 2 degrees higher. The difference between the measured and numerical temperature at sensor D_FL(15) is 3 °C.

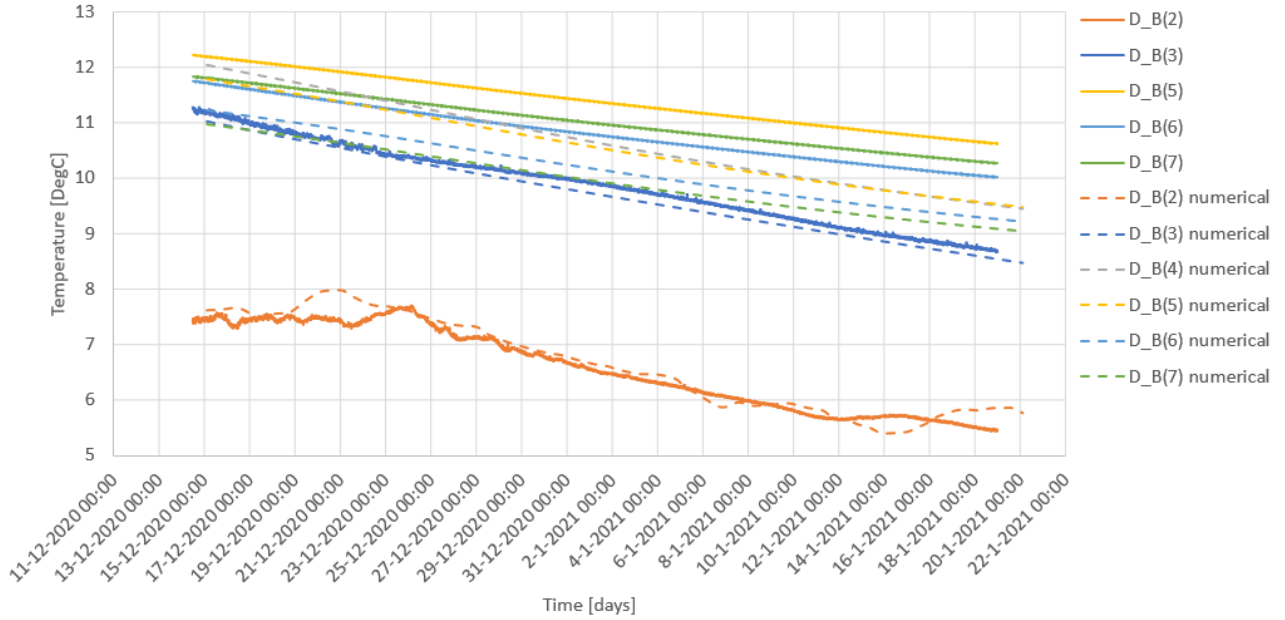

Figure 7.18: Comparison of the field test data of thermistor string D_B and baseline heat conduction model in the (activated) deep section. (2/2)

The numerically determined temperature of the thermistor string located at the back in the deep section (Figure 7.13) coincides well with the data measured. The sensor closest to the surface shows a good agreement while the deeper sensors are approximately 0.5 °C to cold.

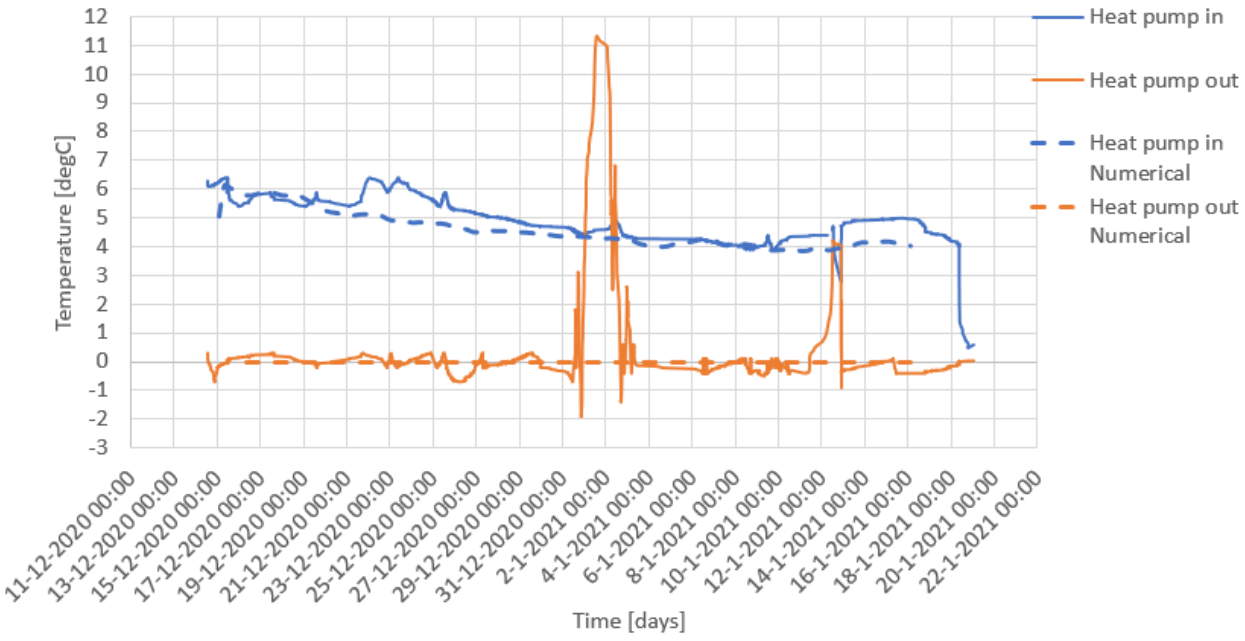

Figure 7.19: Comparison of the temperature going in and out the heat pump - measured and calculated.

The temperature that is extracted by the heat pump is shown in Figure 7.19. The temperature of the fluid exiting the heat pump is still fixed at 0 °C while the temperature going into the system drops from approximately 6 to 4 °C. The numerical approach and measured data show a good fit.

7.2.4 Conclusion

After analysing the measured and numerically determined temperatures in the soil and heat pump, the following observations can be concluded:

- The modelled temperature of the soil is generally too low.
- Water temperature governs the upper part of the soil.
- In the last phase, the numerical temperature is an offset (always 2 degrees lower) but the extraction is more or less te same. This shows that the fit could be better if initial temperatures are better. Exchange can be too much so much energy is lost in the top.

7.3 Validation of the Geotechnical Stability Model

Measurements at two locations have been performed throughout the phases, one in the deep and one in the shallow section. The measurements in the deep section are taken up to a depth of 13 metres and in the shallow section up to a depth of 10 metres. Furthermore, the inclinometer has an error margin of 0.25 mm/m. This means that the deep section measurements have a possible maximum error of 3.25 millimetres and the shallow section measurements one of 2.5 millimetres. To make the deformation as a result of the thermal activation in PLAXIS clearer, the sand backfill is added as a plastic analysis before the time-dependent analysis performed. To isolate the thermal influence on the deformation, the deformation resulting from the backfill is subtracted from the total deformation. This is 6.6 millimetres in the numerical analysis and 2.79 millimetres in the measured data.

7.3.1 Phase 1a: Single Side Shallow Activation

Figure 7.20 shows the maximum displacement of the sheet pile in the shallow section. Figure 7.22 shows the corresponding contour plot. The measured deformation shows little to no distortion of the sheet pile wall the first few days. This is a result of technical issues. After resolving these, the deformation ranged between 1.25 and 2.25 millimetre. The numerically approached values oscillate slightly, averaging at approximately 1.75 millimetre. The measured deformation shows a larger variation in measured values. In the analysis of the deformation of the sheet pile in Chapter 4, it is established the oscillations in the measured deformation result from an in-situ measurement error, warm/cold days (radiation levels) or fluctuating canal/groundwater levels. Precipitation is not included in the THM analysis. The air temperature, shown in Figure 7.21, is added as a boundary condition. The water temperature included by setting a temperature boundary condition on the water surface. The increase in numerically approached deformation coincides with increased temperatures leading to the conclusion that the oscillations result from the boundary condition temperature fluctuations. The fit of the measured and numerically approached values is good.

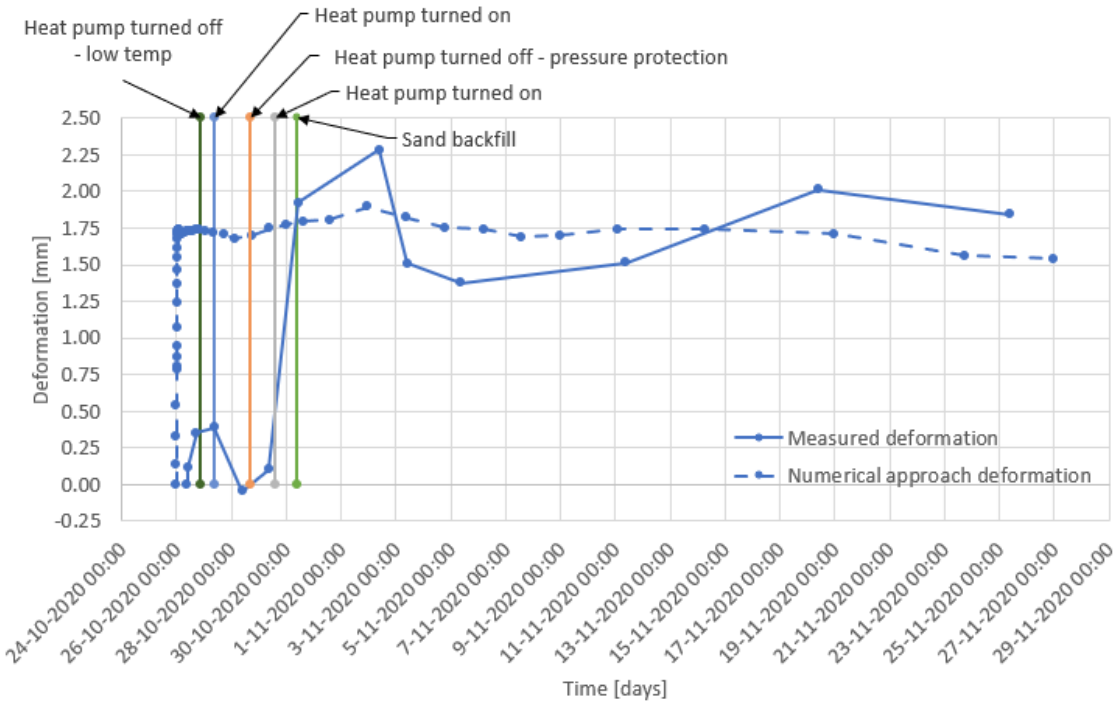

Figure 7.20: The maximum displacement of the sheet pile in the shallow section in phase 1a. The positive direction of movement is into the canal.

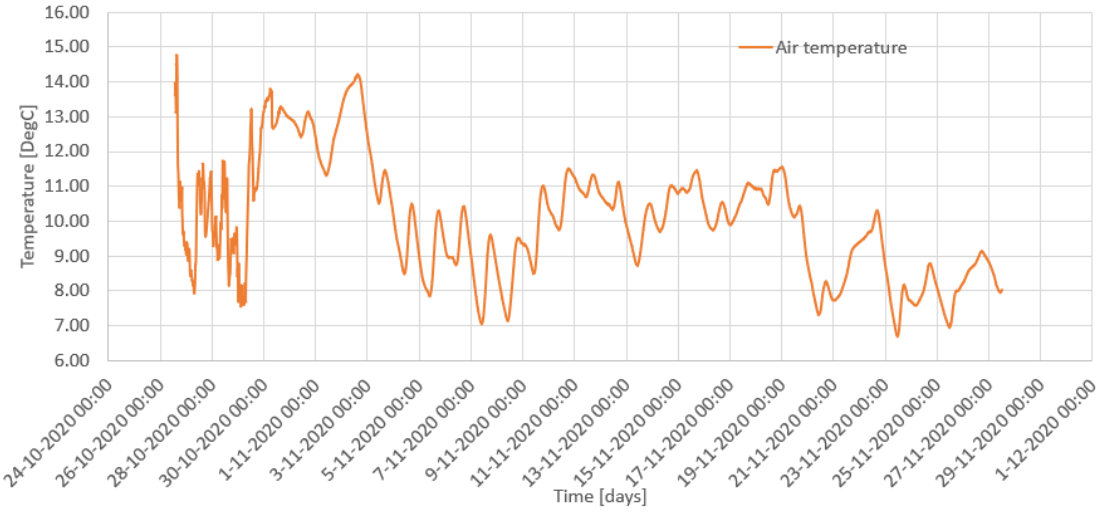

Figure 7.21: The air temperature in phase 1a.

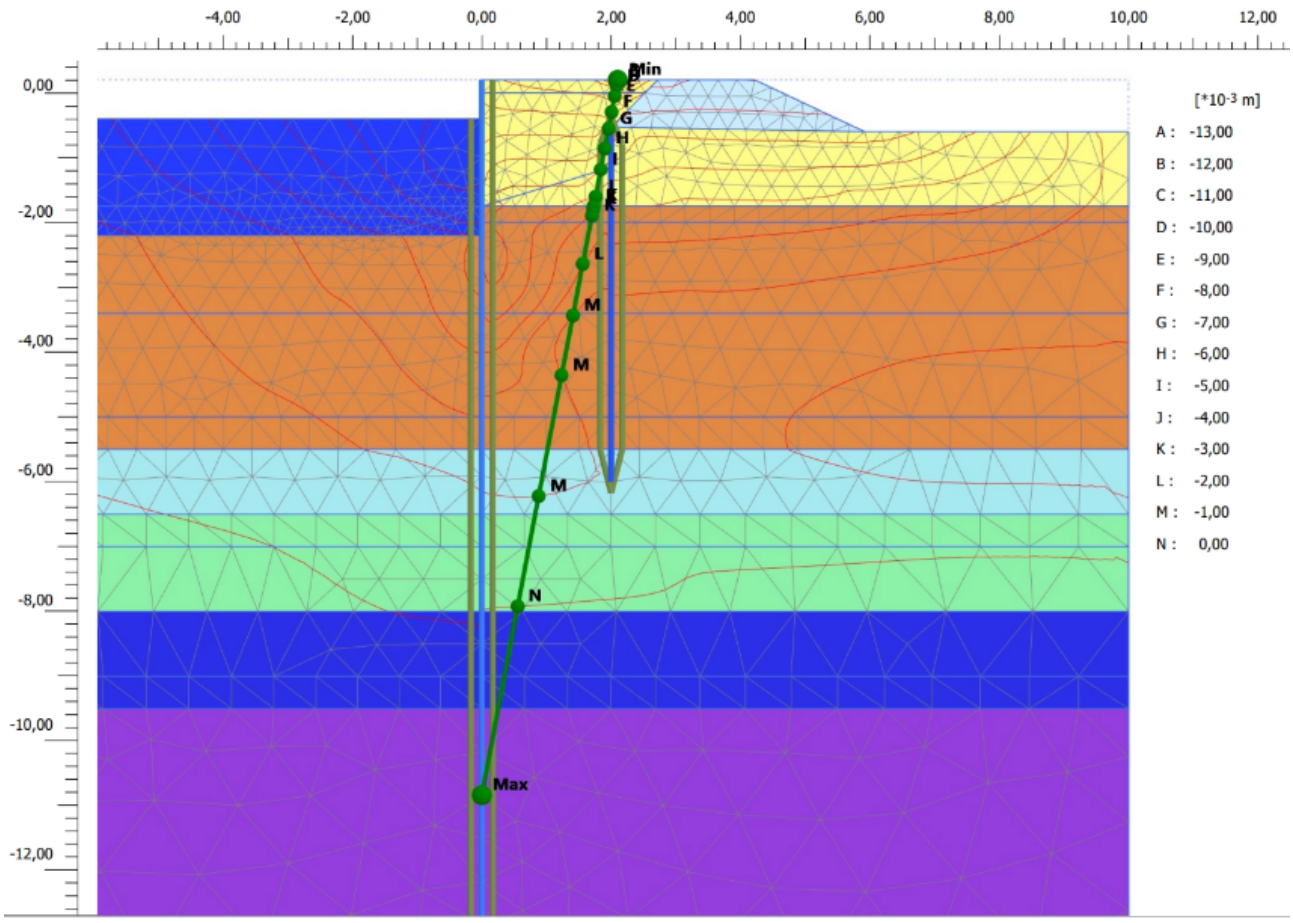

Figure 7.22: A contour plot of the deformation in x-direction in phase 1a.

Figure 7.23 shows the temperature of the soil at the end of phase 1a in PLAXIS. The temperature in the soil around the sheet pile is too cold, because a fixed temperature is used. As the goal of this computation is to maximally load the sheet pile, this overestimated temperature is intended. Moreover, the cold penetrates the soil too deep. This is most likely the result of the excellent colliding properties of the steel. A more realistic distribution is that the cold below 4 metres does not experience any influence from the sheet pile wall and water. Overall, the temperatures in the soil monitored in the field test are less influenced by the thermal activation.

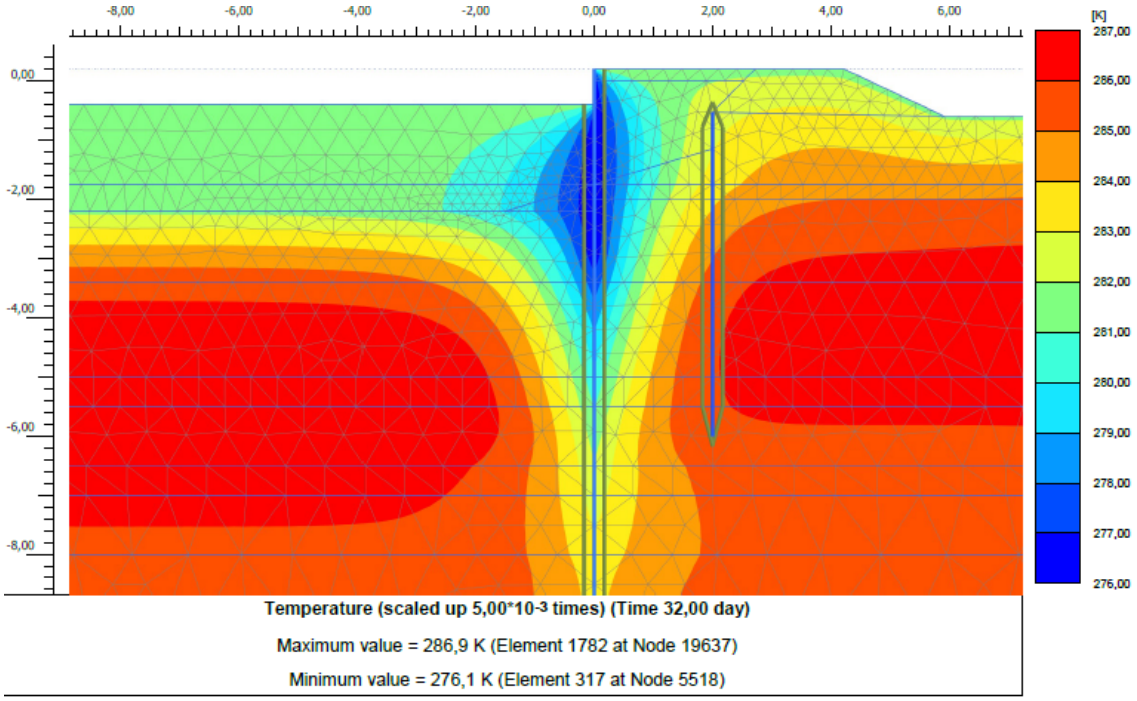

Figure 7.23: The temperature of the soil in phase 1a.

7.3.2 Phase 1b: Single Side Deep Activation

The numerically determined deformation increases slightly at the start of phase 1b after which it shows a linear slightly downward trend. The measured values fluctuate much more as a result of air temperature and precipitation, as determined in Chapter 4. The air (and water) temperature are again responsible for the small oscillations in the numerical values. The measured deformation is on average 2.5 millimetre, approximately 1 millimetre larger than the numerically determined deformation. This means the numerical determined values fall within the error margin of 3.25 millimetre. Figure 7.26 shows the corresponding contour plot.

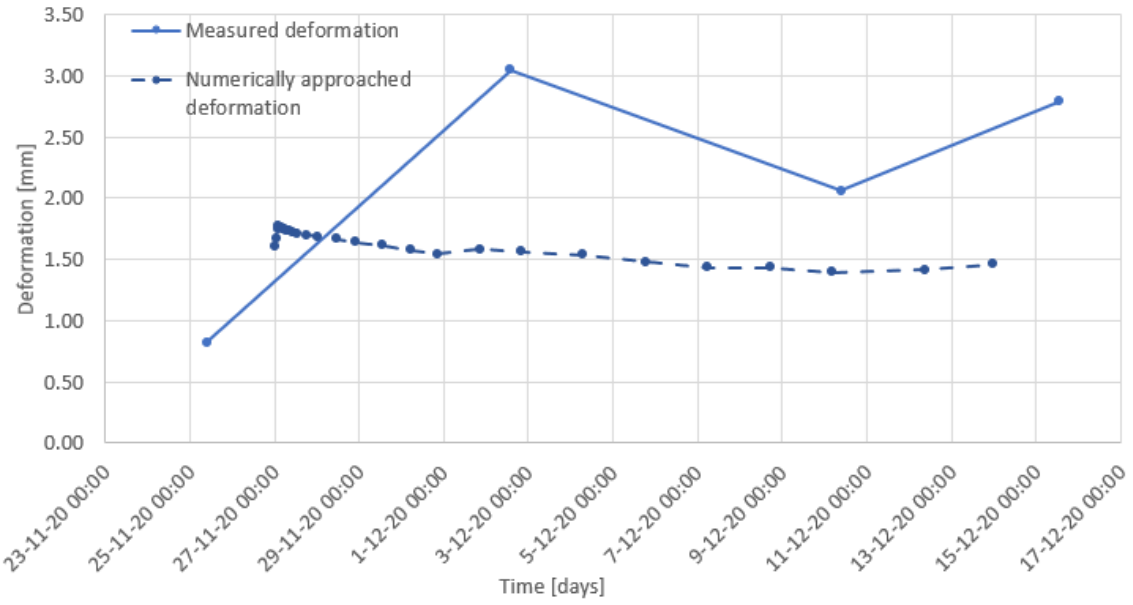

Figure 7.24: The displacement of the sheet pile in the shallow section in phase 1b per metre. The positive direction of movement is into the canal.

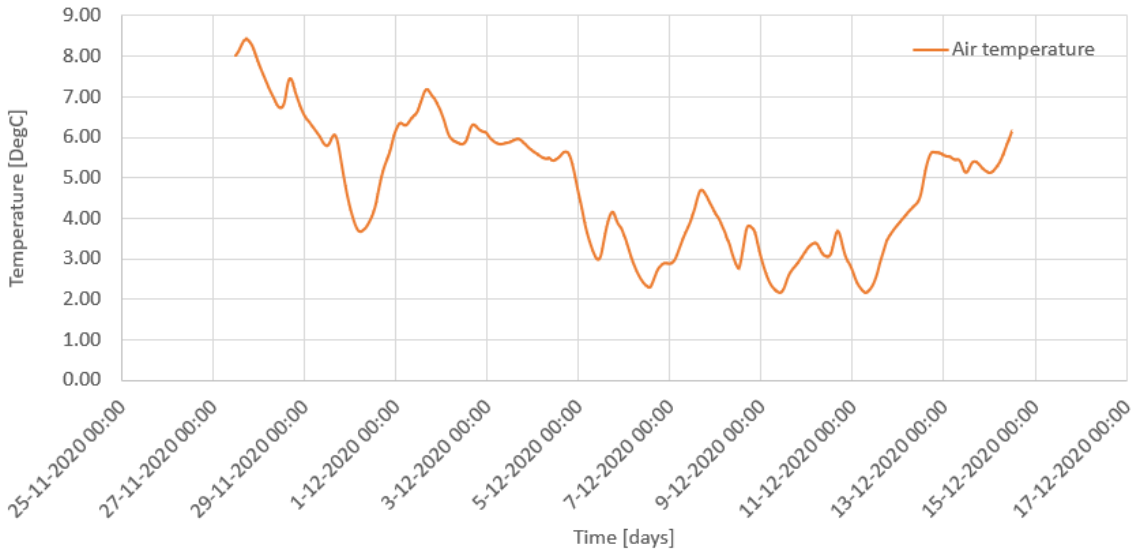

Figure 7.25: The air temperature in phase 1b.

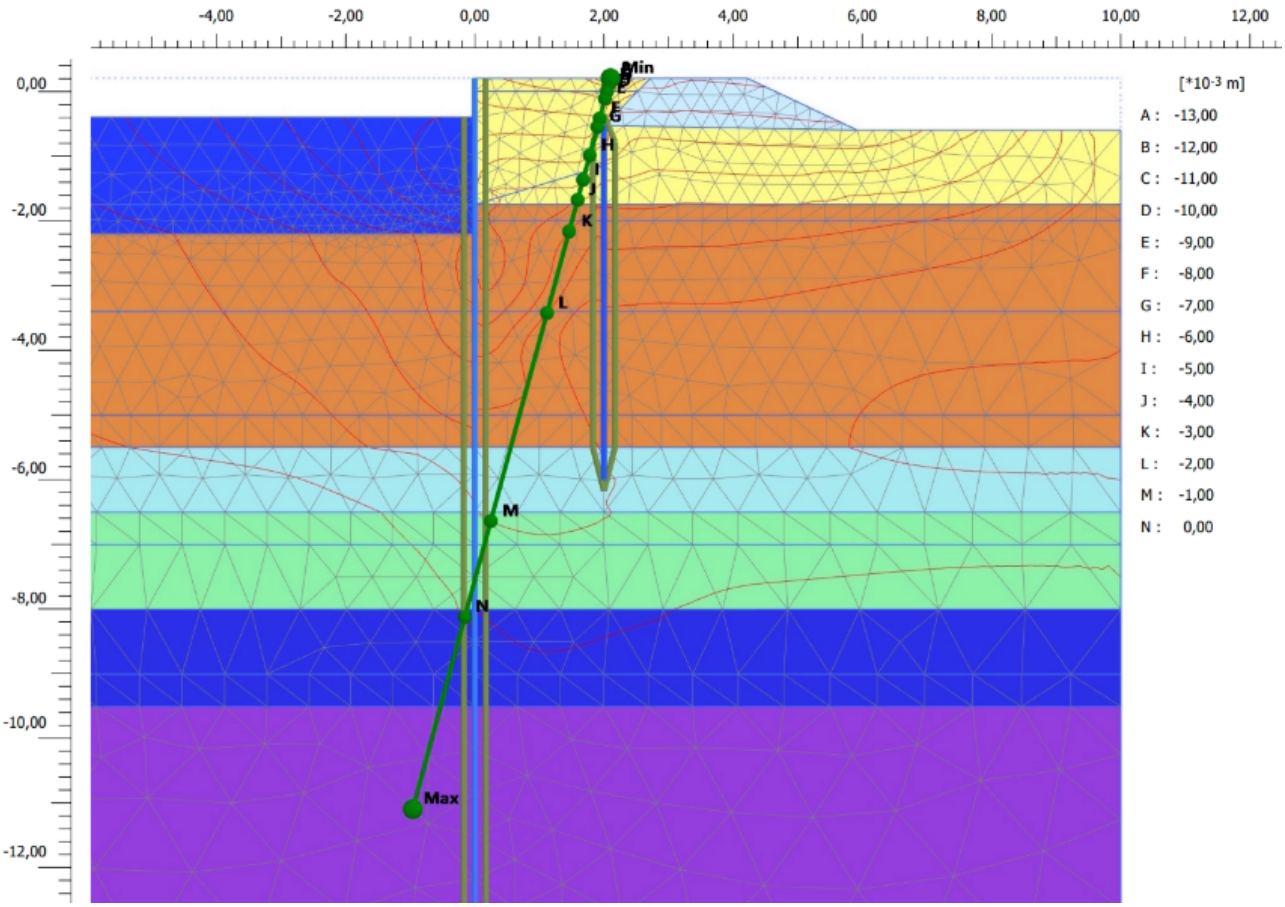

Figure 7.26: A contour plot of the deformation in x-direction in phase 1b.

As a result of the excessively large influence of the thermal activation of the sheet pile in phase 1a, the soil temperatures at the end of phase 1b are too low as well. This can be seen in Figure 7.27. The cooling of the subsurface to 2 °C is limited to the close vicinity of the sheet pile. However, a significant cooling has also occurred up to 2 metres away from the sheet pile. In the field test, this is localized to less than 1.5 metres away.

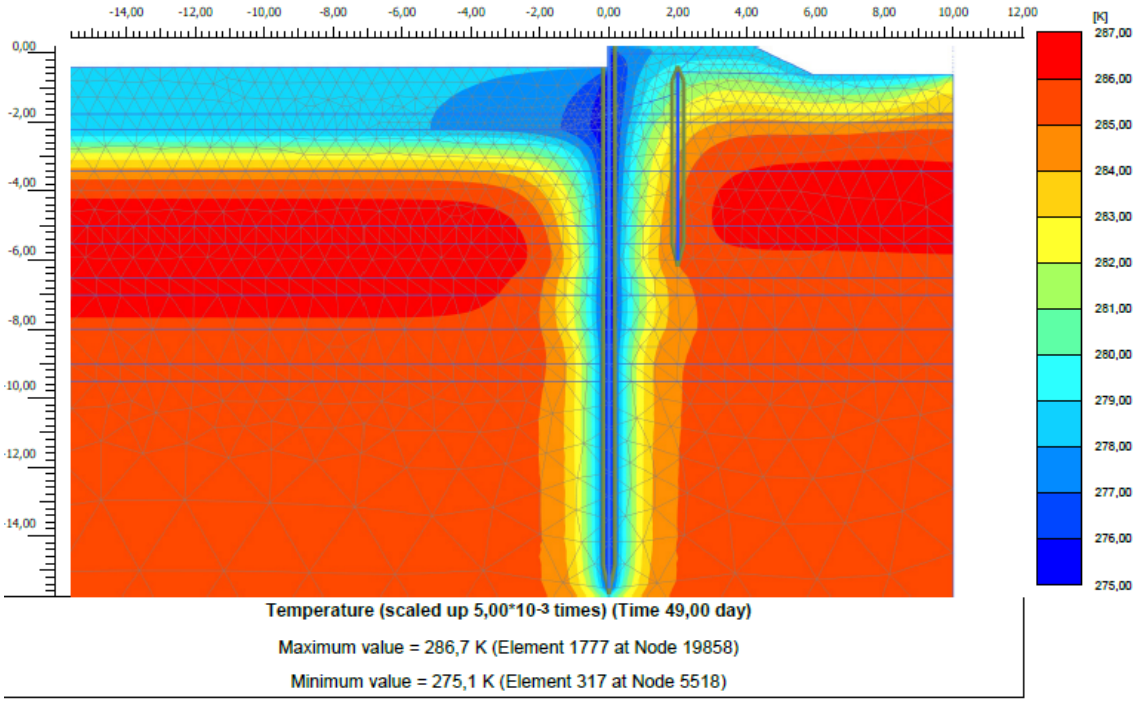

Figure 7.27: The temperature of the soil in phase 1b.

7.3.3 Phase 2: Double Side Deep Activation

Figure 7.28 shows the measured and numerically approached maximum deformation of the sheet pile in the deep section and Figure 7.26 the corresponding contour plot.The numerically determined deformation has barely changed in the 36 days the double deep loops are activated. The in-situ measured value shows a different trend. The largest deformation varies between 4 and 6 millimetres.

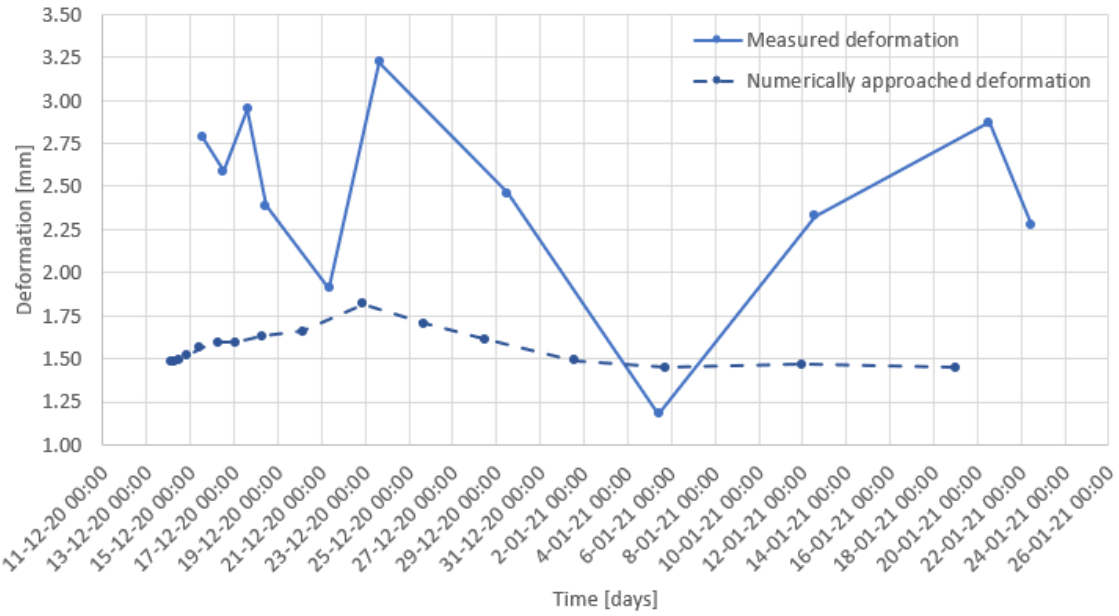

Figure 7.28: The displacement per metre of the sheet pile in the shallow section in phase 2. The positive direction of movement is into the canal.

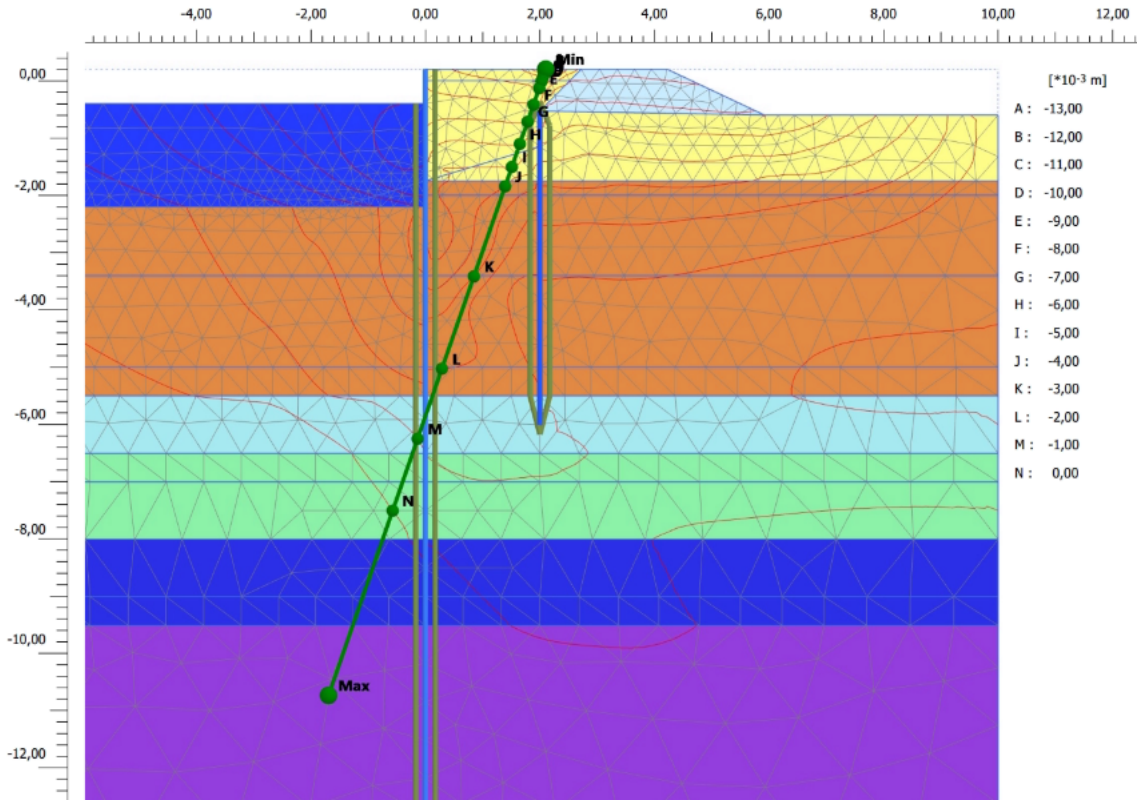

Figure 7.29: A contour plot of the deformation in x-direction in phase 2.

Figure 7.30 shows the air temperature registered in phase 2. The temperature increase at December 21st coincides with an increasing deformation. Moreover, at that time, a large amount of rain fell which undoubtedly contributed to the deformation. As the temperature and precipitation declines afterwards so does the distortion. The increase at the end of the phase cannot be correlated to the air temperature and precipitation.

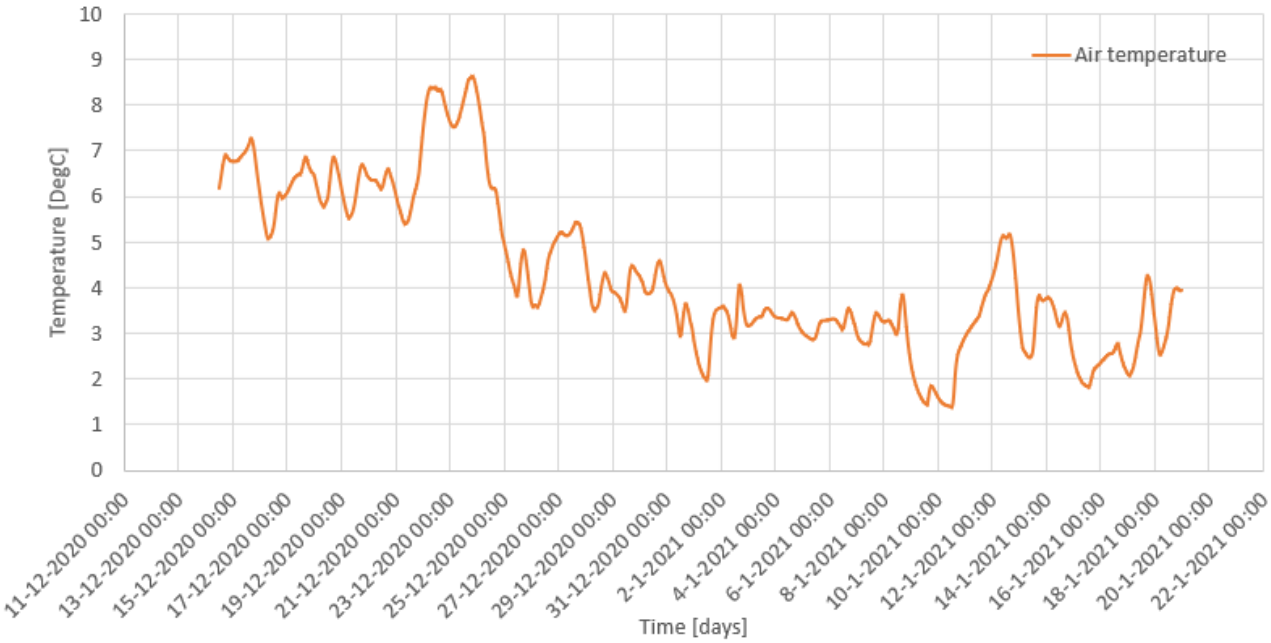

Figure 7.30: The air temperature in phase 2.

Figure 7.31 shows the soil temperatures at the end of phase 2. Just like in the previous phases, the soil cooled down too much as a result of the temperature boundary condition imposed on the sheet pile. Moreover, the thermistor string

in the quay 1.5 metres away from the sheet pile monitored a very limited influence of the thermal activation. In the computation in PLAXIS, the influence of the thermal activation spreads well beyond 2 metres.

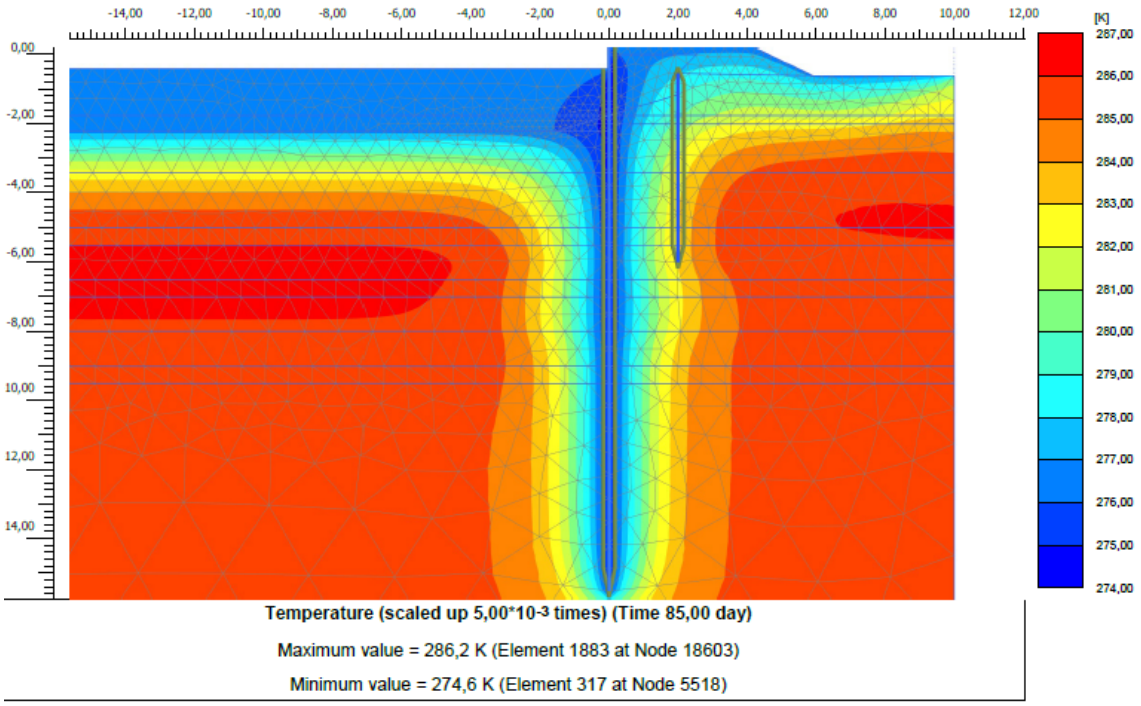

Figure 7.31: The temperature of the soil in phase 2.

7.3.4 Comparison of the Complete Dataset

The measured deformation shows a peak in deformation after the backfill followed by a decrease to the pre-backfill distortion. The deformation of the sheet pile wall prior to the thermal activation is subtracted from the inclinometer data. The both datasets are shown in Figure 7.32. Only the maximum deformation is shown, at the top of the sheet pile, as this data is of most interest.

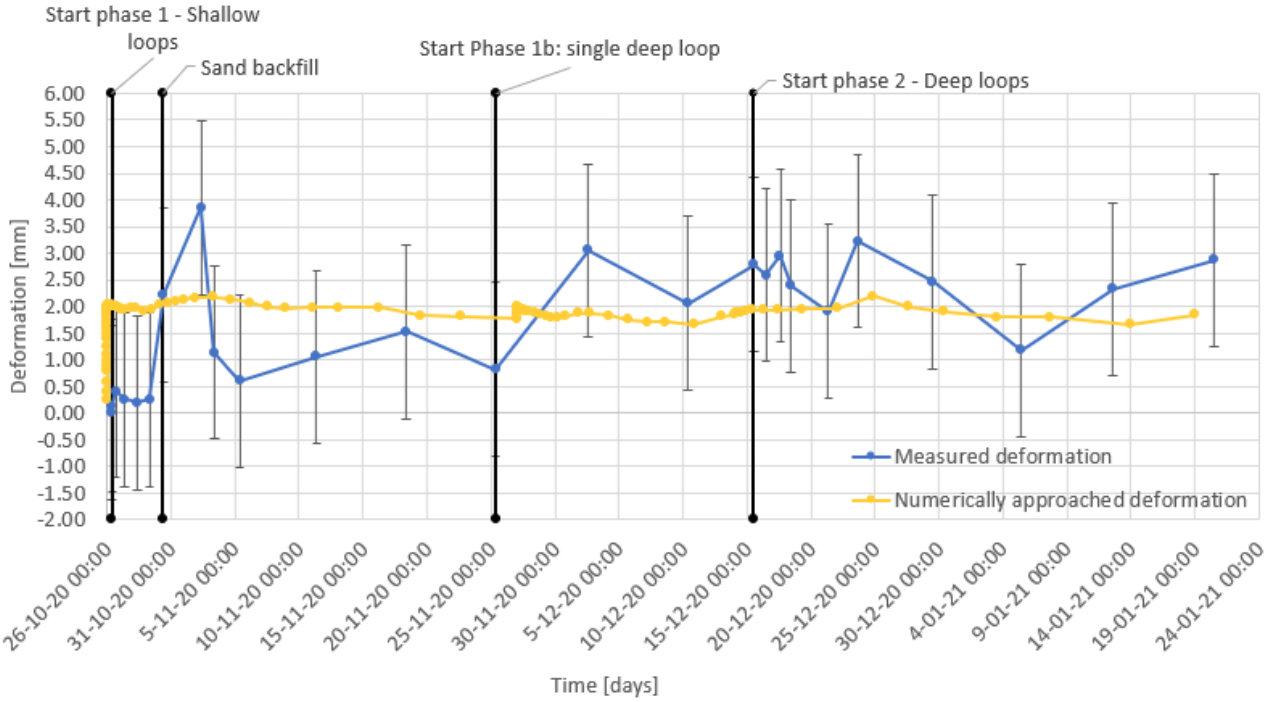

Figure 7.32: The measured and numerically approached maximum deformation of the sheet pile wall with the inclinometer measurement error.

The numerically approached distortion of the sheet pile wall lies within the oscillations of the in-situ measurements. Moreover, the numerical approach lies well within the boundaries of the 3.25 millimetres error margin of the in-situ measurements (1.625 millimetre to both sides). An additional HM analysis points out that the increase on the first day in the computations occurs with and without the thermal component activated. Therefore, if this deformation is ignored, the thermal activation in a PLAXIS analysis results in an oscillating distortion varying with a bandwidth of approximately 0.6 millimetres. However, this increment is not disposed as the in-situ measurements experience non-thermal influences too. Overall, the numerically approached and measured deformation match well.

7.3.5 Conclusion

After analysing the measured and numerically determined deformation and temperature change of the soil, the following observations are concluded:

- In-situ deformation is generally larger than the numerical deformation. This most likely results from additional influences unaccounted for in the numerical analysis such as precipitation and a measurement error.
- Both ambient temperature and precipitation have a clear influence on the in-situ sheet pile wall deformation.
- The soil cools down too much from temperature boundary condition. If a more natural distribution is desired, the heat flux boundary condition is needed.
- Oscillations in numerically approached values result from the fluctuating temperature of the air and water.

7.4 Heat Conduction Model Sensitivity Analysis and Calibration

This section contains the investigation into the sensitivity of several parameters of the heat conduction model. Based on the findings in this investigation, the model is calibrated after which the model is declared validated.

7.4.1 Sensitivity analysis

To calibrate the model and investigate the sensitivity of the constructive and soil parameters, a sensitivity analysis is performed based on the literature study. The following parameters are investigated:

- f_D: this is the Darcy friction factor in the pipes of the loops. To investigate the sensitivity, this factor is varied by a factor 10.
- C_p: this is the heat capacity and is the amount of energy needed to raise the temperature of 1 kg by 1 degree. This parameter is raised by 25%.
- λ: the thermal conductivity of the soil. This parameter is raised by 25% as well.
- Water flow in the canal. The initial analysis has a flow velocity of 0.01 m/s. This is compared to a computation in which there is no flow.
- Groundwater flow is the flow velocity in the soil. Based on the research of Kürten et al. (2014), this velocity is initially set to 0 m/s as the influence is marginal. A flow parallel and perpendicular to the sheet pile is investigated.

Table 7.3 contains the results of the sensitivity analysis. The investigation is carried out by using the data of phase 2. The first and second column contains parameter and value tested, respectively. The third column contains the average temperature flowing into the heat pump and column four contains the root mean square error between the measured heat pump data and the result of the value alteration.

Table 7.3: Parameters altered in the sensitivity analysis, the corresponding average heat pump value and RMSE.

Parameter	**Altered value**	**Average heat pump inlet temp [°C]**	**RMSE [-]**
Measured heat pump data	-	4.82	-
Initial numerical	-	4.49	0.57
f_D	0.01 / 0.1 [-]	4.37 / 4.37	0.56 / 0.63
C_p	2647.5 J/(kg · K) (+25%)	4.73	0.42
λ	1.89 W/(m · K) (+25%)	4.87	0.38
Water flow canal	0 [m/s]	4.24	0.75
Groundwater flow	10^{-7} [m/s]	4.57	0.49

Changing the heat capacity and thermal conductivity results in the biggest alteration. Moreover, the groundwater flow parallel to the sheet pile changes the error by a little less than 0.1. Therefore, it is advised to add this to the computation.

In this sensitivity analysis, the friction factor is varied by using a user defined value. As it shows that this factor does not have a large influence on the heat outlet, the default settings are used. This is determining the friction factor by means of Churchill's formula, described in COMSOL Multiphysics (2017). This is applicable to laminar, transitional and turbulent flow. When setting the open water flow to a flow velocity of 0 m/s, the extracted heat decreased drastically - in agreement with the research by Kürten et al. (2014). Therefore, the flow velocity of 0.01 m/s is maintained.

7.4.2 Calibration of the Heat Conduction Model

The following changes are implemented:

- The thermal properties (C_p and λ) are raised by 25%.
- A groundwater flow of 10^{-7} m/s running parallel to the sheet pile wall.
- The soil domain in the deep section is enlarged to prevent the boundaries from having influence.
- The water temperature is defined based on the measurements of sensor D_C(2), which is located just below the canal in the soil.

The aforementioned improvements result in a better fit of the numerically determined temperatures the measured temperatures. As expected, the temperature of the water in the canal is governing temperatures in the upper 4 metres of soil, emphasizing the importance the canal temperature boundary condition. This influence is so large that the soil temperature in the shallow section in phase 1a, in which only the shallow blue loop is activated, follows the water temperature instead of continuously declining. The metres below the upper 4 metres have a closer fit to the measured data. The temperatures in phase 1a are still too high and too low in the subsequent phases. The numerically approached energy extraction in phase 1b has a better fit in the first half of the phase, but a worse one in the second, as can be seen in Figure 7.33. Phase 2 shows a better fit throughout the whole phase (Figure 7.34). Based on the fact

that only phase 1a has barely improved and that the performance of the heat pump is difficult to model as a result of technical difficulties, it is determined that the data acquired in phase 1a is not useful for the validation.

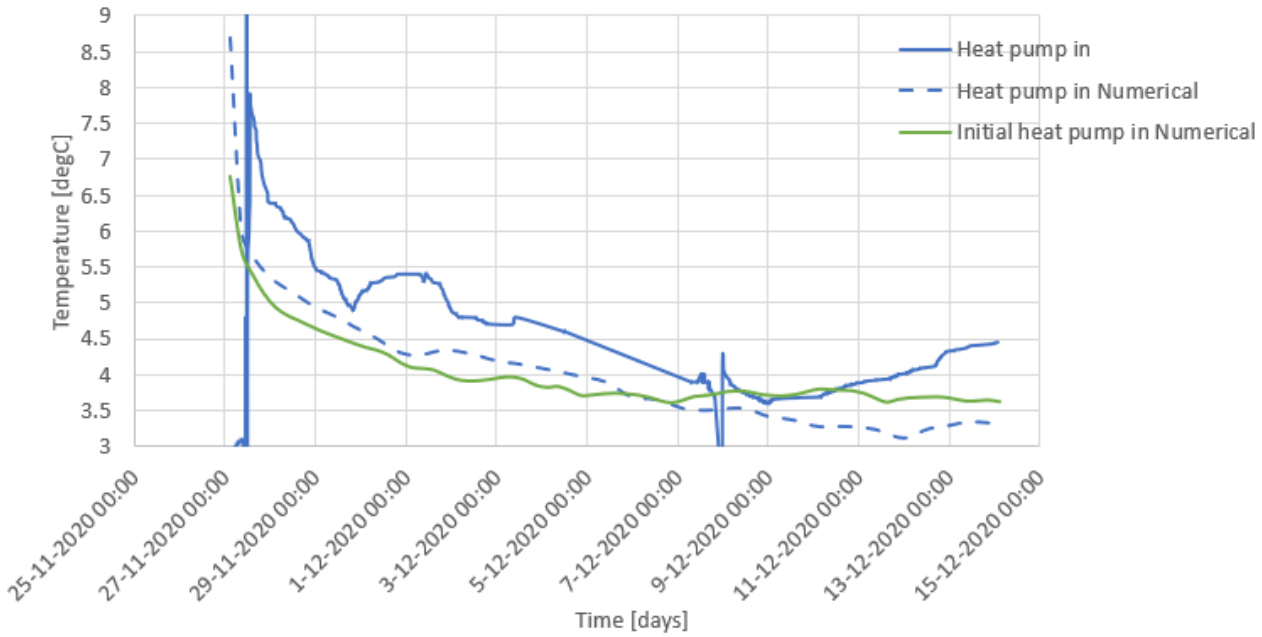

Figure 7.33: The calibrated numerical values of the heat pump compared to the measured values in phase 1b.

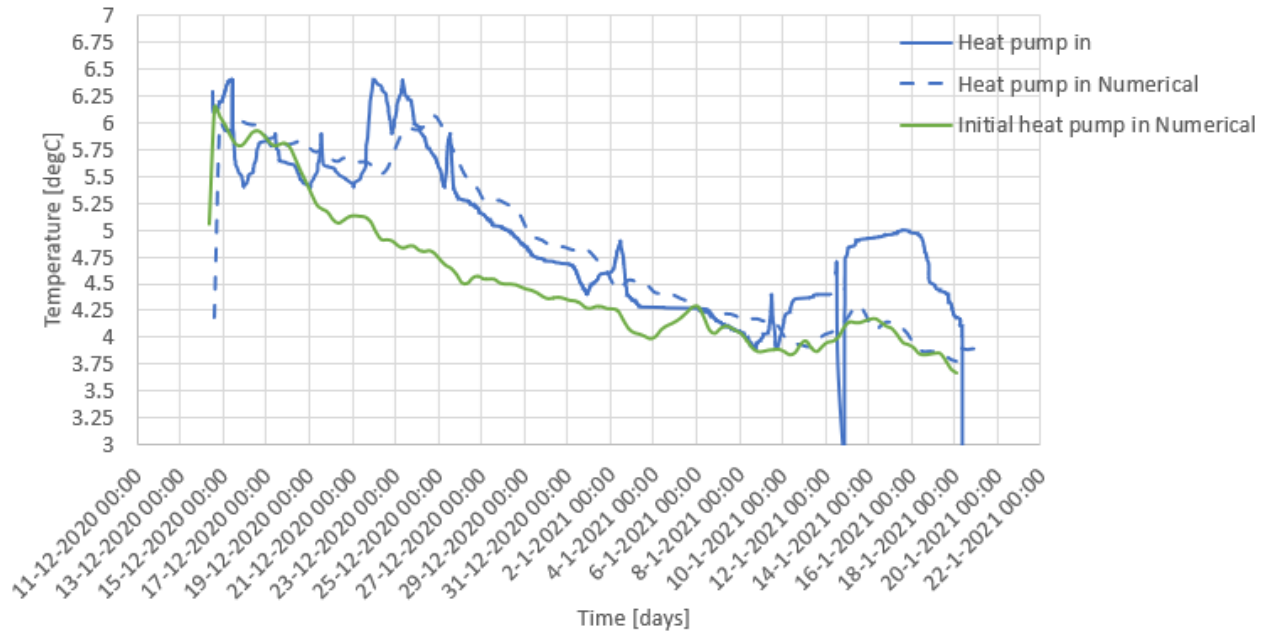

Figure 7.34: The calibrated numerical values of the heat pump compared to the measured values in phase 2.

7.5 Geotechnical Stability Model Sensitivity Analysis

This section contains the investigation into the sensitivity of several parameters of the geotechnical stability model.

7.5.1 Sensitivity Analysis

Table 7.4 shows the deformation at the end of four stages of a computation with and without the thermal component activated. The deformations lie very close to each other. Figure 7.35 shows the time discretized deformation of the top of the sheet pile with and without the thermal component. As can be seen, the computation in which the thermal component is activated oscillates while the non-thermal computation does not. This highlights the importance of looking at the deformation – and the forces on the sheet pile – throughout the computation rather than looking at the end result.

Table 7.4: The deformation ($|u_x|$) of the sheet pile wall into the canal with (THM) and without (HM) the thermal component.

Thermal component [m^2K/kW]	**Sand backfill stage [mm]**	**Phase 1a [mm]**	**Phase 1b [mm]**	**Phase 2 [mm]**
Activated	6.15	8.54	8.56	8.43
Non-activated	6.94	8.46	8.47	8.46

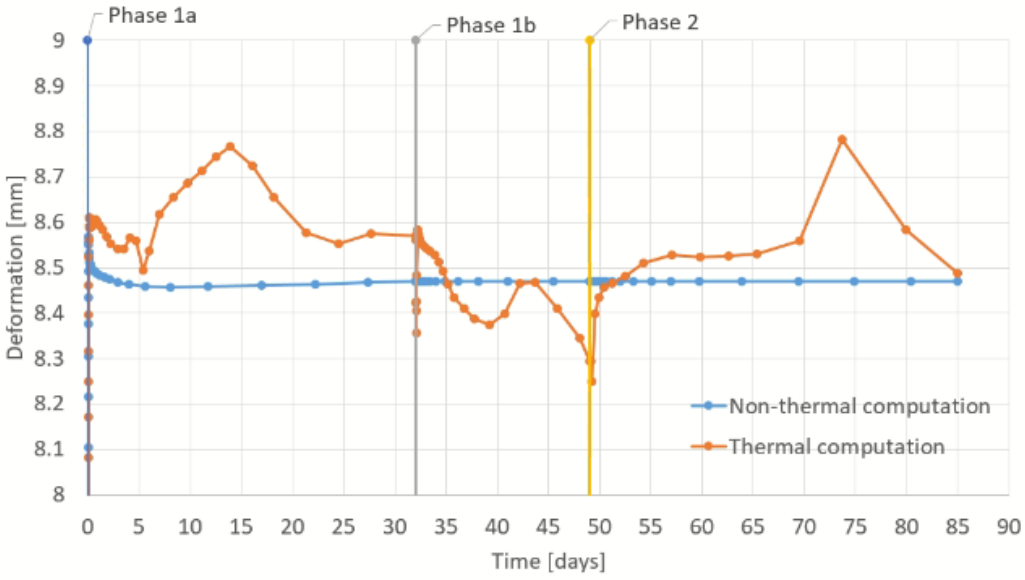

Figure 7.35: The deformation of the top of the sheet pile of a thermal and non-thermal computation

Table 7.5 contains the forces on the sheet pile in an HM and a THM analysis. The forces are close to constant throughout the whole analysis. The only force that changes significantly is the axial force in the THM analysis - in line with the findings in Chapter 6. At the start of phase 1b, the single side deep activation, the changing temperature of the sheet pile and soil results in a temporarily increased axial force. This suggests that the thermal activation contributes little to the total deformation of the sheet pile wall.

Table 7.5: The working on the sheet pile with (THM) and without (HM) the thermal component.

Force	**Type of calculation [THM/HM]**	**Max Value P1a (min/max)**	**Max Value P1b (min/max)**	**Max Value P2 (min/max)**
Axial force [kN/m]	HM	(-19.65/0.4)	(-19.66/0.44)	(-19.66/0.44)
Axial force [kN/m]	THM	(-18.65/0.4)	(-17.66/2.01)	(-18.77/0.49)
Shear force [kN/m]	HM	(-19.88/20.51)	(-19.88/20.51)	(-19.88/20.51)
Shear force [kN/m]	THM	(-20.14/20.53)	(-19.88/20.51)	(-20.08/20.6)
Bending moment [kNm/m]	HM	(0/85.75)	(0/85.75)	(0/85.75)
Bending moment [kNm/m]	THM	(0/86.37)	(0/85.75)	(-0.2/85.50)

Based on the research performed in Chapter 6, the volumetric thermal expansion coefficient (TEC) is expected to have

the largest influence on the deformation of the sheet pile. Therefore, in this calibration, this parameter is decreased separately for each soil layer by 25% to investigate its influence. The input parameters for solids and fluids are split and based on the porosity, the program defines the composed soil parameters. The top sand layer is investigated first, followed by the peat and clay. As peat is consists of mostly water, the volumetric TEC for the solids is not very influential and initially set at 0 1/K. As the the research into the TEC of organic material is a rarity, the volumetric TEC used in the investigation is that of wood, a material scarcely found in peat in the Netherlands. The linear (alpha) TEC of water is 0.21e-3 1/K.

Table 7.6: The deformation ($|u_x|$) of the sheet pile wall into the canal with various volumetric thermal expansion coefficients for sand.

Volumetric thermal expansion coefficient [1/K]	**Sand backfill stage [mm]**	**Phase 1a [mm]**	**Phase 1b [mm]**	**Phase 2 [mm]**
0.1e-3	6.39	8.06	8.17	8.12
0.075e-3	6.6	8.31	8.39	8.48
0.125e-3	6.67	8.29	8.34	8.25

The top two metres of the stratigraphy consist of sand. The variation in the volumetric TEC is described in Table 7.6. The sand backfill stage is added as a plastic analysis, in which a backfill of 0.25 metres of sand is placed and the initial soil temperatures are defined, after which a time dependent analysis is performed in phase 1a, 1b and 2. The deformation of the sheet pile in phase 1a is a result of the thermal activation and approximately 1.7 millimetres. In phase 1b and 2, the deformation increases slightly to approximately 1.8 millimetres. The variation in the volumetric TEC results in a deformation increase in the sand backfill stage of 0.2 - 0.3 millimetre. The consecutive stages have a deformation comparable to the initial value.

Table 7.7: The deformation ($|u_x|$) of the sheet pile wall into the canal with various volumetric thermal expansion coefficients for peat.

Volumetric thermal expansion coefficient [1/K]	**Sand backfill stage [mm]**	**Phase 1a [mm]**	**Phase 1b [mm]**	**Phase 2 [mm]**
0	6.39	8.06	8.17	8.12
9e-6 (parallel)	6.51	8.18	8.43	8.37
90e-6 (perpendicular)	6.77	8.55	8.81	8.79

Table 7.7 contains the data of the analysis of the volumetric TEC of peat. For the first value, 0 1/K, there is no expansion of the solids in the peat. The expansion of the water, of which peat mostly consists, is defined separately. Little information is found on the thermal expansion of organic materials. Therefore, the volumetric TEC of wood is used. Two values are found, one for expansion parallel to the grain and the other perpendicular to the grain (Engineering_Toolbox, 2003). As can be seen, the deformations in the plastic sand backfill stage increase slightly and, consequently, the deformations as a result of the thermal activation do too. It is recommended that additional research is performed into the TEC of peat, but based on this investigation peat does not seem to have a large influence on the deformation of the sheet pile.

Table 7.8: The deformation ($|u_x|$) of the sheet pile wall into the canal with various volumetric thermal expansion coefficients for clay.

Volumetric thermal expansion coefficient [1/K]	**Sand backfill stage [mm]**	**Phase 1a [mm]**	**Phase 1b [mm]**	**Phase 2 [mm]**
0.102e-3	6.39	8.06	8.17	8.12
0.0765e-3	6.42	8.07	8.10	8.06

Table 7.8 gives the initial value for the volumetric TEC of clay and and 25 % smaller. This variation has close to zero influence on the deformation.

Table 7.9: The deformation ($|u_x|$) of the sheet pile wall into the canal with more detailed ambient temperatures.

Altered boundary condition [-]	**Sand backfill stage** [mm]	**Phase 1a** [mm]	**Phase 1b** [mm]	**Phase 2** [mm]
initial	6.39	8.06	8.17	8.12
water	6.40	8.11	8.14	8.19
air	6.6	8.30	8.22	8.22

Besides altering the TEC, the boundary conditions of the model are changed as well. Initially, the water and air temperatures are averaged and are defined by bi-linear curves. To investigate the influence, the data from the field test is used. Table 7.9 contains the results. The precise water temperature has little influence on the deformation and the precise air temperature has slightly more. Still, the change is less than 0.5 millimetre. Therefore, it is determined it is not necessary to define the water and air temperature precisely and an approximation is enough.

Table 7.10: The deformation ($|u_x|$) of the sheet pile wall into the canal with a verying the thermal resistance of the top sand layer.

Thermal resistance sand [m^2K/kW]	**Sand backfill stage** [mm]	**Phase 1a** [mm]	**Phase 1b** [mm]	**Phase 2** [mm]
3.089	6.39	8.06	8.17	8.12
2.317	6.5	8.4	8.5	8.5

Table 7.10 contains the deformation of the sheet pile when the thermal resistance of the top sand is varied. This value is defined as:

$$R = \frac{d}{\lambda}$$

in which d is the thickness of the sheet pile [m] and λ the thermal conductivity of the soil [kW/(m · K)]. This value is used to control the heat transfer through the sheet pile. This variable is varied by 25% as well and by decreasing this value, the exchange between the sand and the water is smaller. This results in higher temperatures in the quay which results in a slightly increased deformation. Still, this extra deformation is very small reaching the conclusion that this is not influential. Based on the first comparison and the sensitivity analysis, none of the parameters are adjusted.

7.6 Investigation Into the Behaviour of the Energy Sheet Pile Wall Over 4 Year

Using the validated geotechnical stability model a long term THM calculation of 4 years is conducted to investigate the behaviour of the sheet pile wall. The calculation starts at January 1st 2017 and ends at January 1st 2021. The calculation is divided in multiple stages: the cold period of the year (October - April) in which buildings are heated and the warmer period in which the soil regenerates. Two types of regeneration are investigated: natural regeneration and regeneration using the energy sheet pile wall. In the calculation of the former the line boundary condition of the sheet pile is deactivated while during the latter the water temperature is imposed on the energy sheet pile wall. By doing this, the heat extracted from the water is stored in the subsurface which can be used during winter. It is expected that it increases the yield considerably and is easily achieved by letting the fluid flow through the loop system without the heat pump extracting heat.

Figure 7.36 shows the numerically determined deformation for three situations. The 'no energy extraction' (gray) line is the deformation of a conventional sheet pile wall, i.e. a sheet pile wall which is not used for extracting energy but is influenced by temperature changes throughout the year. The 'natural regeneration' (blue) line shows the deformation when the soil recharges naturally during the warm period of the year and the 'forced regeneration' (yellow) shows the deformation when the sheet pile stores heat in the subsurface.

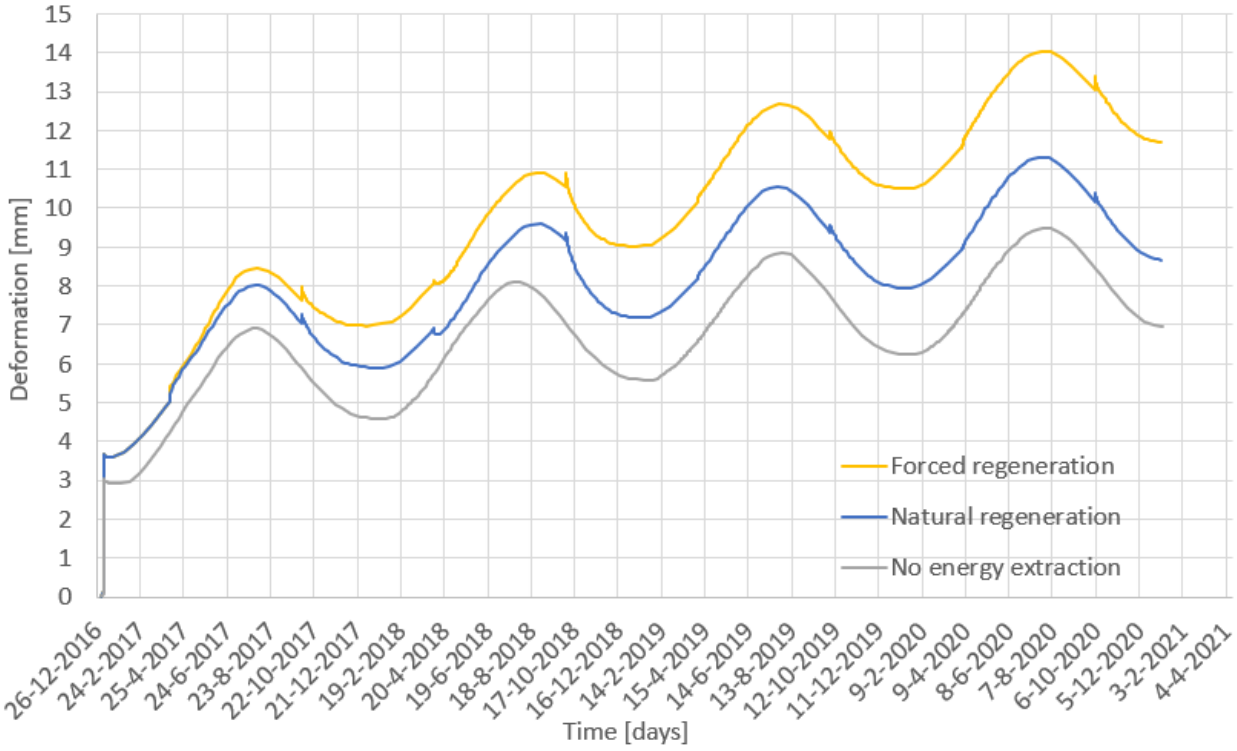

Figure 7.36: The maximum deformation of the energy sheet pile wall resulting from different activation settings.

The gray line is the deformation resulting from the natural temperature fluctuation. In reality, this might be even larger as radiation is not accounted for in the model. The computation starts with a sudden increase of 3 millimetre (and the other two almost 4 millimetres). This increase occurs regardless of whether the sheet pile is thermally activated. It is not completely clear if this is a numerical deviation or a direct effect from implementing the thermal boundaries. Therefore, it is advised to investigate this in more detail. Shifting attention to the other calculations, the maximum difference between the gray and blue line is approximately 2 millimetre and between the gray and yellow line a maximum difference of 5 millimetre is present. Even though the deformation of the energy sheet pile wall with forced regeneration is larger, the increase tapers off as can be seen clearly when comparing the yearly lows in the sinus curve. This deformation is a result from the yearly temperature fluctuations: water temperatures of 5 °C in the winter and 23 °C in the summer. The air temperature is approximately the same and the energy sheet pile is 2 °C in the winter. To put these temperature fluctuations in perspective: during the summer the temperature of the sheet piles in a lock can increase up to values of 40/50 °C as a result of radiation. In the winter, the temperature can drop to -1 °C. This 50 °C temperature difference poses no problem. As this natural temperature fluctuation is not a design condition for standard quay walls it is expected that the numerical influence from activation does not pose a risk to the function of the quay wall. However, it is recommended to investigate this behaviour further and compare it to the natural seasonal displacement behaviour of the quay.

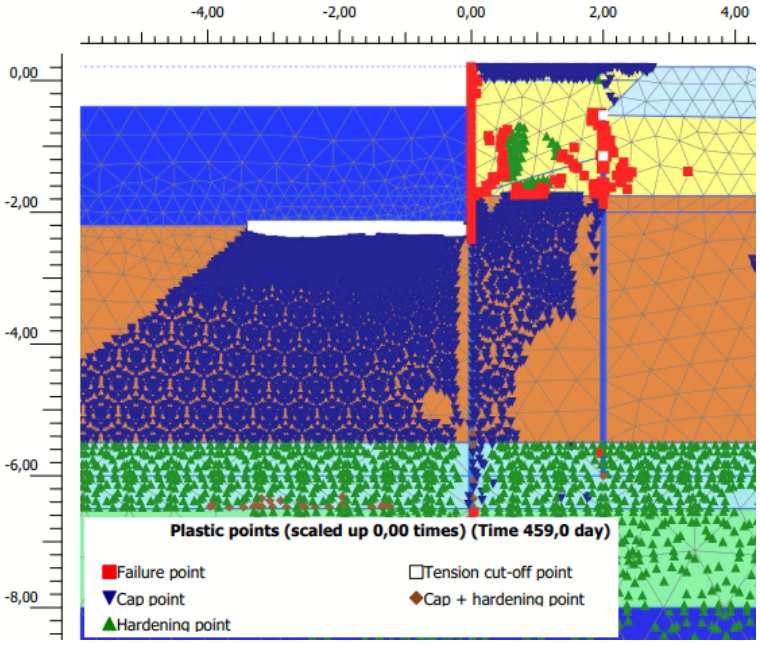

Figure 7.37: The plastic points in April 2018.

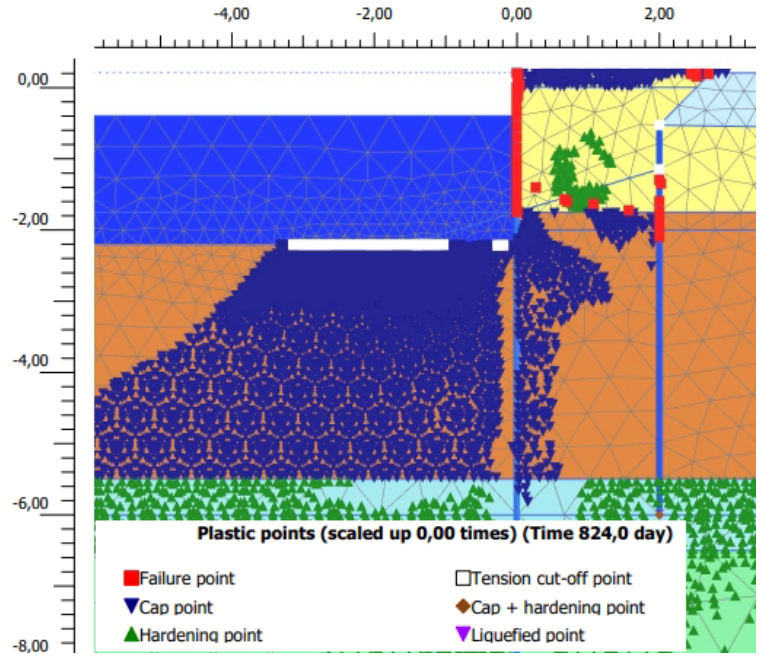

Figure 7.38: The plastic points in April 2019.

Figure 7.37 shows a plot with plastic points. These points indicate the consequences on the state of the soil as a result of the temperature change by showing the stress points that are in a plastic state (PLAXIS, 1994):

- Red cube (failure point) = indicate that the stresses lie on the failure envelope;
- White cube (tension cut-off point) = tension cut-off criterion is applied;
- Blue upside-down pyramid (cap point) = a state of normal consolidation where pre-consolidation stress is equivalent to the actual stress state;
- Brown diamond (cap + hardening point) = points that are on the shear hardening and cap hardening envelope.
- Green pyramid (Hardening point) = points on the shear hardening envelope.

Comparing Figures 7.37 and 7.38 show that after one year the amount of cap and hardening points decrease indicating a hardening effect caused by the temperature induced displacement. This hardening effect is also what causes the

displacement effect to taper out over time as the soil starts to react stiffer to the alternating sheet pile displacements. By extrapolating the data, it is determined that after an additional two years the yearly increase becomes zero. It is expected the maximum deformation as a result of the thermal activation with forced regeneration will be approximately 6 millimetres.

7.7 Concluding Remarks

In this chapter the two models developed are validated using the thermal and mechanical measurements performed at the field test location at Zweth. The heat conduction model improved significantly after adjusting thermal properties of the soil and defining the air and water temperature in more detail. Still, the temperature of the soil is generally too low while the extracted energy has an acceptable fit. The somewhat limited time period analysed in this chapter poses no direct problems. However, when simulating the extraction over multiple years, incorrect soil temperatures might possibly result in an incorrect yield. The deformation determined using the geotechnical stability model shows a good agreement with the in-situ measured deformations. The sensitivity analysis showed that the thermal component in the computation has little influence on the overall deformation of the sheet pile. However, as the in-situ measurements consist of a thermally and mechanically induced distortion too, the overall deformation is used in the assessment.

The insights and conclusions resulting from the research described in this chapter, in combination with the finding of Chapter 5 and 6, are meant to be used to answer research question 3: 'Can an industry standard finite element method program capture the long-term thermal and mechanical behaviour of an energy sheet pile quay and the subsurface?' When validating a specific period of time, very precisely measured boundary conditions are needed for the heat conduction model, as well as an improvement on the energy extraction from the water in the canal. Besides this, the simulated and measured extracted energy is a close fit. Therefore, it is safe to say that the heat conduction model can capture this behaviour. The deformation of the sheet pile wall is approached reasonably by the geotechnical stability model. The computation with a time span of 4 years shows that the air temperature influences the deformation considerably. This is not spotted in the validation, most likely the result of the short time span. The radiation and precipitation is also expected to wield large influence on the deformation, both of which not accounted for in the model. These influences occur regardless of the sheet pile wall being thermally activated hence this is standard behaviour. Investigating this is not standard practice so it is recommended to investigate this into further detail. Referring back to Figure 7.36, the natural (blue line) and forced (gray line) regeneration are, like the natural behaviour, sinus-like curves. The thermal activation and regeneration amplifies this curve thus increasing the deformation. Extrapolating the data, the trend tapers off after 6 years to a total increase of 6 millimetres. Answering research question 3: yes, PLAXIS and COMSOL can approach the behaviour of the sheet pile wall with acceptable accurately.

Chapter 8

Discussion

The Validity of This Thesis

Two types of measurements are performed in the field test used in this thesis. To measure the distortion of the sheet pile wall, inclinometer measurements are performed. The temperature change in the soil is measured with the help of thermistor strings connected to a data logger. The inclino measurements are done manually by the author. When processing the data, a measurement error to take into account. The error is 0.25 mm/m which means the possible error at the top of the sheet pile in the deep section is 3.25 millimetres and in the shallow section 2.5 millimetres. As the objective of this thesis is to determine if the energy sheet pile wall is safe to use, the exact deformation is not that important - the order of magnitude of deformation is. The temperature change in the soil is measured every 15 minutes by every sensor in the thermistor string. In addition to the missing data of several sensors due to technical issues, the possibility exists that the sensors close to the surface experience a lot of influence from the ambient temperature. The steel pipes in which the thermistor strings are placed conduct heat well - possibly transporting the cold from the air into the soil. Moreover, the pipes were initially filled with air damps the temperature. Half way through phase 1a, the pipes were filled with water which damps much less. After filling the pipes with water the monitored temperatures became less linear indicating more precise measurements. These pipes are not present in the heat conduction model and might explain some of the differences in measured and numerically approached temperatures. Generally, the acquired data is reliable and valid and, by validating the heat conduction and geotechnical model, predictions can be made based on the simulations of these models.

Discussion of the Results

The aforementioned measurements are used to validate the heat conduction and geotechnical stability model. The simulated temperature in the heat conduction model is initially overestimated in the quay adjacent to the canal. This is the result of the water temperature in the canal being higher - emphasizing the importance of a precisely measured water temperature. The data acquired in phase 1a fits poorly with the numerical data. As a result of technical difficulties the conditions in this phase are difficult to capture in the model. Therefore, it is determined that the data of phase 1a is not useful. In phase 1b and 2, the numerically approached temperatures showed a better fit. However, the temperatures deeper in the soil are generally simulated too low while the extracted energy fits well, indicating a mismatch between the remaining and extracted energy. Possibly, the initial amount of energy in the soil is not enough or the supply of energy from the surroundings is too little. In addition, the energy supply of the water is poorly modelled. The convection in the water is accounted for by a constant flow but the turbulence of the water and the resulting energy is not simulated. This technique distinguishes itself from other shallow geothermal systems by extracting energy from flowing water and, therefore, needs to be added to the model. In this investigation, the most important is the fit of the extracted energy - which is very close. This shows it is possible to simulate the energy extraction and the temperature of the sheet pile and loops as a result of this extraction. Neither the deformations determined in the field test nor those determined in the numerical approach are excessively large. The measured deformation oscillates while the computed data is almost linear and lies close to the average of the in-situ measurements. Moreover, an analysis is done simulating a 4 years time period in which the maximum deformation of the sheet pile which, among others, is used for heat extraction during cold times and heat storage during warm periods is investigated. The yearly temperature difference in the 4 year analysis is approximately 20 °C. In situations where a large area of the sheet pile wall is exposed to the air, the temperature can increase up to values of 40/50 °C. Therefore, to put in perspective, the thermal activation does not result in excessively large temperature loads. The maximum deformation is 5 millimetre larger than the case with a conventional sheet pile wall. Extrapolating the data, it is expected that – in this particular

case – the maximum deformation resulting from the thermal activation is expected to be approximately 6 millimetres. The natural temperature fluctuation is not a standard design condition for quay wall but, based on this analysis, it is expected the influence from the thermal activation does not pose a risk to the function of the quay wall.

Effects of the Results of This Thesis

The conclusion drawn up in this thesis implies that a thermally activating a sheet pile wall does not negatively impact the primary function of the sheet pile wall. The temperature leads to some wall displacements but the amount is assumed to be within the boundaries of the seasonal displacement behaviour without activation. Use of the technology as an adaptation on standard sheet pile wall does not negatively impact is primary function as a quay wall. As a result, this technology has great potential to be implemented on a large scale in densely populated areas with lots of quays, such as Amsterdam. By extracting energy from the open water and subsurface, the dependency on fossil fuels is reduced. An additional benefit is that the water temperature decreases as energy is extracted from it which leads to cooler temperatures during the summer in the city centre making the city more liveable for all.

Chapter 9

Conclusions and Recommendations

Conclusions

The results from the field test show that in phase 1a (single side shallow activation) the soil cools down by 0.5 °C per week. In phase 1b (single side deep activation) by 1 °C and in phase 2 by 0.375 °C. This temperature decrease is measured in the close vicinity of the sheet pile wall, right between the bulges. The thermistor string in the quay, 1.5 metres away, monitored a small temperature decrease. This decrease includes the influence of the ambient air temperature and the possible influence of the energy extraction. Moreover, the amount of loops activated in one section (single or double activation) did not show a linear relation. Double side activation shows only a slightly larger temperature decrease in the subsurface.

The comparison of the temperature decline in the soil in the heat conduction model and the acquired data in the field test show that the temperature decline in the soil of the heat conduction model is too large. The numerically approached extracted temperature from the soil corresponds well to the measured data from the field test. Moreover, the temperature of the water in the canal is found to govern the temperature in the soil adjacent to the canal. Therefore, to model the energy extraction in the (shallow) subsurface correctly, the water temperature has to be implemented in the model as precise as possible.

The geotechnical stability model approaches the measured deformation of the sheet pile wall well. The deformation measured in the field test oscillates while the numerically approached data is almost linear. Very small oscillations in distortion, in the order of tens of millimetres, are calculated over time. This is a result of the fluctuating ambient air/water temperature. In a 4 year analysis in which energy is extracted during the cold period of the year and the soil regenerates during the warm period as a result of the transport of heat from the surface to the subsurface by the loop system, the forced regeneration results in the largest theoretical deformation. The maximum calculated distortion of the sheet pile wall is approximately 5 millimetres more than without thermal activation. The main research question of this thesis is: 'Can the structural safety of a sheet pile quay wall be guaranteed when the sheet pile is thermally activated'? In the 4 year analysis, the deformation increases progressively and tapers off at approximately 5 millimetres. Therefore, the main research question is answered with: yes, as the deformation of the thermally activated sheet pile wall can be approach with acceptable accuracy and is not excessively large, it is strongly expected the primary function will not be negatively impacted by the thermal activation.

Recommendations

For future investigations it is recommended that the behaviour of the water in the heat conduction model is improved. The model does not account for the influence of turbulence of the water flow parallel to the sheet pile. Research has indicated that a significant amount of energy is extracted from this phenomenon. Moreover, it is recommended to investigate if the presence of soil layers – with different thermal properties – are of influence on the regeneration of the soil as a result of the changing seasonal temperature. Regarding the deformation of the energy sheet pile as a result of thermal loading, various aspects deserve additional research. The thermal loading of a sheet pile wall not a design parameter and; therefore, the deformation of a sheet pile wall resulting from the natural seasonal temperature fluctuations should be investigated so that the additional influence from the thermal activation can be quantified. In addition, at the start of a time dependent analysis (both HM and THM), an immediate deformation of a few millimetres occurs. It is advised to investigate this increase as it is unclear if this is an actual occurring deformation or a numerical occurrence.

Appendices

Appendix A

13.1 Phase 1a - Single Side Shallow Activation

This appendix contains the analysis of the single side activation phase. All measurements in each thermistor string are plotted in a single graph.

13.1.1 Deep Section

Originally, this phase was supposed to have the duration of one month. However, no fluid ran through the deep (purple) loop during this month (from October 29th 2020 to November 27th 2020). As the energy sheet pile wall deep section did not functioned properly, the temperature measured over depth is the natural distribution. These temperatures give a valuable insight into the reaction of soil to the changing weather conditions and temperatures. In order to have at least some data of the deep activation section, the first phase has been extended by two weeks which has been called phase 1b.

Deep Front Left Figure 13.1 contains the measurements of the deep front left (D_FL) thermistor string. The number in brackets in the legend is the depth at which the sensor hangs; hence, D_FL(1) lies 1 metre below surface and D_FL(15) 15 metres below the surface. What catches the eye immediately is the dip on 2020-11-18. This is due to the filling of the tubes with water in which the thermistor strings are placed. Water has a higher thermal conductivity than air resulting in a more accurately measured soil temperature. This is especially visible at sensor D_FL(4) where the measured temperature drops 0.5 degrees Celsius after the filling.

The temperature distribution visible is as one would expect in the autumn. The five upper sensors (D_FL(1) – D_FL(5)) show a large temperature difference. The coldest is D_FL(1), varying between 9 and 13 °C, and is influenced by the ambient temperature a lot. When focussing on deeper sensors, this daily variation becomes smaller. D_FL(5) varies between 13.5 and 14.5 degrees Celsius. This warmth is a result of the summer heating up the soil. As air temperature cooled down, the cold hasn't had time to penetrate to 5 metres depth yet. D_FL(2) to D_FL(4) lie between these two extremes, as temperature increases with depth. The downward going trend is the soil catching up with the season temperature. All sensors deeper than D_FL(5) are cooler, converging to slightly less than 12 °C quickly. This observation is in line with expectations as the soil in the Netherlands at 6 metres below ground level is around 12 degrees year around (Sedighi et al., 2015). The deepest sensors monitor an increasing temperature. This is most likely the delayed heat from the summer only now penetrating to this depth.

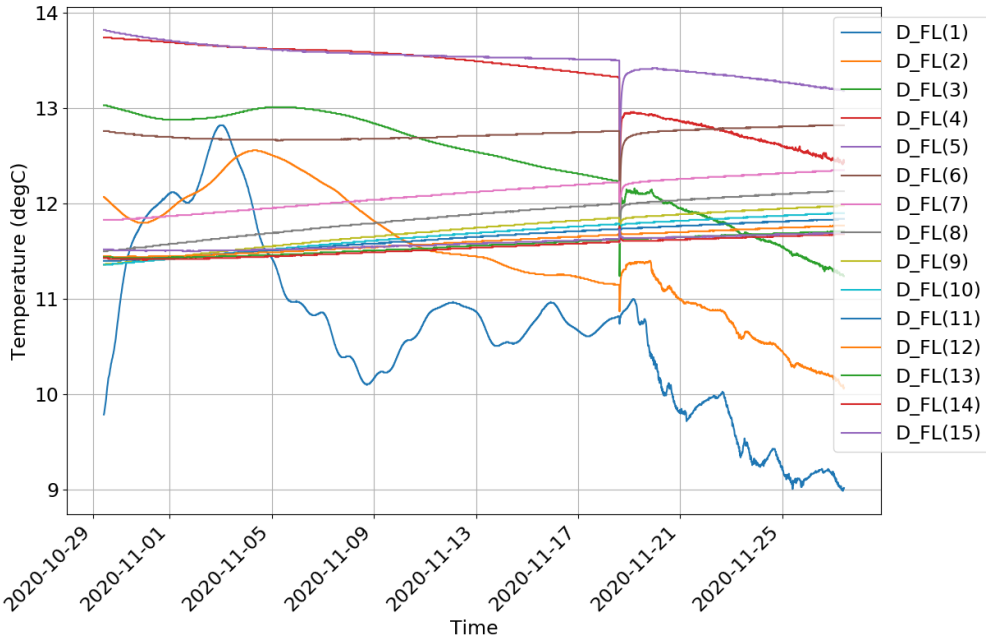

Figure 13.1: The data of deep front left thermistor string measurements in phase 1a.

Deep Front Right Figure 13.2 shows the measurements from thermistor string deep front right (D_FR). The same behaviour is recognised in this dataset and the extremes are even larger. D_FR(5) starts at 14.5 °C dropping to 13.5 °C over the course of one month. This is about 0.5 °C warmer than the measurements from D_FL. Most likely, the water in the canal governs this difference as D_FL lies closer to the canal and is more exposed to its influence as it lies in the bulge of the quay (as can be seen in Figure 4.6).

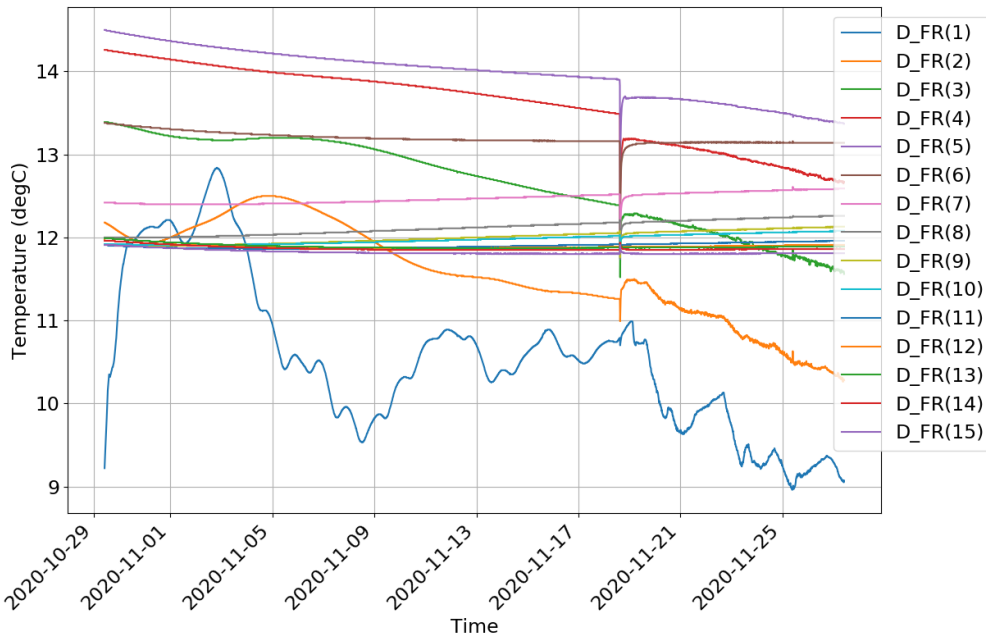

Figure 13.2: The data of deep front right thermistor string measurements in phase 1a.

Deep Back The measurement of thermistor string deep back (D_B) are shown in Figure 13.3. This thermistor string contains fewer sensors than the previous two discussed. Also, the highest sensor (D_B(1)), is located on the surface instead of in the pipe resulting in the measurement of the ambient temperature. Nevertheless, the six sensors that are in place show the same soil temperature behaviour. The sensors clearly show that the summer heat has penetrated the soil less deep but with the same magnitude (D_B(3) lies about 2.5 m below the surface). This suggests that the presence of a canal aids the heating of the soil during summer. Due to radiation, convection, diffusion and the flow

in the canal, water heats up more or less uniformly to even higher temperatures than the soil in the summer. In addition, as the heat capacity of water is relatively high, a large amount of energy is captured on the canal surface and transported to the bottom of the canal where it transfers the energy to the soil. Therefore, comparing this dataset with datasets acquired closer to the canal, it can be – cautiously – concluded that the presence of a canal greatly increases the possible yield of the energy sheet pile wall.

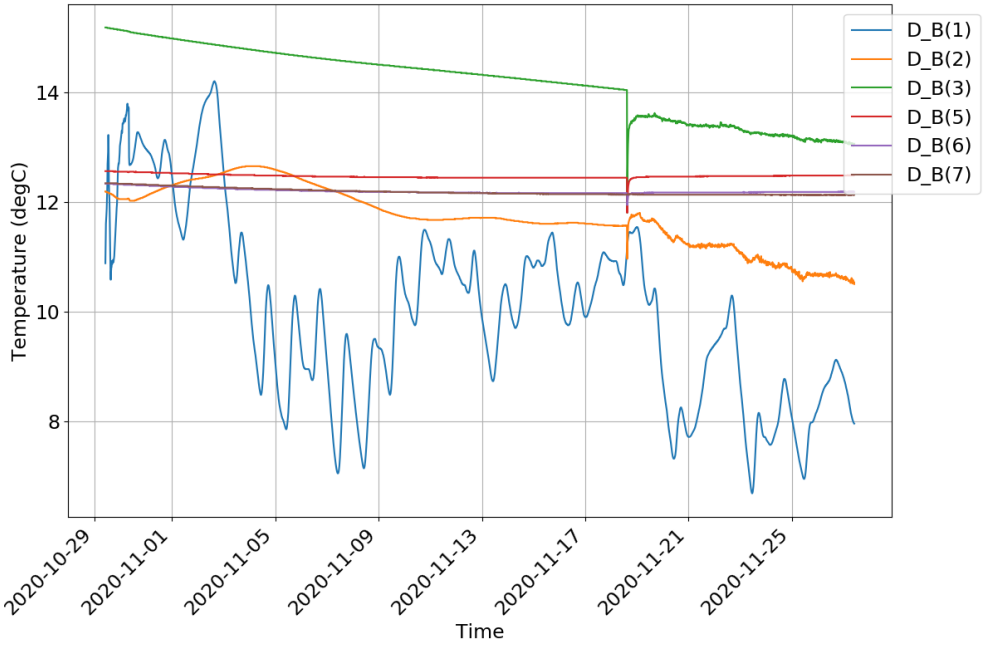

Figure 13.3: The data of deep back thermistor string measurements in phase 1a.

Deep Canal The final set of measurements is shown in Figure 13.4, which is from the thermistor string placed in the canal (D_C). The temperature fluctuation in the water just below the surface is large, as can be deduced from sensor D_C(1). This is most likely not correct because temperatures of 20 degrees Celsius have not occurred in November. The most probable explanation is that radiation from the sun heated the pipe and its inside temperature to vary between 20 and 2.5 °C as the steel is oxidated thereby absorbing a lot of energy. One metre lower, sensor D_C(2) is a lot less fluctuating but still clearly influenced by the air temperature. Below D_C(2), the sensors are placed in the soil and, as expected, the temperature just below the canal bottom (D_C(3)) is relatively warm. Below that, the temperature cools down to 12 degrees Celsius quickly. As a result of the large unrealistic temperatures fluctuations, the sensors used to measure the water temperature are not used in this thesis. That does not count for the sensors measuring the soil temperature.

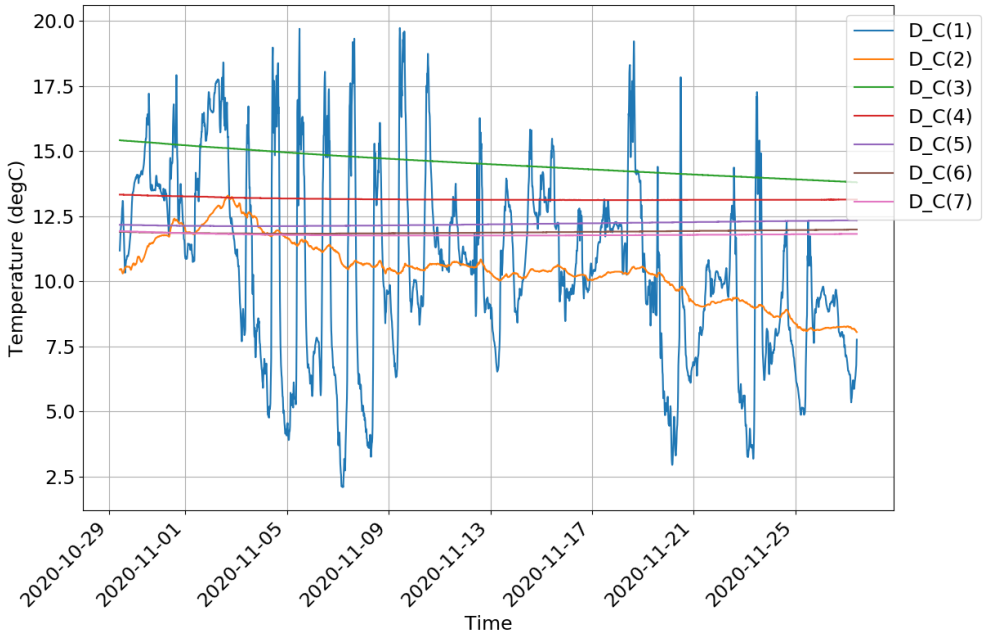

Figure 13.4: The data of deep canal thermistor string measurements in phase 1a.

Temperature Over Depth Figure 13.5 and Figure 13.6 show the temperature distribution over depth of deep front left and right. It's clearly visible that the soil above 5 metres cools down while the soil beneath warms up. This is in agreement with the previously described analysis.

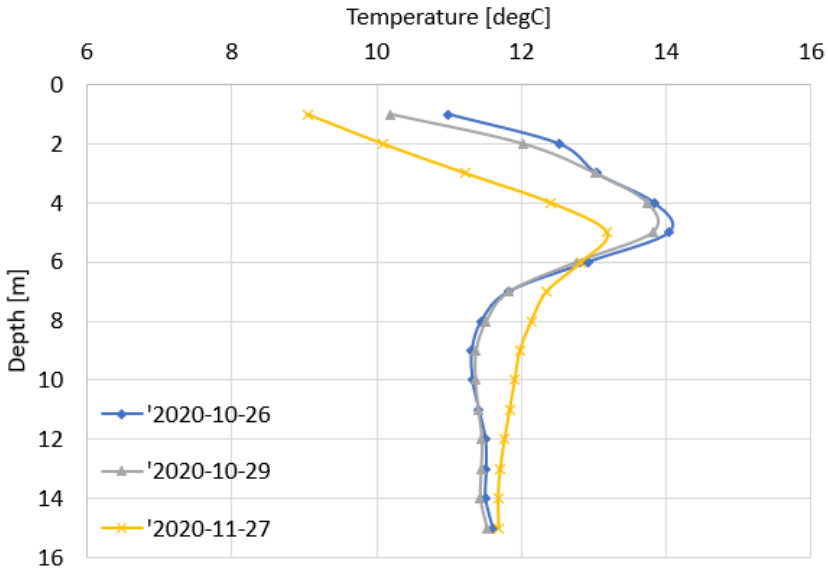

Figure 13.5: Deep front left temperature versus depth in phase 1a.

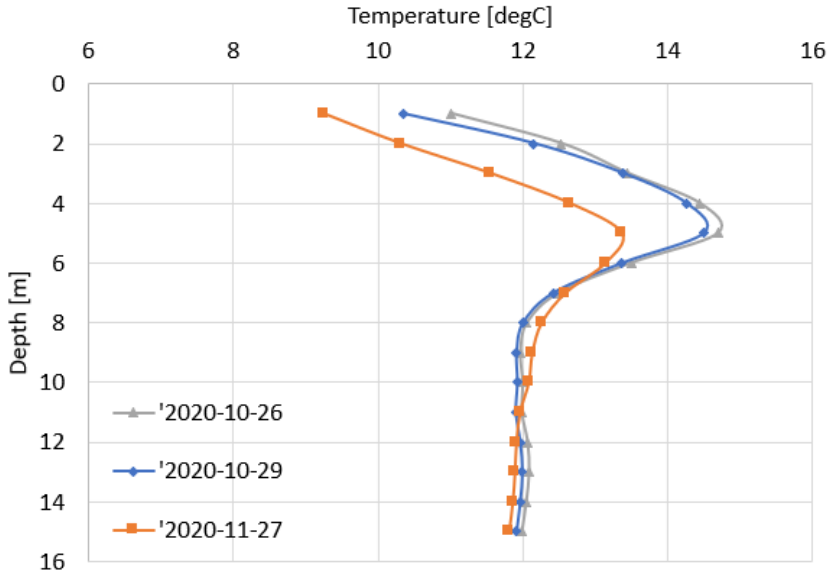

Figure 13.6: Deep front right temperature versus depth in phase 1a.

13.1.2 Shallow Section

The interpretation of the thermistor strings in the shallow section in phase 1a is described here.

Shallow Front Left The same measurements have been performed in the shallow activation section, yet with less sensors. Figure 13.7 shows the measurements of thermistor string shallow front left (S_FL). Only two sensors are shown in the graph while the string contains four. The datalogger doesn't pick up a signal from the bottom two sensors. Nevertheless, the data available indicates a clearly down going trend – the soil cools down by approximately 3 °C. The temperature change measured by the top sensor doesn't differ that much compared to the course of D_FL(1); however, S_FL(2) and D_FL(2) do and even though the magnitude is the same, in terms of extremes S_FL(2) is much lower.

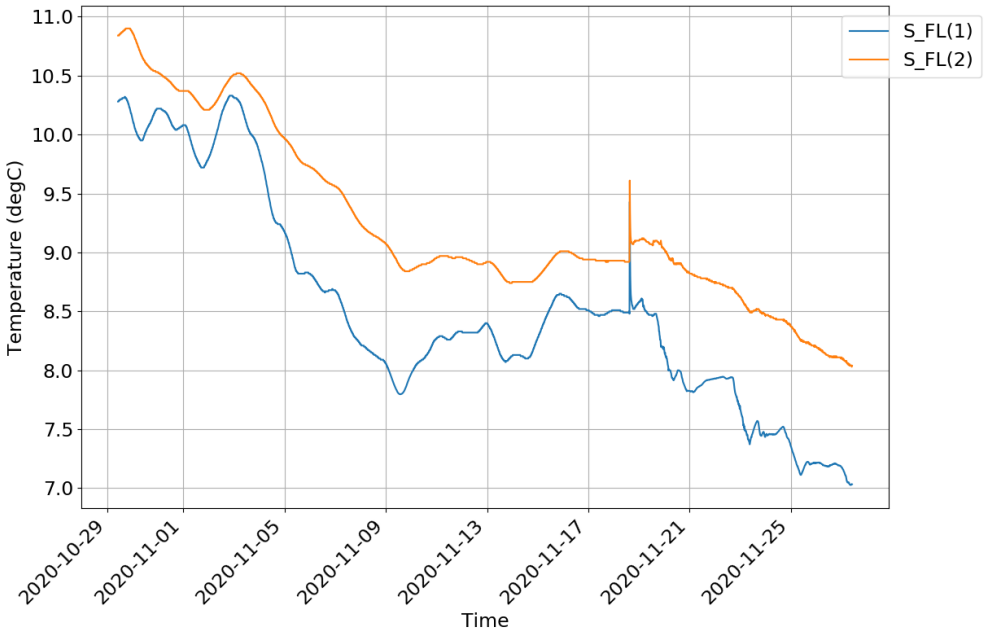

Figure 13.7: The data of shallow front right thermistor string measurements in phase 1b.

Shallow Front Right Figure 13.8 contains the measurements of the shallow front right (S_FR) thermistor string. This string has four working sensors giving a better look into the temperature distribution. Instantly capturing the attention is the jump of lines S_FR(3) and S_FR(4) - the air in the pipes has had a lot of influence on the temperature

measurements. S_FR(3) becomes half a degree warmer while S_FR(4) becomes half a degree cooler. The dotted lines show an approximation of the expected curve taking the start value and the horizontal part after the filling with water as start and end point. These lines are much more probable – especially for S_FR(3) as it isn't likely the temperature of the soil is the same as one metre higher (at S_FR(2)).

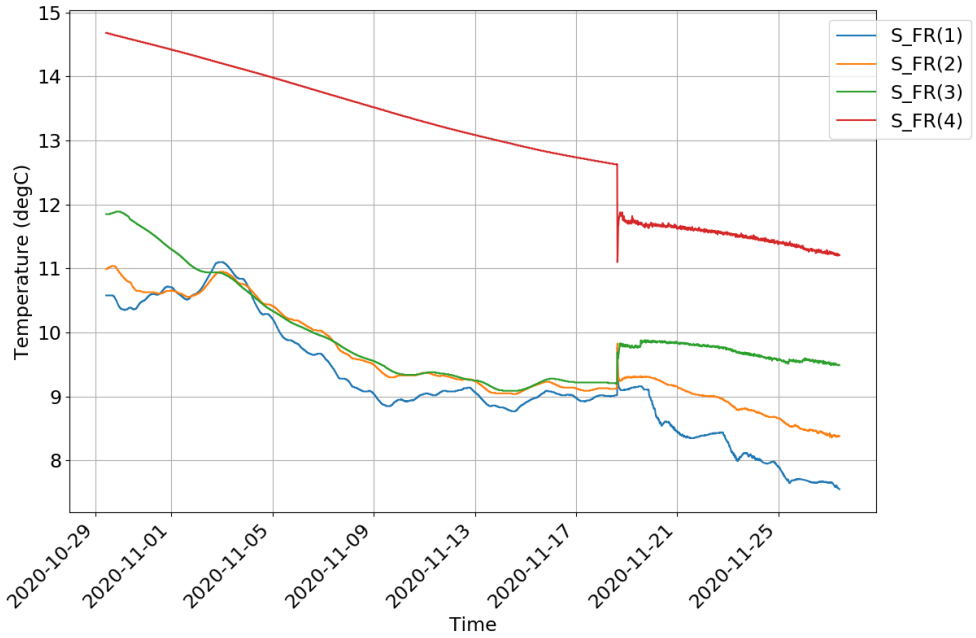

Figure 13.8: The data of shallow front right thermistor string measurements in phase 1b.

Shallow Canal Like the thermistor string in Figure 13.7, the shallow canal thermistor string (in Figure 13.9) has some non-working sensors. Only one line is plotted showing that the temperature of the canal one metre below the surface is decreasing almost linearly. When comparing this to the measurements done in the deep section, the two paths of the sensor closest to the surface are very different, Figure 10 shows this. Due to the limited amount of information and the improbability that the water temperature decreases linearly this data is not used in this thesis.

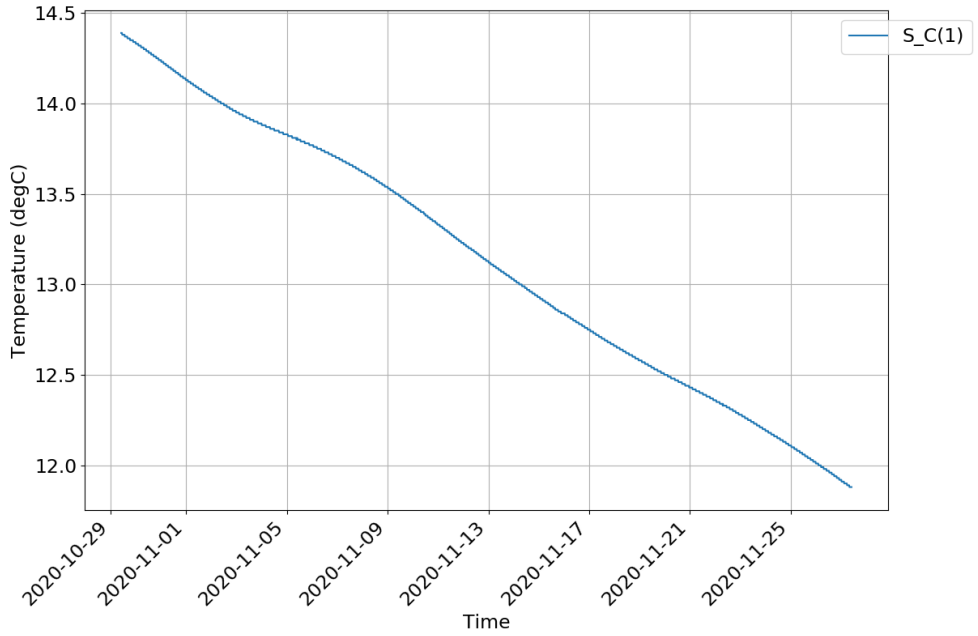

Figure 13.9: The data of shallow canal thermistor string measurements in phase 1b.

Temperature Over Depth Figure 13.10 shows the temperature distribution over depth of the shallow front right thermistor string. The gray line (26-10-2020) shows the distribution three days before the start of the test. The blue line shows it at the start of the test. A relatively large temperature drop has occurred in these three days. Based on the data acquired by sensor D_B(1), which measures the air temperature, temperatures dropped from 14 degrees to an average of 10 degrees Celsius from 26-10-2020 to 30-10-2020. This, in combination with the air moving in and out of the steel thermistor sting pipes, might be an explain for the drop. The orange line (27-11-2020) displays the temperature at the end of the month of measuring. An overall temperature drop of approximately 1.5 degrees Celsius has occurred. Referring back to Figure 4.6, this thermistor string is placed 0.5 metres from the sheet pile and not in the direct vicinity of the loops.

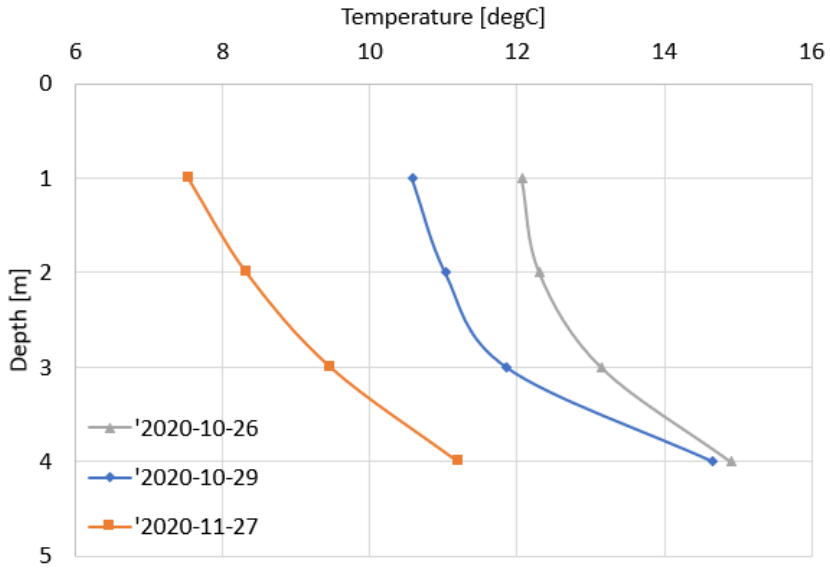

Figure 13.10: Shallow front right temperature versus depth in phase 1b.

13.2 Phase 1b - Single Side Deep Activation

This section contains the aforementioned two week timespan in which the single side deep loop has been activated the entire time. As a result of technical issues, a considerable flow rate flowed for only for the first few days through the single shallow loop. The rest of the phase this loops is considered inactive.

13.2.1 Deep Section

This subsection contains the interpretation of the thermistor strings in the deep section in phase 1b.

Deep Back Figure 13.11 contains the monitored data during the two weeks of activation of the single deep loop. As one can see, the three thermistors closest to the surface show responsiveness to the generally decreasing air temperature. The sensors below don't experience that influence but, around 09-12-2020, a downward going trend is noticed. This may be due to the decreasing air temperature as all but one lie above the 6 metre boundary. However, it is expected, as the temperature is constant up to December 9, this temperature decrease is the result of the thermal activation.

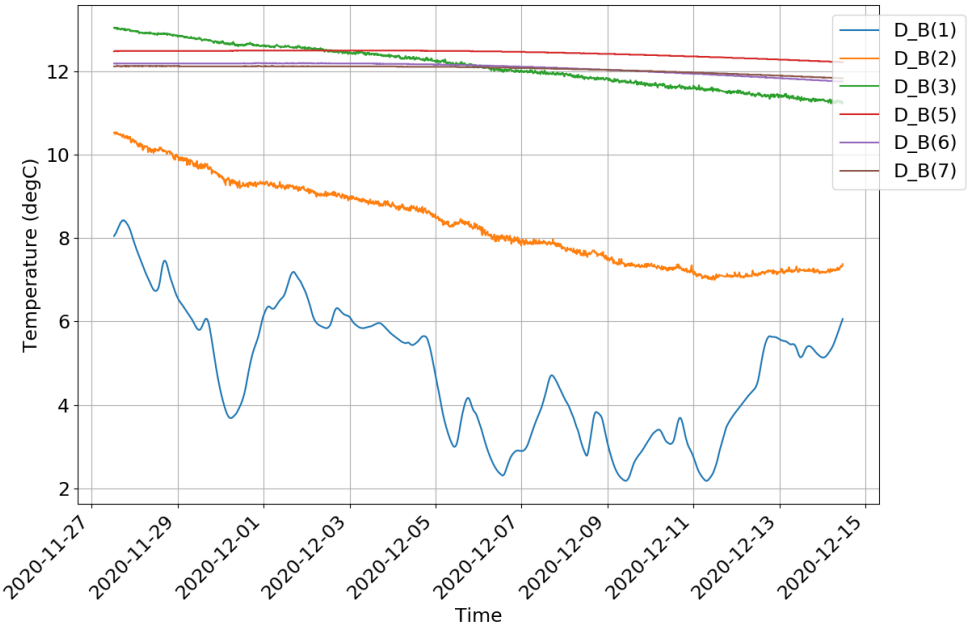

Figure 13.11: The data of deep back thermistor string measurements in phase 1b.

Deep Canal The behaviour identified in Figure 13.11 is seen in Figure 13.12 as well. The two thermistors closest to the surface respond to the air temperature strongly while deeper sensors pick up a small but gradual temperature decrease. Most likely, this is partly caused by the changing water temperature – especially for the soil in direct vicinity of the water – but, in agreement with the analysis of the deep back thermistor string, this partly due to energy extraction al well.

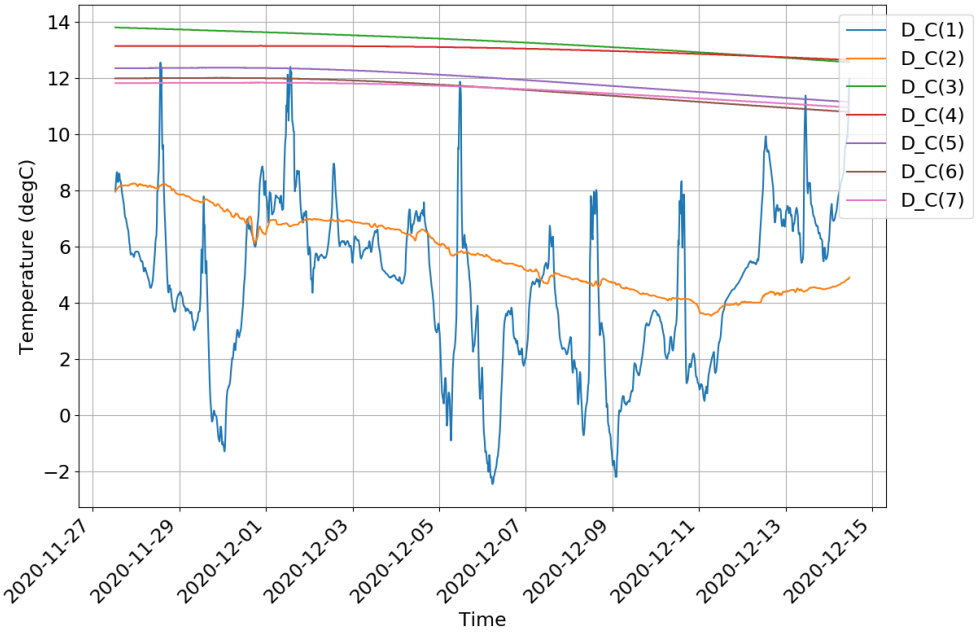

Figure 13.12: The data of deep canal thermistor string measurements in phase 1b.

Deep Front Left Figure 13.13 shows a very clear decrease of the temperature in deeper regions. This decline starts a few days after the activation of the deep loop and decreases from an approximate 12 °C to 9 °C.

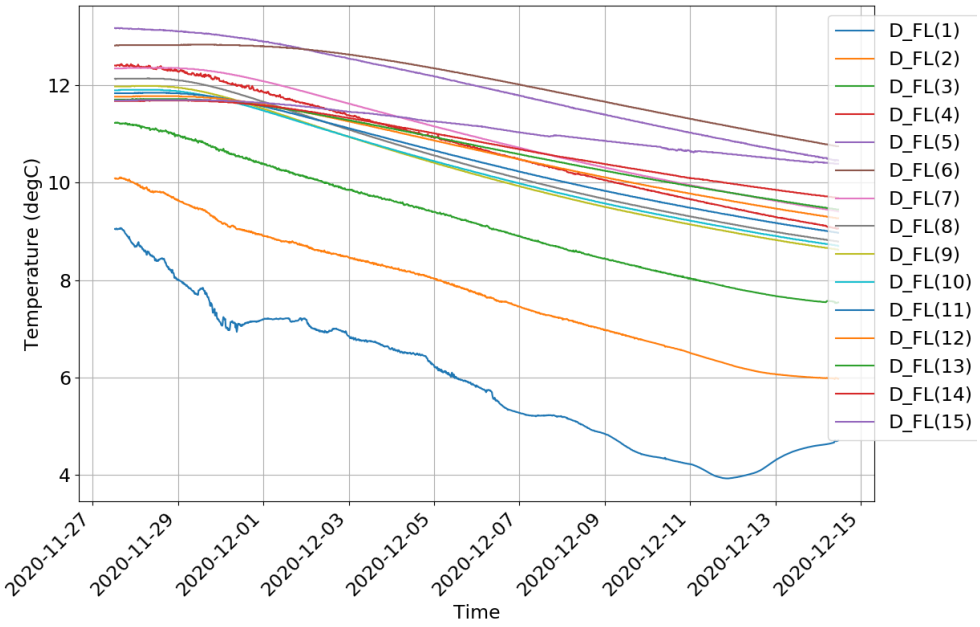

Figure 13.13: The data of deep front left thermistor string measurements in phase 1b.

Deep Front Right Figure 13.14 shows the temperature decrease monitored by thermistor string deep front right. Comparing the graph to the previously analysed data, the first three sensors register the same behaviour. Shifting attention to the deeper sensors, one can see a generally downward going trend. However, in opposition to thermistor string deep front left, the temperature decrease has not the same magnitude - the temperature drop slows down over depth. Where the temperatures up to approximately 11 metres were higher than the deeper layers, these drop quickly after which the lines intersect on December 4. This is due to the glycol-water mixture heating up in the metres loop before reaching the deepest point. This heating results in a smaller temperature gradient between the soil and glycol-water mixture.

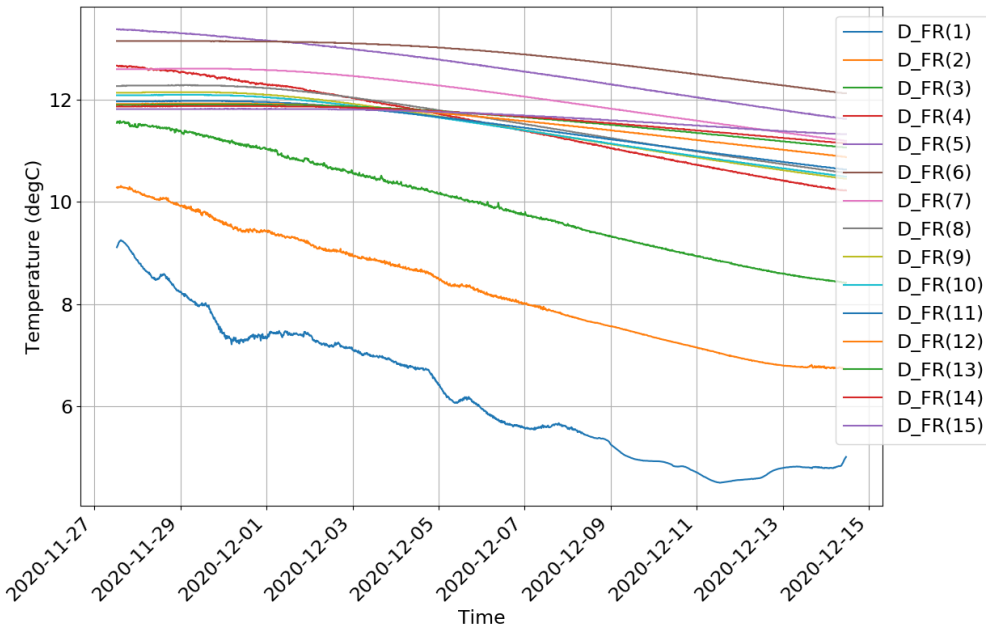

Figure 13.14: The data of deep front right thermistor string measurements in phase 1b.

13.2.2 Shallow Section

This section contains the data of the thermistor strings on the shallow side of the sheet pile wall.

Shallow Canal The data of the temperature of the water is shown in Figure 13.15. This is a linear line and it is expected that this is not accurate. Most likely, the temperature is damped heavily inside the metal tube. Therefore, it shows no influence from changing ambient temperature. As a result, this data is not used in this thesis.

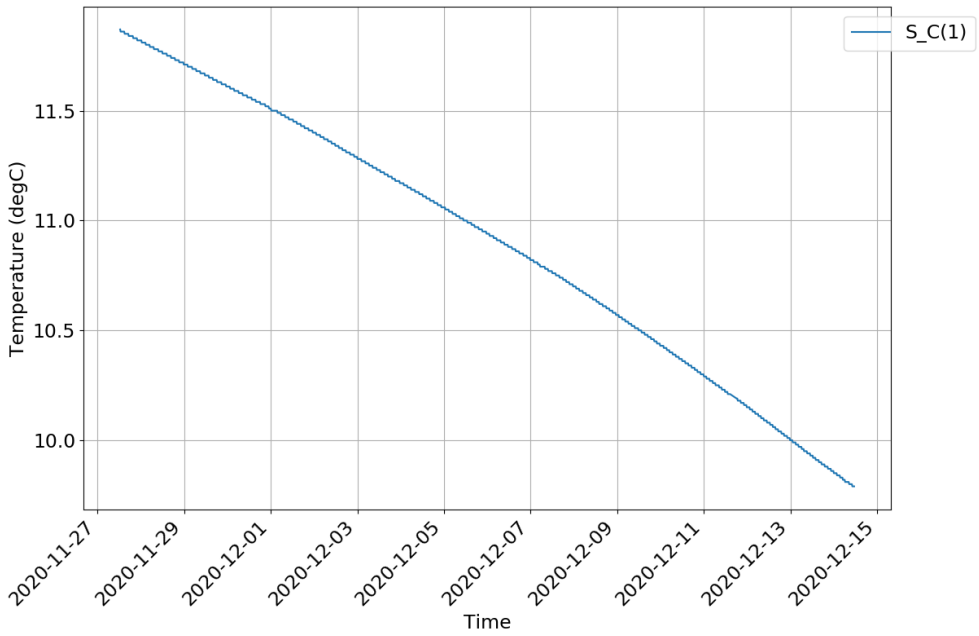

Figure 13.15: The data of shallow canal thermistor string measurements in phase 1b.

Shallow Front Left Figure 13.16 contains the soil temperature monitored by the shallow front left thermistor string. The difference between the two lines is approximately 1 °C and almost continuously declining. The thermistor closest to the surface is influenced by the air temperature as a daily temperature variation is visible. At the end of the phase the monitored temperature increases as a result of increasing water and air temperatures.

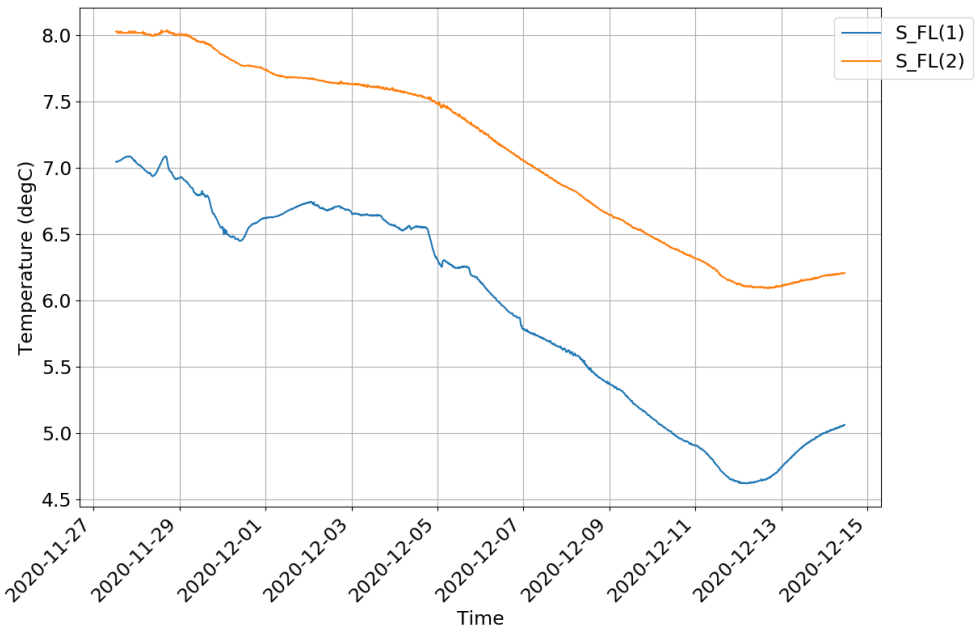

Figure 13.16: The data of shallow front left thermistor string measurements in phase 1b.

Shallow Front Right The temperature change in phase 1b is visible in Figure 13.17. The deepest sensor is barely influences while the sensor closest to the surface is the most. Comparing the latter to Figure 13.16, the temperature declines more gradual and is less influenced by the water temperature which is important to recognize.

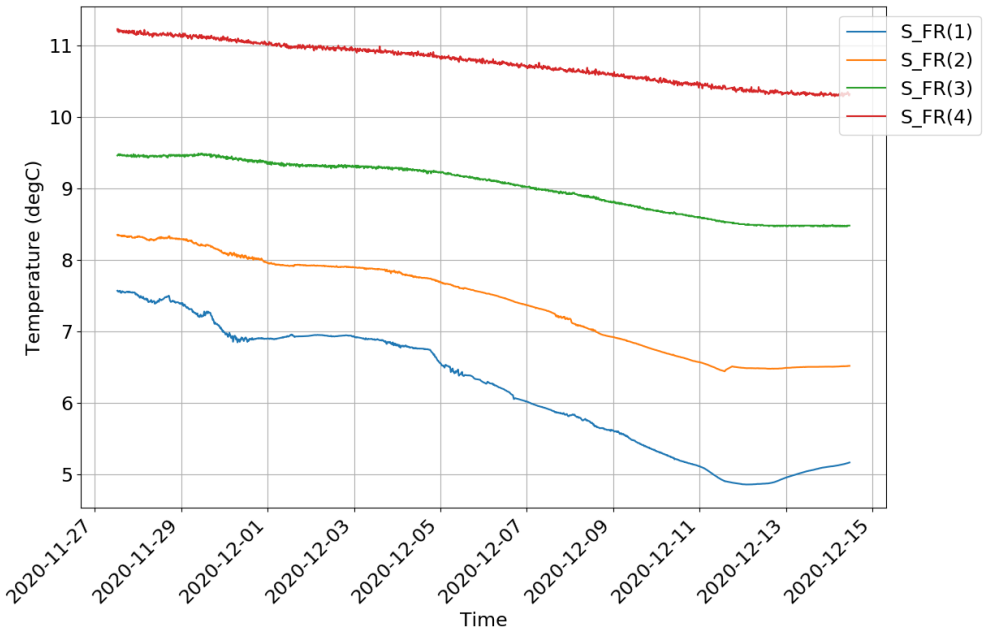

Figure 13.17: The data of shallow front right thermistor string measurements in phase 1b.

13.3 Phase 2 - Double Side Activation

The second phase comprises the activation of the two deep loops. These have been activated from 27-11-2020 to 14-12-2020. The power of the heat pump at the start of the test was approximately 2.5 kW and slowly declined to 2 kW. This decline is further elucidated in the analysis of the heat pump performance. First, the two datasets from the thermistor strings that are located the furthest away from the sheet pile are analysed after which the datasets from the strings closer by are interpreted.

13.3.1 Deep Section

Deep Back Figure 13.18 shows the temperature measurements of the thermistor string placed the furthest away from the sheet pile. As assumed, the energy sheet pile has little no influence on the soil near this thermistor string as it is located 1.5 metres away. Thermistor D_B(1) and D_B(2) sense cooler temperatures, ranging from approximately 6 - 3 °C and 7.5 - 5.5 °C, respectively. D_B(1) is located outside the metal tube, buried a few centimetres below the surface. Therefore, it is assumed this thermistor registers the air temperature. The four sensors underneath the aforementioned thermistors monitor higher temperatures: D_B(3) registers a decline from 11 to 9 °C and D_B(5) to D_B(7) cools down from approximately 12 to 10 °C.

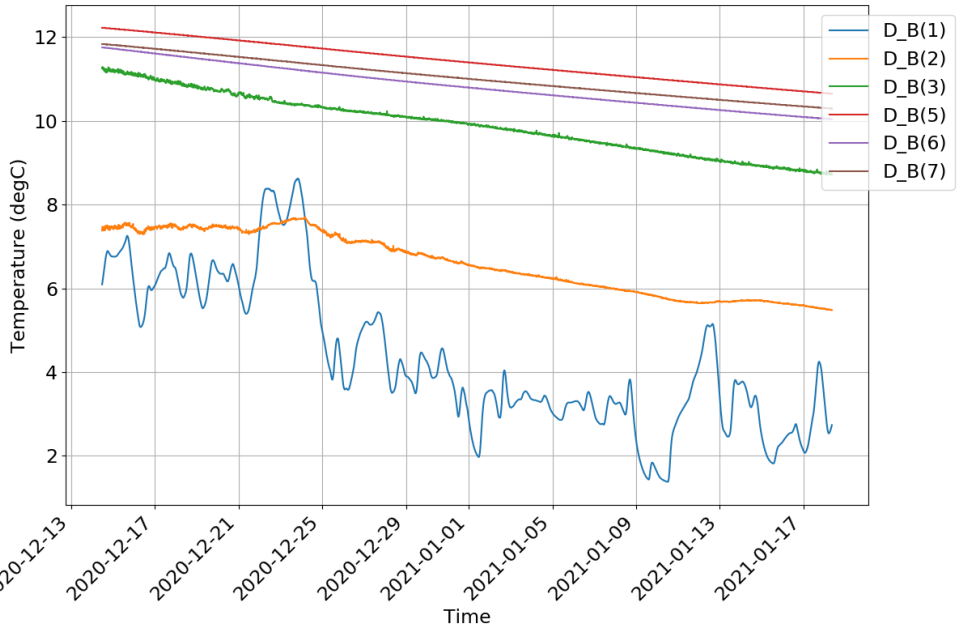

Figure 13.18: The temperature change monitored by the deep back (D_B) thermistor string

Deep Canal The temperature change in the canal is shown in Figure 13.19. The thermistor string contains seven thermistors of which two are located in the water and the rest in the soil underneath the canal. The biggest temperature variation can be seen, as expected, in the data registered by the thermistor one metre under the water surface. This sensors is located in the water. The temperature declines from approximately 10 to 3 °C. The thermistor underneath, D_B(2), monitors the temperature decreasing from approximately 5 to 2.5 °Cand is located just below the bottom of the canal. The temperature at this depth is still very responsive to the air temperature, resulting in the sudden temperature rise at 23-12-2020. The linearity of the lines indicates that the temperature change in the soil under the canal is uninfluenced by the air temperature. The first two metres of soil underneath the canal are slightly hotter than the metres below but cool down faster too. The deepest three thermistors have approximately the same temperature and register a temperature decrease of 2 °C, from 11 to 9 °C.

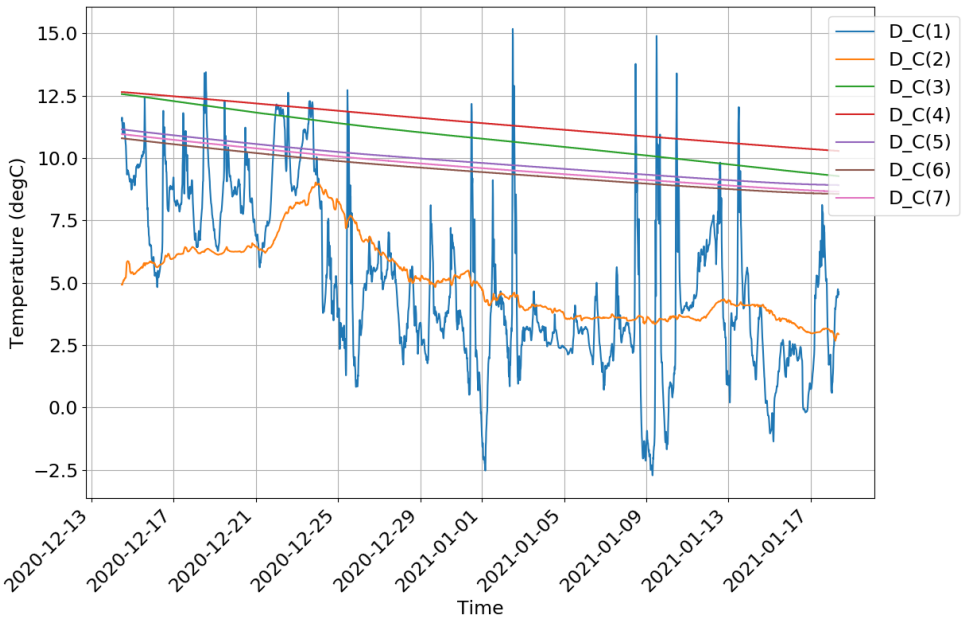

Figure 13.19: The temperature change monitored by the deep canal (D_C) thermistor string.

Deep Front Left Figure 13.20 contains the measurements of the thermistor string located closest to the sheet pile. A clear decline in subsurface temperature is present. In the upper 6 metres, D_FL(1) - D_FL(6), this is the result of de-

creasing air temperatures and heat extraction, but in the metres below that the ambient temperature has no influence. As a result, the complete decline is due to the extraction by the energy sheet piles. Quantifying this temperature decrease, the deepest thermistors monitor a temperature between 9.5 and 11.5 °C at the start of the phase and between 6.5 and 8.5 °C at the end - meaning an approximate 2 °C temperature decrease. Such a quantification proves more difficult for the upper 6 metres as the soil experience influence from the air en water. However, the thermistor closest to the surface is a smooth line showing a generally negative trend, in contrast to the upper thermistor temperature paths in Figure 13.18 and 13.19. The same smooth line is seen for the second thermistor. This indicates a continuous heat sink (the energy sheet piles) rather than ambient influences (i.e. air and water).

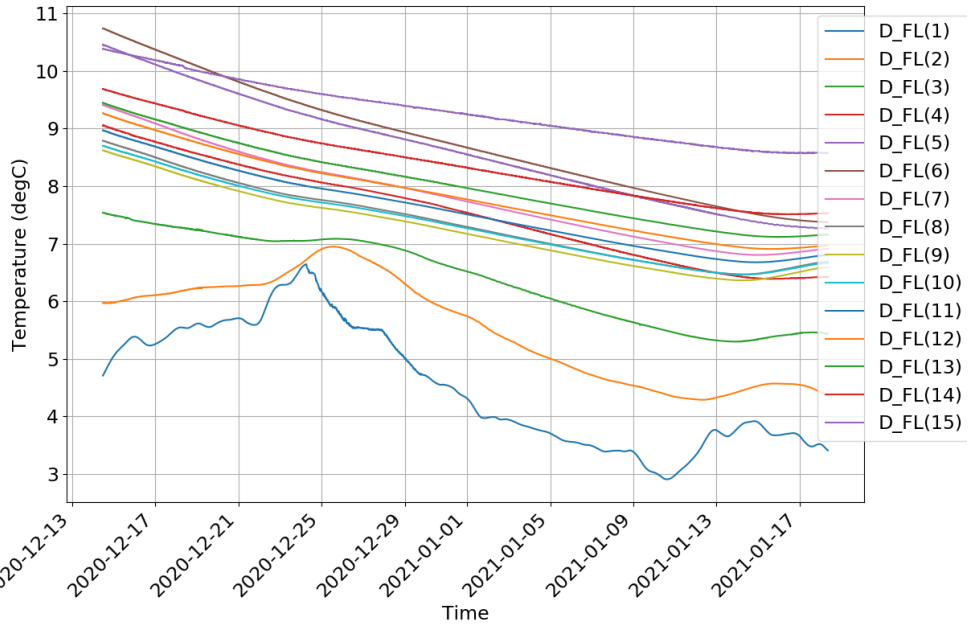

Figure 13.20: The temperature change monitored by the deep front left (D_FL) thermistor string.

Deep Front right Figure 13.21 shows the registered temperatures by thermistor string deep front right. This figure is very alike Figure 13.20, according to expectations, as these strings are located close to each other. Especially the first five thermistors give very similar temperature paths. However, the paths below 5 metre show a subsurface that is generally 1 °C warmer than thermistor string D_FL.

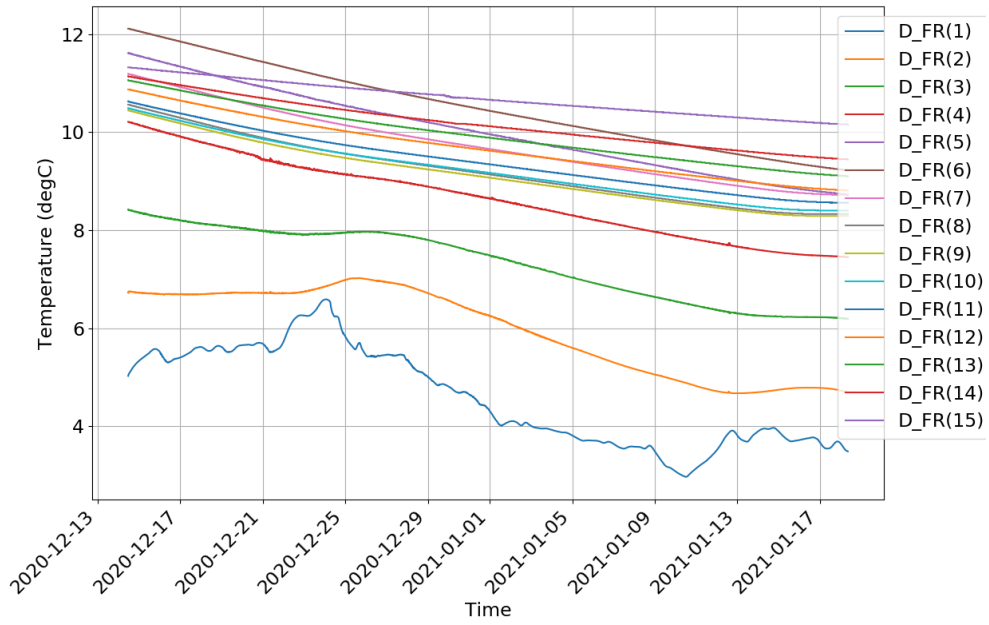

Figure 13.21: The temperature change monitored by the deep front right (D_FR) thermistor string.

13.3.2 Shallow Activation Section

This section contains the analysis of the shallow activation section. On this side of the sheet pile, the loops were inactive for the duration of one month.

Shallow Back In this phase, the shallow back thermistor string was activated and registered temperatures at two depths: 1 and 2 metres below the surface. S_B(1) is expected to follow more or less the air temperature - which is does. S_B(2) lies deeper and is more sheltered from this influence - this too is visible. Quantifying the temperature change: the S_B(1) registers a 2 °C drop and S_B(2) an approximate 1.5 °Cdrop.

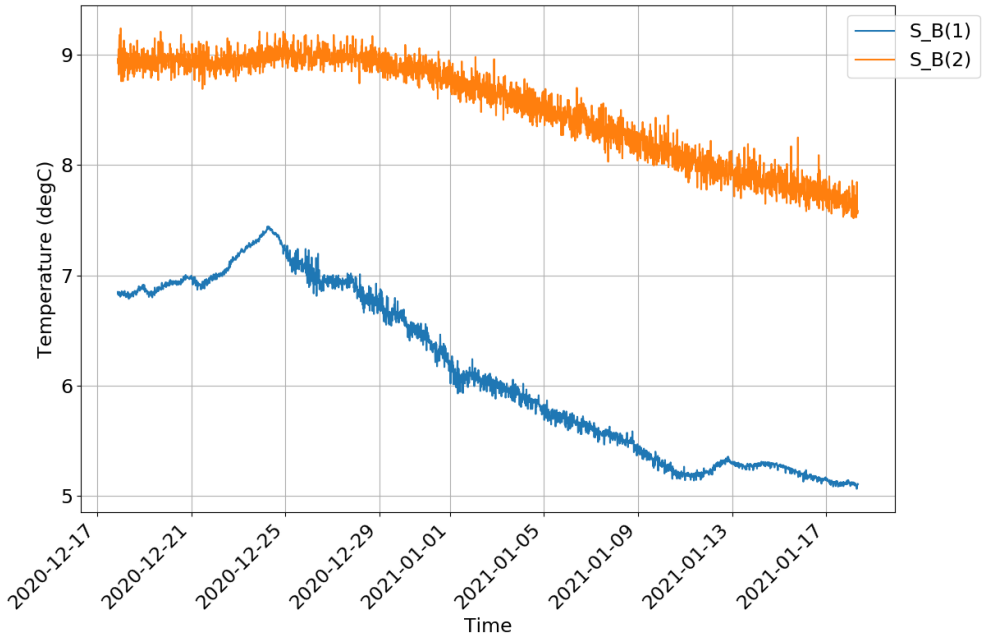

Figure 13.22: The temperature change monitored by the shallow back (D_B) thermistor string.

Shallow Canal In contrast to the previous phase, both thermistors in the canal thermistor string are working properly. At 18-12-2020, a sudden temperature drop and revive can be seen. No adjustments where made at that time

so this sudden change is most likely a measurement error. The temperature gradient monitored by the thermistor closest to the surface is less linear than in the previous phase, yet it the temperature decreases almost constantly from approximately 10 to 8 °C. One metre below, temperatures are much higher and fall less quickly: from 14 tot 13 °C.

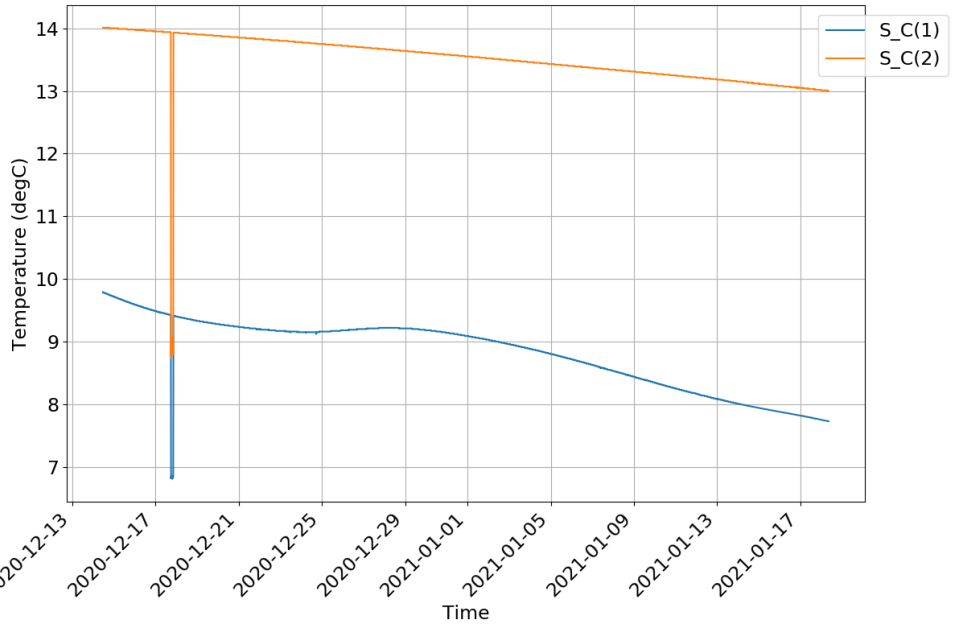

Figure 13.23: The temperature change monitored by the shallow canal (D_C) thermistor string.

Shallow Front Left Two out of four thermistors are working in this thermistor string. The temperature paths visualized in Figure 13.24 show a bigger response to external influences than in Figure 13.22. This is due to either the air temperature, the temperature decrease of the sheet pile as a result of the thermal activation in the deep section or a combination of both. Nevertheless, S_FL(1) shows an increase of 3 °C after which is falls below 4 °C. S_FL(2) follows more or less the same path but registers temperatures 1 - 1.5 °C higher. This temperature change is in agreement with the air temperature.

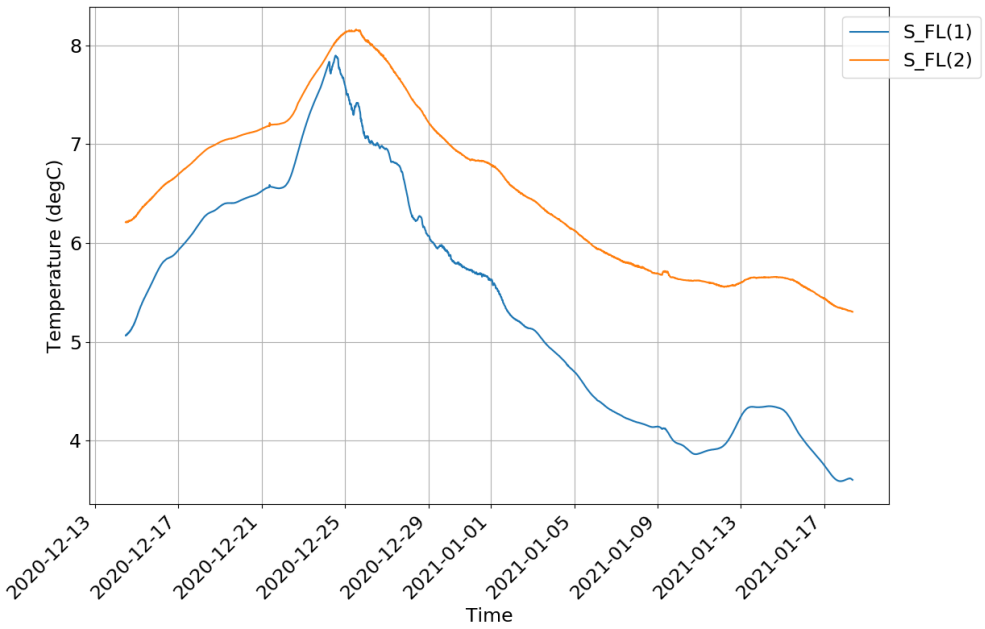

Figure 13.24: The temperature change monitored by the shallow front left (D_FL) thermistor string.

Shallow Front Right S_FR(1) and S_FR(2) in Figure 13.25 show very similar behaviour to the temperature paths in Figure 13.24. The two thermistors below that show a small temperature decrease of approximately 0.5 °C.

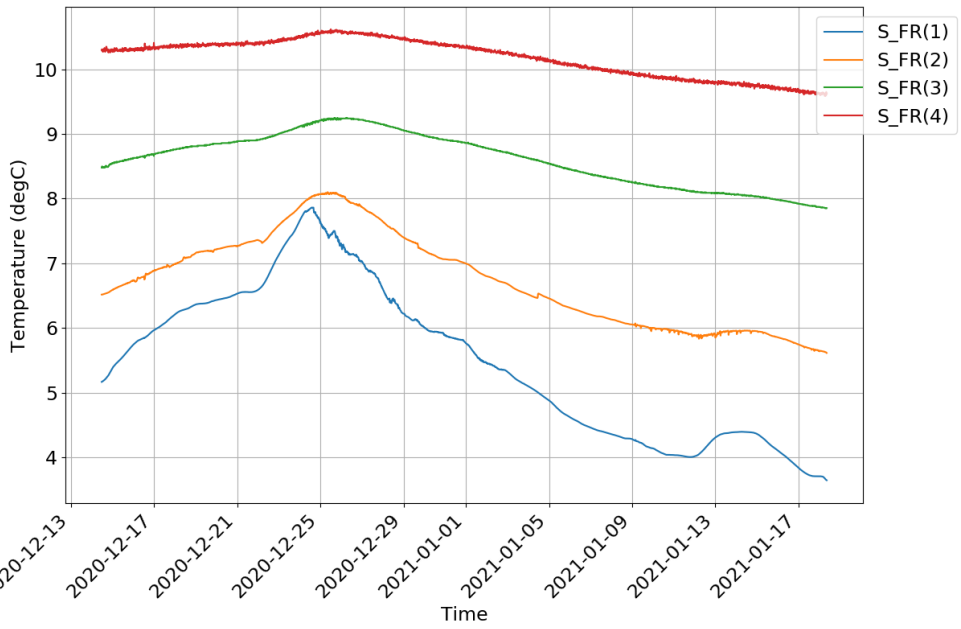

Figure 13.25: The temperature change monitored by the shallow front right (D_FR) thermistor string.

Appendix B

This appendix contains the governing equations of the packages used in COMSOL Multiphysics and PLAXIS 2D. These equations account for the heat transport through the models, fluid flow through the models and deformation of the matter in the models.

COMSOL Multiphysics

Theory for heat transfer in Porous Media

This equation is a transient convection-conduction equation where this first term is transient, recognizable by the temperature changing over time. The second term represents the convection; the velocity field vector indicates this. The third term accounts for the conduction: Fourier's law makes use of the thermal conductivity and the temperature gradient.

$$(\rho C_p)_{eff}\frac{\delta T}{\delta t} + \rho C_p \mathbf{u}\cdot\nabla T + \nabla \mathbf{q} = Q + Q_{vd} \tag{13.1}$$

$$\mathbf{q} = -k_{eff}\nabla T \tag{13.2}$$

Where:

- ρ is the fluid density [kg/m^3]
- C_p is the fluid heat capacity at constant stress [J/(kg · K)]
- $(\rho C_p)_{eff}$ is the effective volumetric heat capacity at constant pressure, defined by:

$$(\rho C_p)_{eff} = \theta_p \rho_p C_{p,p} + (1-\theta_p)\rho C_p$$

- k_{eff} is the effective thermal conductivity (a scalar or tensor if the thermal conductivity is anisotropic)
- **u** is the velocity field, either an analytic expression or computed from a fluid flow interface. It should be interpreted as the Darcy velocity, that is, the volume wflow rate per unit cross sectional area. The average linear velocity (the velocity within the pores) can be calculated as $\mathbf{u}_f$ = **u** / (1 - θ_p), where (1 - θ_p) is the fluid's volume fraction or equivalently the porosity.
- **q** is the heat flux by conduction [W/m^2]
- Q are heat sources [W/m^2]

Theory for the Heat Transfer in Pipes

The governing equation for the heat transfer in pipes interface is a transient convection-conduction equation too, but for a line element. The first two term are the same as the aforementioned explanation in the heat transfer in porous media interface. The second term on the right hand side is a convection factor as well, yet in the pipes rather than the soil. The conduction term is again recognizable by the thermal conductivity: this is the first term on the right hand side.

$$\rho A C_p \frac{\partial T}{\partial t} + \rho A C_p \mathbf{u}\cdot\nabla T = \nabla\cdot(Ak\nabla T) + \frac{1}{2} f_D \frac{\rho A}{d_h}|\mathbf{u}|^3 + Q + Q_{wall} \tag{13.3}$$

With:

- ρ is the density [kg/m^3]
- A is the pipe cross area [m^2]
- C_p is the specific heat capacity at constant stress [J/(kg · K)]
- T is the temperature [K]
- f_D is a friction factor [-]
- **u** is the velocity field [m/s]
- k is the thermal conductivity [W / (m · K)]
- Q represents a general heat sources [W/m]
- Q_wall represents external heat exchange through the pipe wall [W/m]

PLAXIS

Heat Transfer

$$\rho C \frac{\partial T}{\partial t} - \nabla \cdot (\lambda \, \nabla T) \left[\frac{k_{rel}}{\mu} \, \kappa_{ij}^{int} \, (\nabla p_w + \rho_w \, \mathbf{g}) \right] \cdot T + \rho_w \, C_w \, T \left[\nabla \cdot (\frac{k_{rel}}{\mu} \kappa_{ij}^{int} \, \nabla p_w + \rho_w \, \mathbf{g}) \right] - Q_T - C_{as}(T - T_a) = 0 \quad (13.4)$$

With:

- ρC = heat capacity of the porous medium [J/(kg ·K)]
- T = temperature [K]
- λ = thermal conductivity of the porous medium [W/(m · K)]
- k_{rel} = relative permeability [-]
- μ = dynamic viscosity [kg/(m · s)]
- κ_{ij}^{int} = intrinsic permeability [m^2]
- p_w = water pressure [kPa]
- ρ_w = water density [kg/m^3]
- g = gravitational acceleration [m/s^2]
- Q_T = heat source term [W/m^3]
- C_{as} = the convective heat transfer coefficient at the surface in contact with air [$W/(m^2 \cdot K)$]
- T_a = air temperature [K]

Fluid Flow

The formula for the equilibrium for groundwater flow is (Galavi, 2010):

$$\mathbf{q} = K_{ij}^{int}(\nabla p_w + \rho_w \cdot \mathbf{g}) \quad (13.5)$$

Where $\mathbf{K}^{int}$ is:

$$K_{ij}^{int} = \begin{bmatrix} \kappa/\mu & 0 & 0 \\ 0 & \kappa/\mu & 0 \\ 0 & 0 & \kappa/\mu \end{bmatrix}$$

In which :

- **q** is the specific discharge
- p_w = water pressure [kPa]
- ρ_w = water density [kg/m^3]
- g = gravitational acceleration [m/s^2]
- κ^{int} = intrinsic permeability [m^2]
- μ = dynamic viscosity [kg/(m · s)]

More information can be found in PLAXIS (2015)

Deformation

The deformation equation is based on the linear momentum balance of a representative elemental volume of soil, the infinitesimal strain theory and the effective stress equation. This results in the governing equation for the deformation model (Galavi, 2010):

$$L_{ij}^T \, [\mathbf{M} \, (L_{ij} \, \cdot d\mathbf{u}) + S_e \, d p_w \, \mathbf{m}] + d(\rho \, \mathbf{g}) = \mathbf{0} \quad (13.6)$$

In which:

$$L_{ij}^T = \begin{bmatrix} \frac{\delta}{\delta x} & 0 & 0 & \frac{\delta}{\delta y} & 0 & \frac{\delta}{\delta z} \\ 0 & \frac{\delta}{\delta y} & 0 & \frac{\delta}{\delta x} & \frac{\delta}{\delta z} & 0 \\ 0 & 0 & \frac{\delta}{\delta z} & 0 \frac{\delta}{\delta y} & \frac{\delta}{\delta x} & \end{bmatrix}$$

And:

$$\mathbf{m} = (1 \; 1 \; 1 \; 0 \; 0 \; 0 \; 0)^T \quad (13.7)$$

Where:

- $\mathbf{L}^T$ is the transpose of the differential operator [-]
- **M** the stress-strain matrix [-]
- **u** an element [-]
- S_e the effective saturation [-]
- p_w the water pressure [kPa]
- **m** a vector containing unity terms for normal stress components and zero terms for the shear stress components [-]
- **g** the gravitational acceleration [m/s^2]

More information about the composition of the equation can be found in Galavi (2010).

Appendix C

This appendix contains the parameters of the soil present at the test location. The parameters are used in the geotechnical stability model in which the deformation of the sheet pile and the distortion of the soil is investigated.

Material Strength Properties

Table 13.1: Soil properties.

Name	Level Top Layer [m NAP]	γ/γ_{sat} [kN/m^3]	c' [kPa]	ϕ' [°]	n [-]
Sand Top Layer	0.2	18/20	0	27	0.33
Peat	-1.75	11/11	10	15	0.6
Clay, Weakly Silty	-5.5	15/15	1	22.5	0.6
Clay, Strongly Sandy	-6.5	18/18	0	27.5	0.4
Clay, Weakly Silty	-8.0	15/15	1	22.5	0.6
Clay	-9.5	14/14	3	17.5	0.6
Sand	-17.0	17/19	0	30	0.33

Table 13.2: Strength parameters PLAXIS.

Name	Level Top Layer [m NAP]	γ/γ_{sat} [kN/m^3]	E'$_{50;ref}$ [MPa]	E'$_{oed;ref}$ [MPa]	E'$_{ur;ref}$ [MPa]	G'$_{0;ref}$ [MPa]	Y$_{0.7}$ [-]	R_0^{NC} [-]
Sand Top Layer	0.2	18/20	41.9	41.9	125.8	142.0	9.8E-5	0.5460
Peat	-1.75	11/11	1.0	0.5	6.0	12.0	9.79E-4	0.7412
Clay, Weakly Silty	-5.5	15/15	2.0	1.0	10.0	34.0	3.84E-4	0.6173
Clay, Strongly Sandy	-6.5	18/18	26.9	20.7	134.6	149.0	9.4E-5	0.5383
Clay, Weakly Silty	-8.0	15/15	2.0	1.0	10.0	34.0	3.84E-4	0.6173
Clay	-9.5	14/14	1.4	0.7	7.0	29.0	4.17E-4	0.6993
Sand	-17.0	17/19	34.1	34.1	102.4	124.0	1.17E-4	0.5000

Where:

- γ/γ_{sat} is the (saturated) volumetric weight;
- E'$_{50;ref}$ is the secant stiffness in standard drained triaxial loading;
- E'$_{oed;ref}$ is the tangent stiffness for primary oedometer loading;
- E'$_{ur;ref}$ is the unloading/reloading stiffness;
- **G'**$_{0;ref}$ is the shear modulus at very small strains;
- **Y**$_{0.7}$ is the shear strain at which G'$_s$ = 0.722 G$_0$;
- R_0^{NC} is the stress ratio $\sigma_{xx}'/\sigma_{yy}'$ in 1D primary compression;
- ν_{ur} is Poisson's ratio, fixed for all layers at 0.2;
- p$_{ref}$ is the reference pressure, fixed for all layers at 100 kPa;
- R$_f$ the failure ratio q_f/q_a, fixed for all layers at 0.9.;
- m the rate of stress dependency in stiffness behaviour, fixed for all layers at 0.5.

Table 13.3: Strength parameters plates.

Name	EA_1 [kN/m]	EA_2 [kN/m]	EI [kNm^2/m]	d [m]	w [kN/m/m]	ν [-]
Stiff Plate	1E9	1E9	1E9	3.464	0	0
ZZ 17-700	2.793E6	2.793E6	76.49E3	0.5733	1.04	0.2

Where:

- EA_1 is the in-plane axial stiffness;
- EA_2 is the out of plane axial stiffness;
- EI is the flexural rigidity;
- d is the (equivalent) thickness;
- w is a specific weight entered as force per unit of length per unit width in out of plane direction;
- ν is Poisson's ratio.

References

Andersland, O. B. and B. Ladanyi
1994. *An Introduction to Frozen Ground Engineering*, 1 edition. Springer US.

Bourne-Webb, P., S. Burlon, S. Javed, S. Kürten, and F. Loveridge
2016. Analysis and design methods for energy geostructures. *Renewable and Sustainable Energy Reviews*, 65:402–419.

Bovelander, R.
2020. Water Temperature Delftsche Schie. Technical report, Hoogheemraadschap Delfland, Delft.

Brinkgreve, R. B.
2019. CIE4361 Behaviour of Soils and Rocks.

COMSOL Multiphysics
2015. *Heat Transfer Module User's Guide*.

COMSOL Multiphysics
2017. *Pipe Flow Module User's Guide*.

De Jong, F.
2020. Proefopzet Energie Damwand De Zweth. Technical report, CRUX Engineering B.V., Delft.

Delage, P.
2013. On the thermal impact on the excavation damaged zone around deep radioactive waste disposal. *Journal of Rock Mechanics and Geotechnical Engineering*, 5(3):179–190.

Engineering_Toolbox
2003. Coefficients of Linear Thermal Expansion.

Galavi, V.
2010. Internal Report Groundwater flow , fully coupled flow deformation and undrained analyses in PLAXIS 2D and 3D Vahid Galavi Research department. *Plaxis BV*, P. 285.

Kürten, S., D. Mottaghy, and M. Ziegler
2014. A new model for the description of the heat transfer for plane thermo-active geotechnical systems based on thermal resistances. *Acta Geotechnica*, 10(2):219–229.

Kürten, S., D. Mottaghy, and M. Ziegler
2015. Design of plane energy geostructures based on laboratory tests and numerical modelling. *Energy and Buildings*, 107:434–444.

PLAXIS
1994. *Reference manual*.

PLAXIS
2015. Thermal and coupled THM analysis. *Essential for Geotechnical Professionals*.

Sedighi, M., B. D. Hepburn, H. R. Thomas, and P. J. Vardon
2015. Energy balance at the soil atmospheric interface. *Environmental Geotechnics*, 5(3):146–157.

Snoeren, J.
2019. The Influence of Freezing-thawing Cycles on the Geotechnical Performance of an End-bearing Energy Pile. Technical report, Delft University of Technology.

Ziegler, M., D. Koppmann, R. Pechnig, and D. Knapp
2019. Energy sheet pile walls – Experimental and numerical investigation of innovative energy geostructures. *XVII European Conference on Soil Mechanics and Geotechnical Engineering*, 1(1).